

# Long Coherence Time and Precision Measurement of Atomic Interactions in a Bose-Einstein Condensate

M. Egorov, V. Ivannikov, R. Anderson, I. Mordovin, B. Opanchuk,  
B.V. Hall, P. Drummond, P. Hannaford and A. I. Sidorov

Centre for Atom Optics and Ultrafast Spectroscopy, Swinburne University of Technology,  
Melbourne 3122, Australia  
asidorov@swin.edu.au

**Abstract:** We report a high precision method of measuring  $s$ -wave scattering lengths in a Bose-Einstein condensate (BEC) and a coherence time of 2.8 s in a Ramsey interferometer employing an interacting BEC.

## 1. Introduction

Atomic interactions play a major role in ultracold quantum gases, matter-wave interferometry and frequency shifts of atomic clocks. Precise knowledge of inter-particle interaction strengths is important because the dynamical evolution of a Bose-Einstein condensate is highly sensitive to atomic collisions and BEC interferometry is greatly influenced by mean-field driven dephasing [1] and quantum phase diffusion [2]. Here we demonstrate that in the presence of atomic interactions the interference contrast can be enhanced by mean-field rephasing of the condensate and the timely application of a spin echo pulse [3]. We observe a periodic decrease and revival of the contrast with a slowly decaying magnitude. We also employ collective oscillations of a two-component BEC for the precision measurement of the interspecies scattering length  $a_{12}$  with a relative uncertainty of  $1.6 \times 10^{-4}$ .

## 2. Periodical Rephasing and Long Coherence Time of BEC

A  $^{87}\text{Rb}$  condensate is trapped in a cigar-shaped magnetic trap on an atom chip [4] in two internal states ( $|1\rangle = |F = 1, m_F = -1\rangle$  and  $|2\rangle = |F = 2, m_F = +1\rangle$ ) coupled via a two-photon MW-RF transition. In the Ramsey interferometer (Fig. 1(a)) the first  $\pi/2$  pulse prepares a coherent superposition of two components in a non-equilibrium state due to the different values of scattering lengths  $a_{11}$ ,  $a_{12}$  and  $a_{22}$ . The wavefunctions of two components begin to oscillate out-of-phase along the axial direction of the trap. During the first half of the oscillation the relative phase of the two states grows non-uniformly in space [1] and the component wavefunctions separate in space leading to a rapid decrease in the fringe contrast ( $T = 0.2$  s, Fig. 1(a)) [3]. The relative phase becomes uniform along the condensate when the two wavefunctions complete an oscillation cycle at  $T_{osc} = 0.37$  s and we observe a remarkable recovery of the contrast - a self-rephasing of the two-component BEC.

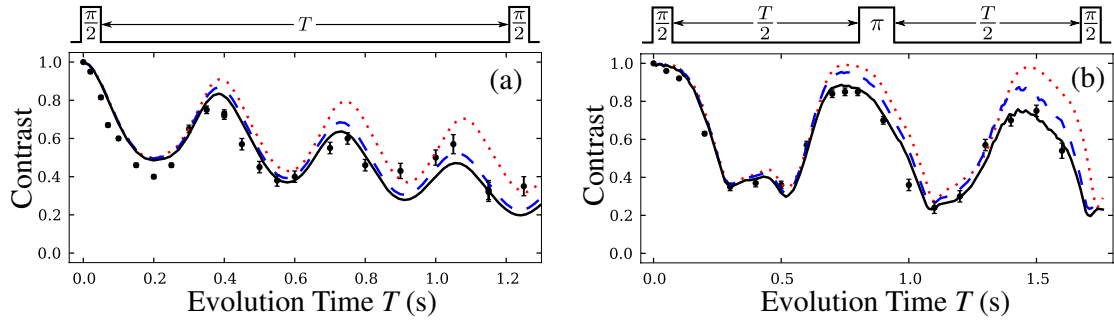


Fig. 1: Dependence of the interferometric contrast (filled circles) on the evolution time  $T$  in the Ramsey (a) and spin echo (b) sequences. Simulations: GPE theory (red dotted), truncated Wigner model without (blue dashed) and with (solid black) technical noise.

We apply a spin echo pulse (Fig. 1(b)) to reverse the relative phase evolution and to compensate for asymmetric losses of the two states by inverting the populations of the BEC components  $|1\rangle$  and  $|2\rangle$ . Maximal revivals of the contrast (0.85 at  $T = 0.75$  s and 0.75 at  $T = 1.5$  s, Fig. 1(b)) are observed when the self-rephasing mechanism and the spin echo are synchronized. This occurs if the  $\pi$  pulse is applied at  $T/2 = T_{osc}$ ,  $2T_{osc}$ , when the relative phase is uniform along the condensate and the two wavefunctions overlap in space. Simulations of the Gross-Pitaevskii equations (GPEs) clearly show the echo-enhanced revivals of the contrast but predict almost 100% recovery of the contrast not seen in the experiments (Fig. 1(b)) due to the presence of beyond-mean-field effects. The inclusion of quantum and technical noise in the simulations provides a better fit with the data and allows to evaluate a coherence time of 2.8 s for the interacting BEC interferometer.

### 3. Measurement of $s$ -Wave Scattering Lengths

Collective oscillations of a three-dimensional (3D) two-component BEC in a cigar-shaped trap can be conveniently described by an effective 1D treatment using Gaussian trial functions [5]. For the transfer of a small atom number to state  $|2\rangle$  the equations show the existence of state  $|2\rangle$  oscillations with the frequency  $f_2 = 4f_{ax}\sqrt{(1 - \sqrt{a_{12}/a_{11}})/3}$ . Accurate measurements of the axial trap frequency  $f_{ax}$  and the state  $|2\rangle$  oscillations with the frequency  $f_2$  make possible a precision measurement of the ratio  $a_{12}/a_{11}$ .

Our trap frequencies (98.23, 101.0, 11.507) Hz are measured by employing dipole oscillations of the condensate. To monitor the state  $|2\rangle$  oscillations we transfer 10% of the condensed atoms from state  $|1\rangle$  to state  $|2\rangle$ , allow the BEC to evolve dynamically in the trap for variable oscillation times, release the atoms from the trap and image both components after a variable time-of-flight [5]. The 2D distribution of the column density of component  $|2\rangle$  is fitted with Gaussian functions to obtain the axial width of the atomic cloud. Oscillations of the extracted axial widths (black dots) with time are presented in the Fig. 2(a). Each point represents one experimental realization and we fit the temporal dependence of the data with the GPE simulations (blue solid line), varying parameters  $a_{12}$ ,  $a_{22}$  and the total atom number and using a converging iteration procedure [5]. We carry out six series of measurements with different times of flight (6.6 ms and 20.1 ms), atom number (from  $6 \times 10^4$  up to  $1.5 \times 10^5$ ) and take systematic uncertainties into account. Using  $a_{11} = 100.40 a_0$  ( $a_0$  is the Bohr radius) as the established value, we evaluate  $a_{12} = 98.006(16) a_0$  from our measurement series.

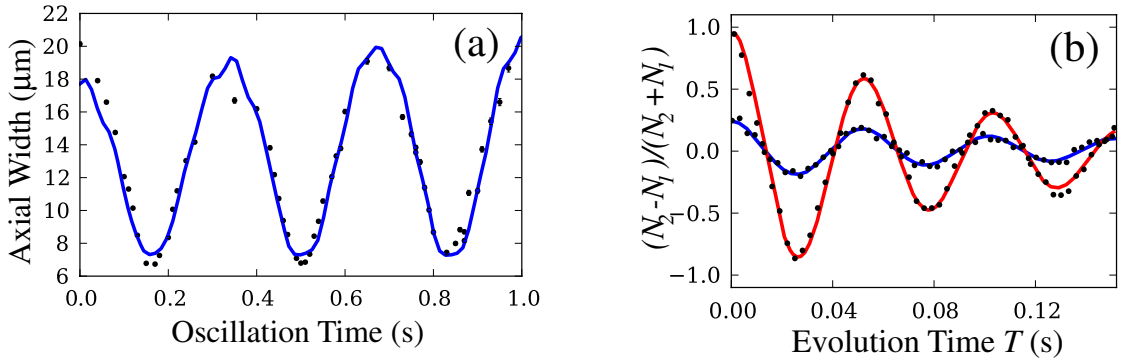


Fig. 2: (a) Temporal evolution of the axial width of component  $|2\rangle$  in a superposition of two states prepared with a  $\pi/5$  pulse; (b) Ramsey fringes in the time domain for the  $\pi/2$  (red solid line) and  $\pi/10$  (blue solid line).

In order to measure the intraspecies scattering length  $a_{22}$ , we perform two Ramsey interferometric sequences with a variable area of the first pulse ( $\pi/10$  and  $\pi/2$ , Fig. 2(b)). The collisional shift for the  $\pi/10$  pulse (the small atom number in  $|2\rangle$ ) is proportional to  $n(r)(a_{11} - a_{12})$  and for the  $\pi/2$  pulse to  $n(r)(a_{11} - a_{22})$ , where  $n(r)$  is the atom number density. The ratio of the two shifts is independent of  $n(r)$  greatly reducing the systematic error on the atom number variations. We run the GPE simulations to fit our data and extract the value  $a_{22} = 95.44(7) a_0$ .

### 4. Conclusion

We show that atomic interactions not only lead to dephasing of a BEC interferometer but under appropriate conditions produce rephasing of the BEC wavefunctions and the recovery of the interferometric contrast. We also demonstrate a method of high-precision measurements of  $s$ -wave scattering lengths in the two-component BEC. Our observations are important for precision measurements and the development of sensors based on quantum degenerate gases.

### 5. References

- [1] R. P. Anderson, C. Ticknor, A. I. Sidorov, and B. V. Hall, "Spatially inhomogeneous phase evolution of a two-component Bose-Einstein condensate," *Physical Review A* **80**, 023603(7), (2009).
- [2] B. Opanchuk, M. Egorov, S. Hoffmann, A. I. Sidorov, and P. Drummond, "Quantum noise in three-dimensional BEC interferometry," *Europhysics Letters* **97**, 50003(5), (2012).
- [3] M. Egorov, R. P. Anderson, V. Ivannikov, B. Opanchuk, P. Drummond, B. V. Hall, and A. I. Sidorov, "Long-lived periodic revivals of coherence in an interacting Bose-Einstein condensate," *Physical Review A* **84**, 021605(R)(4), (2011).
- [4] A. I. Sidorov and P. Hannaford, "From magnetic mirrors to atom chips," in *Atom Chips*, J. Reichel and V. Vuletic, eds., pp. 3–31, (Wiley-VCH, Berlin, 2011).
- [5] M. Egorov, B. Opanchuk, P. Drummond, B. V. Hall, P. Hannaford, and A. I. Sidorov, "Precision measurement of  $s$ -wave scattering lengths in a two-component Bose-Einstein condensate." arXiv:1204.1591, (2012).

# Quantum state engineering with large atomic objects

Eugene Polzik

*QUANTOP - Danish Center for Quantum Optics  
Niels Bohr Institute, Copenhagen University  
Blegdamsvej 17, Copenhagen, Denmark DK-2100*

Recent progress with generation and applications of quantum entangled states in macroscopic systems will be reviewed. Spin polarized atomic gas in a magnetic field behaves as a quantum harmonic oscillator in the ground state even at room temperature. Entanglement generated by dissipation and a steady entangled state with an arbitrary long life time has been demonstrated for such oscillators. Entanglement between two atomic spin ensembles allowed for demonstration of a magnetic field measurement in which suppression of the quantum measurement back action and quantum projection noise has led to a record sensitivity at the sub-femtoTesla level. Recently quantum teleportation of atomic spin states between two spin ensembles has been demonstrated. These methods and ideas are now being transferred to mechanical and electrical oscillators paving the road to quantum state transfer between disparate macroscopic quantum systems.

# Quasi-two-dimensional atomic Fermi gas with tunable interactions

Andrey Turlapov

*Institute of Applied Physics, Russian Academy of Sciences, ul. Ulyanova 46, Nizhniy Novgorod, 603000, Russia  
turlapov@appl.sci-nnov.ru*

A planar Fermi gas of atoms with tunable  $s$ -wave interactions is studied in various smoothly-connected many-body regimes including the regime of Fermi liquid, strong interaction, and molecular Bose gas.

Reduction of spatial dimensionality from three to two has strong effect on many-body quantum systems. In 2D, the phenomena of superfluidity and Bose condensation become clearly separated [1]. High-temperature superconductivity is attributed to 2D structure of the cuprate materials [2]. Semiconductor and oxide interfaces filled with 2D electron gas are at the basis of modern and prospective electronics [3]. Despite significant theoretical progress [2, 4], understanding of 2D systems is far from being complete, even in somewhat basic situations. Ultracold gases of Fermi atoms have been previously used to study fundamentals of 3D many-body quantum systems [5].

In experiment, we have realized and studied a quasi-2D Fermi gas of atoms with widely tunable  $s$ -wave interactions. A gas of lithium-6 atoms has been cooled and confined in a series of planar traps as shown in Fig. 1. Motion along one direction is “frozen” by tight confinement. The interactions are tuned by means of the Fano-Feshbach resonance. Different values of the interaction parameter correspond to physically different, smoothly-connected many-body states: Fermi gas of weakly attractive particles, strongly-interacting matter in a profoundly many-body regime, and a Bose gas of tightly-bound diatomic molecules. The system is characterized quantitatively by local *in situ* measurements of the pressure and density. For a weakly attractive Fermi gas, the pressure is somewhat above a Fermi-liquid theory prediction [6]. In the strongly-interacting regime, the pressure is significantly below the values obtained by Monte Carlo simulation within a strictly two-dimensional model [7]. This suggests that strong interactions break dimensionality two by populating excited states of motion along the tightly-confined direction. Interestingly, most of cuprate superconductors are not purely 2D systems either because some interlayer hopping of electrons is possible [2]. In the Bose regime, the measured pressure agrees with calculations for a weakly-interacting Bose gas, with no adjustable parameters.

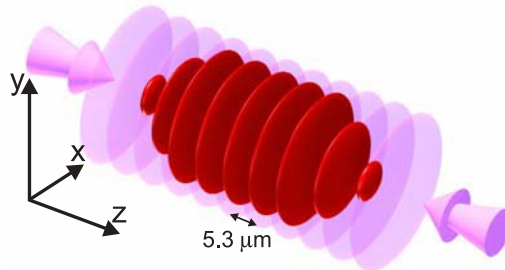


Fig. 1. Trapping ultracold atoms in antinodes of a standing optical wave. The isolated clouds of atoms shown in dark red, the standing-wave intensity shown in light purple.

Generally, for a 2D Fermi system, calculations of thermodynamic quantities are more sensitive to the choice of model than those in 3D. Reported measurements, therefore, may serve for sensitive testing of many-body theoretical methods applicable across different disciplines including nuclear and condensed matter physics.

[1] V. L. Berezinskii, “Destruction of long-range order in one-dimensional and two-dimensional systems with a continuous symmetry group. II. Quantum systems.” *Sov. Phys. JETP* **34**, 610 (1972) [*Zh. Eksp. Teor. Fiz.* **61**, 1144 (1971)].

[2] V. M. Loktev, R. M. Quick, and S. G. Sharapov, “Phase fluctuations and pseudogap phenomena,” *Phys. Rep.* **349**, 1 (2001).

[3] T. Ando, A. B. Fowler, and F. Stern, “Electronic properties of two-dimensional systems,” *Rev. Mod. Phys.* **54**, 437 (1982); J. Mannhart, D. H. A. Blank, H. Y. Hwang, A. J. Millis, and J.-M. Triscone, “Two-dimensional electron gases at oxide interfaces,” *MRS Bull.* **33**, 1027 (2008).

[4] Y. Yanase, T. Jujo, T. Nomura, H. Ikeda, T. Hotta, and K. Yamada, “Theory of superconductivity in strongly correlated electron systems,” *Phys. Rep.* **387**, 1 (2003).

[5] I. Bloch, J. Dalibard, and W. Zwerger, “Many-body physics with ultracold gases,” *Rev. Mod. Phys.* **80**, 885 (2008); A. Turlapov, “Fermi gas of atoms,” *JETP Lett.* **95**, 96 (2012) [*Pis'ma Zh. Eksp. Teor. Fiz.* **95**, 104 (2012)].

[6] P. Bloom, “Two-dimensional Fermi gas,” *Phys. Rev. B* **12**, 125 (1975).

[7] G. Bertaini and S. Giorgini, “BCS-BEC crossover in a two-dimensional Fermi gas,” *Phys. Rev. Lett.* **106**, 110403 (2011).

# Influence of magnetic field on relaxation processes in ultracold laser plasma

B.B. Zelener<sup>1,2</sup>, E.A. Manykin<sup>2,3</sup>, S.A. Sahakian<sup>1</sup>, V.A. Sautenkov<sup>1,4</sup>, B.V. Zelener<sup>1</sup>

<sup>1</sup> Joint Institute for High Temperatures of Russian Academy of Sciences, Moscow, 125412 Russia

<sup>2</sup> National Research Nuclear University, Moscow, 115409 Russia

<sup>3</sup> Kurchatov Institute, National Research Centre, Moscow, 123182, Russia

<sup>4</sup> P. N. Lebedev Physical Institute of Russian Academy of Sciences, Moscow, 119991 Russia  
e-mail:boboze@mail.ru

**Abstract:** We analyze influence of external magnetic field on relaxation processes in ultracold plasma. Simulations show that magnetic field can strongly reduce of the recombination plasma rate. We assembled setup for preparation and study of ultracold lithium plasma by using tunable lasers. Behavior of laser cooled plasma in external magnetic fields will be investigated.

Our studies of ultracold plasma in magnetic field were initiated by opportunity to control laser cooled plasma and possibility to increase a production of anti-hydrogen atoms from cold antiprotons and positrons. According our preliminary estimations an intermediate magnetic field  $B \sim 0.1$  T can decrease the rate of relaxation processes in ultracold plasma. In the frame of molecular dynamic approach we obtained that external magnetic field can reduce the recombination rate by several orders [1]. The main parameter  $\zeta$ , which defined the relation between magnetic field  $B$  and recombination rate  $\alpha$ , is the ratio of the Lamoure radius and the Landau length. Calculated recombination rates are presented in Fig. 1 as “points” for different electron temperatures.

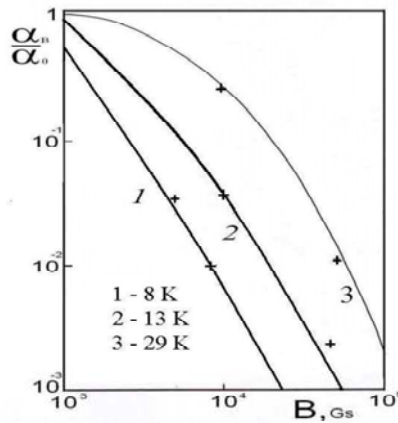


Fig.1. Normalized relaxation rate v.s. magnetic field B.

In Fig. 1. simple extrapolations  $\alpha_B = \alpha_0 [1 - \exp(-\zeta)]$  are presented as solid curves. Here  $\alpha_0$  is the recombination rate at  $B = 0$ .

We assembled setup for preparation and study of ultracold lithium plasma by using different tunable lasers. The vacuum system consists two parts: Zeeman slower and magneto-optical trap (MOT). To cool and trap  $^7\text{Li}$  or  $^6\text{Li}$  atoms we use two external cavity diode lasers. When the lithium atoms are trapped in MOT we ionize the cold atoms by pulsed narrow band titanium-sapphire laser. We can reach initial plasma temperature much bellow 1 K. We have developed several techniques to diagnose of laser ultra-cold plasma. Some of these techniques based on methods which already discussed in literature. The temporal and spectral properties of laser cooled plasma in external magnetic fields will be studied.

This work was supported by grants from the Program for basic research of the Presidium of the Russian Academy of Sciences Study of matter under extreme conditions under the guidance of Academic Fortov V.E., Ministry of Education and science of Russian Federation Grant FCP (№8679, №8513, №8364).

## References

- [1] A.A. Bobrov, S.J. Bronin, B.B. Zelener, B. V. Zelener, E. A. Manykin, D. R. Khikhlikha, JETP **143**, 4 (2013)

# Ultracold Rydberg matter: new phases and effects

**Yu.E.Lozovik**

Institute of Spectroscopy, Troitsk, 142190 Moscow  
Moscow Institute of Physics and Technology (State University), Dolgoprudnyi  
lozovik@mail.ru

Last achievements in the field of ultracold Rydberg matter are reviewed. New theoretical predictions, results of computer simulations and experimental results are discussed (see also [1,2] and cit.lit.).

van der Waals repelling of Rydberg atoms is analyzed. Crystallization of rather rarified Rydberg gas due to the van der Waals repelling is discussed [2, 3]. Two-stage crystallization and melting of mesoscopic clusters from Rydberg atoms are analyzed [2]. When Rydberg gas is excited from ultracold Bose condensed gas in result at ultralow temperatures the formed Rydberg crystal is embedded in Bose condensed, superfluid gas of nonexcited atoms and spatially modulate the last one. Thus the nonexcited Bose gas forms a supersolid first predicted by Andreev and Lifshits [4] – the state with diagonal long range (spatial) order and nondiagonal long range (coherent) order. By other words in the last system the crystal order coexist with superfluidity. Effect of blockade by Rydberg atoms is discussed. Effective masses of Rydberg atoms embedded in nonexcited Bose gas are analyzed. The effects of huge dipoles induced by external electric fields in Rydberg atoms are discussed. Crystallization and roton instabilities in the dipole gas (see [6] and also supersolid mesoscopic dipole clusters (see also [7,8]) are also discussed.

1. Peter Schauss , Marc Cheneau, Manuel Endres, et al., Nature 491, 87 (2012).
2. Lozovik Yu.E., et al (to be publ.)
3. Osychenko O. N., Astrakharchik G. E., Lutsyshyn Y., Lozovik Yu. E., Boronat J., Phys. Rev. A 84, 063621 (2011).
4. A.F. Andreev and I. M. Lifshitz, Sov. Phys. JETP 29, 1107 (1969).
5. G.E.Astrakharchik, J.Boronat, I.L.Kurbakov, Yu.E.Loizovik, Phys.Rev.Lett., 98, 060405 (2007).
6. Golomedov A. E., G. E. Astrakharchik, Yu. E. Lozovik, Phys. Rev. A 84, 033615 (2011).
7. Lozovik Yu.E., Volkov S.Y., Willander M. , JETP Lett, v.79, No.10, p.473-478 (2004).

# Observing a Large Optical Phase Shift from a Single Trapped Atomic Ion

A. Jechow<sup>1,2</sup>, E.W. Streed<sup>2</sup>, B.G. Norton<sup>2</sup>, S. Händel<sup>2</sup>, V. Blüms<sup>2</sup>, D. Kielpinski<sup>2</sup>

1. University of Potsdam, Institute of Physics and Astronomy, Photonics, Karl-Liebknecht Str. 24-25, D-14476 Potsdam, Germany

2. Centre for Quantum Dynamics, Griffith University, Kessels Road, 4111 Nathan, Brisbane, Australia

**Abstract:** We have used a single trapped atomic ion to induce and measure a large optical phase shift of 1.3 radians in light scattered by the atom by utilizing spatial interferometry based on absorption imaging

A laser-cooled trapped atomic ion is a nearly ideal isolated quantum system and is therefore a perfect test bed for fundamental atomic and quantum physics experiments. We have used a single  $^{174}\text{Yb}^+$  ion to measure a large optical phase shift between an illumination field and light scattered by the ion. A schematic of the experimental apparatus is shown in Fig. 1. The ion (blue dot in the figure) is trapped in ultra-high vacuum using a double-needle radio-frequency (RF) quadrupole Paul trap. Laser light at 369.5 nm, near resonance of the ion's cooling transition is weakly focused onto the ion to provide an illumination field that can be approximated as a plane wave. Since the ion is driven by this external field, it will emit a spherical wave. To provide additional laser cooling, an auxiliary 369.5 nm laser beam (not shown in the figure), detuned -200 MHz from atomic resonance, is incident perpendicular to the optical axis and the needle axis. This allowed us to access the blue side of the transition without losing the ion.

When transmitted past the ion, the illumination wave will interfere with the scattered wave emitted by the ion. This light is reimaged onto a cooled CCD camera with a magnification of 585 using a phase Fresnel lens with almost diffraction limited performance and a high numerical aperture  $\text{NA} = 0.64$  [1].

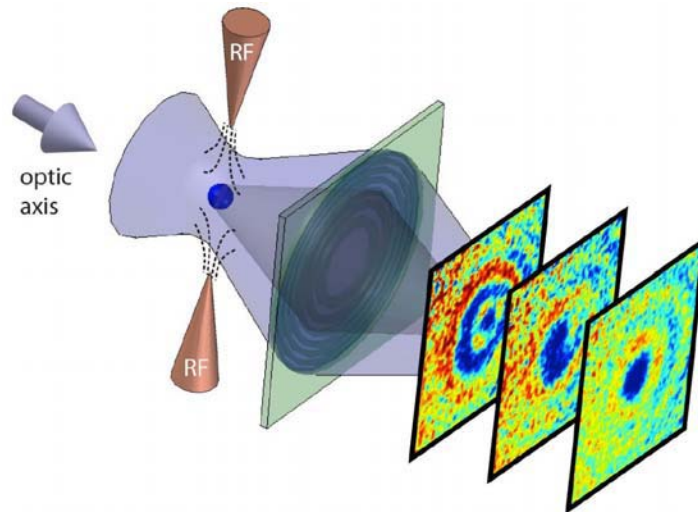


**Fig. 1** Experimental apparatus. An  $^{174}\text{Yb}^+$  ion is trapped in an RF needle trap and illuminated by a weakly focused light field near resonance. The interference between the illumination field and the scattered wave emitted by the ion is acquired with a CCD camera and a high NA phase Fresnel lens (PFL) at different focal planes as indicated by the coloured graphs on the right hand side. Laser cooling is provided by the illumination field and an auxiliary laser beam (not shown) detuned -200 MHz from the illumination beam that is incident perpendicular to the needle axis and optical axis of the illumination beam.

Our data consist of background-subtracted, normalised absorption images obtained for different laser detunings and focusing planes. From these spatial interferograms (as indicated in Fig. 1 right hand side for three focal planes) we are able to isolate the scattered part from the illumination part of the light field. The experimental setup and the data taking process are described in more detail in [2, 3].

Figure 2 shows spatial interferograms for two different detunings (a) -13 MHz and (b) +9 MHz. For each detuning three images at different focal planes are shown in rows. The left column for each detuning shows the measured data which is compared to the theoretical prediction depicted in the right column.

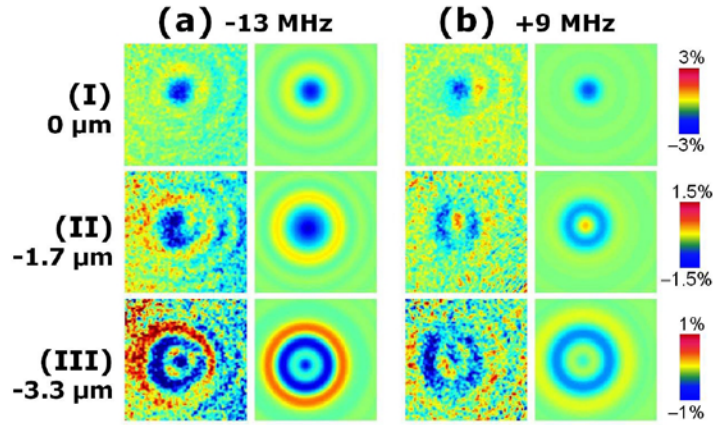


**Fig. 2** Spatial interferograms of the scattered wave for (a) -13 MHz detuning and (b) +9 MHz detuning. Each row of images corresponds to a fixed observation plane as indicated in the experimental setup with row I being the nominal plane of the ion, row II being at 1.7  $\mu\text{m}$  and row III at 3.3  $\mu\text{m}$  upstream of the ion. The colorbars indicate the fractional change in transmission for the images in each row. The theoretical prediction for each interferogram is shown in the right column of each data set.

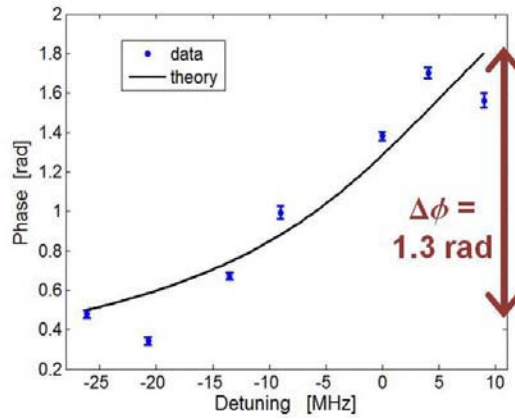


**Fig. 3** Phase of the scattered wave as a function of laser detuning obtained from the interferograms shown in Fig. 1.

Figure 3 shows the phase shift of the scattered wave as a function of the laser detuning. Each data point was obtained from a spatial interferogram as shown in Fig. 2. The measured phase shift is in good agreement with semiclassical theory were the ion is modelled as a damped harmonic oscillator driven by the laser field. The model and the way how the data was extracted is described in Ref. [3].

In conclusion we have observed a large optical phase shift of  $1.3 \pm 01$  radian from a single ion. This phase shift can be controlled by changing the detuning of the illumination laser. Our observation of single-atom phase shifts at the theoretical limit holds wide implications for microscopy and nanophotonics. Our results verify that the large optical phase shifts predicted by quantum theory can actually be observed in practice, calibrating the capabilities of techniques based on phase shifts. This scheme might find application in quantum computing and quantum information processing.

## References

- [1] A. Jechow, E.W. Streed, B.G. Norton, M. Petrasianus, and D. Kielpinski, "Wavelength-scale imaging of trapped ions using a phase fresnel lens," *Opt. Lett.* 36, 1371 (2011).
- [2] E.W. Streed, A. Jechow, B.G. Norton, and D. Kielpinski, "Absorption imaging of a single atom," *Nat. Commun.* 3, 933 (2012).
- [3] A. Jechow, B. G. Norton, S. Händel, V. Blüms, E. W. Streed, D. Kielpinski "Controllable optical phase shift over one radian from a single isolated atom," arXiv:1208.5091

# Quantum Computation in an array of trapped Rydberg Atoms

M. Saffman

*Department of Physics, University of Wisconsin, Madison, Wi., 53706, USA  
msaffman@wisc.edu*

**Abstract:** We report on progress towards multi-qubit quantum logic using an array of optically trapped neutral atom qubits. Rydberg state mediated long range interactions enable gate operations beyond nearest neighbors for scalable computing.

## 1. Introduction

Neutral atom hyperfine qubits localized in an array of optical traps represent a promising and actively pursued approach to implementing multi-qubit quantum information processing (QIP) devices[1,2,3,4]. Far detuned optical traps provide strong confinement with low photon scattering rates and low decoherence. Quantum information can be stored with excellent coherence properties in atomic hyperfine states. Entangling gate operations are enabled by exciting atomic ground states to high lying Rydberg levels with strong long-range van der Waals interactions. When the interaction range exceeds the lattice spacing gates beyond nearest neighbors can be performed. This is advantageous for multiple qubit interactions[5] such as are needed for quantum error correction.

## 2. Multi-qubit architecture

We report on experiments implementing an architecture designed to be scalable to tens of qubits in a two-dimensional array. We use blue detuned trap potentials for magic trapping of ground and Rydberg state atoms. A novel Gaussian beam array architecture provides phase stable, and optically resolvable trap sites. Trap lifetimes for Rydberg states that are limited only by spontaneous decay are demonstrated. A fluorescence image of 6 single atom qubits in a 2D trap array is shown in the figure.

Single qubit gate operations are performed with two-photon stimulated Raman transitions at 459 nm. The use of short wavelength Raman light allows for better focusing and reduced crosstalk between sites. Rydberg excitation is achieved with two-photon transitions via an intermediate p-level.

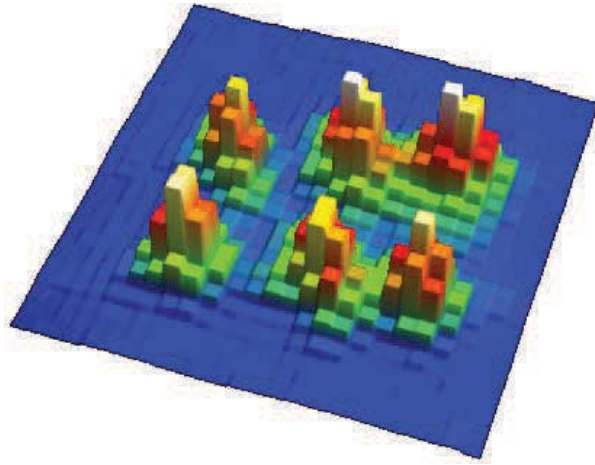


Figure 1: Fluorescence image of six Cs atom qubits in a  $4\ \mu\text{m}$  spacing trap array.

Characterization of one- and two-qubit gates, and plans for implementation of quantum algorithms will be discussed.

This work was supported by IARPA, through ARO, and DARPA through AFOSR.

### 3. References

1. D. Meschede and A. Rauschenbeutel, *Adv. At. Mol. Opt. Phys.* **53**, 75 (2006).
2. M. Saffman, T. G. Walker, and K. Mølmer, *Rev. Mod. Phys.* **82**, 2313 (2010).
3. A. Negretti, P. Treutlein, and T. Calarco, *Quantum Inf. Process.* **10**, 721 (2011).
4. M. Schlosser, S. Tichelmann, J. Kruse, and G. Birkl, *Quantum Inf. Process.* **10**, 907 (2011).
5. L. Isenhower, M. Saffman, and K. Mølmer, *Quant. Inf. Proc.* **10**, 755 (2011).

# Ultra Cold Magnesium Atoms for an Optical Frequency Standard: State of the Art and Future Trends.

A.N. Goncharov, A.E. Bonert, D.V. Brazhnikov, A.M. Shilov,  
A.V. Taichenachev, V.I. Yudin and S.N. Bagayev

*Institute of Laser Physics SB RAS, pr. Lavrent'eva 13/3, 630090 Novosibirsk, Russia*  
*Novosibirsk State University, st. Pirogova 2, 630090 Novosibirsk, Russia*  
*Novosibirsk State Technical University, pr. Karla Marksa 20, 630092 Novosibirsk, Russia*  
gonchar@laser.nsc.ru

**Abstract:** The paper presents the last results on ultra-high resolution spectroscopy of laser cooled and trapped magnesium atoms. Application of cold Mg atoms for an optical frequency standard with relative uncertainty  $\Delta\nu/\nu < 10^{-16}$  is discussed.

Frequency standards play an important role as powerful instruments for fundamental science and numerous metrological and navigation applications. Relative uncertainty of a primary frequency standard based on a fountain of cold  $^{133}\text{Cs}$  atoms, most probably, come up to their limit at  $10^{-16}$ [1]. Further progress in accuracy is connected with frequency standards in optical range. To realize an advantage of the optical range the key problem is a suppression of Doppler effects relative influence of which is independent on absolute frequency -  $\Delta\nu/\nu \sim v/c$ . Spatial localization of single ion/atoms inside a trap with a size less than wavelength, at least in the direction of an observation, is needed to suppress Doppler and the recoil effects. With this localization (Lamb-Dicke regime) [2] motional effects are strongly suppressed. Nowadays, uncertainty of the most precise optical standard based on  $\text{Al}^+$  ion reaches down to  $10^{-17}$ [3]. This is order of magnitude less than uncertainty of the most accurate microwave frequency standard. Optical frequency standards based on cooled and localized neutral Ca, Sr, Mg, Yb, Hg atoms are less accurate at the moment. With experimental realization of cooling and trapping of  $10^5 - 10^6$  atoms inside a dipole optical trap (optical lattice) formed by standing wave at "magic" wavelength[4] the situation may change in neutral atoms favour. The advantage is larger signal/noise ratio that leads up to higher frequency stability. Nowadays, Sr optical lattice frequency standard shows the best result - uncertainty is  $10^{-16}$ [5]. Magnesium atoms have some advantages as compared with Sr atoms. Internal electronic shells of Mg atom are completely filled that simplify calculations of the influence of various physical factors on the frequency shift of the clock transition. The Black Body Radiation (BBR) shift of the Mg clock transition is one of the lowest among other alkaline-earth atoms [6]. For the development of Mg frequency standard both the  $^1\text{S}_0 - ^3\text{P}_1$  transition with a natural width of 30 Hz and the ultra narrow transitions  $^1\text{S}_0 - ^3\text{P}_2$  and  $^1\text{S}_0 - ^3\text{P}_0$  are of interest (see Fig. 1). In the case of the  $^1\text{S}_0 - ^3\text{P}_0$  transition, the use of the magneto-induced spectroscopy method [7] is promising. The most serious disadvantage of Mg is the problem of a sub-Doppler cooling. Two-photon and quenching sub-Doppler cooling [8,9] were proposed and realized but these methods failed to cool down Mg atoms to a temperature of  $\sim 10 \mu\text{K}$  that is necessary to load atoms into an optical lattice. Only recently magnesium atoms were cooled down to  $5 \mu\text{K}$  and were loaded into a dipole trap [10].

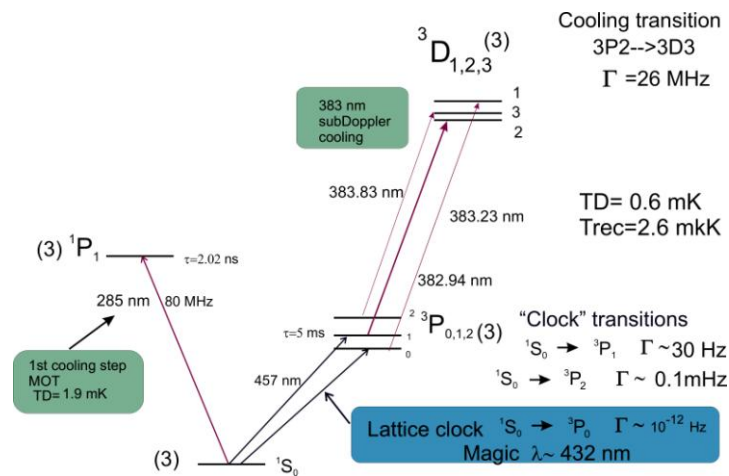


Fig.1 Level scheme of Mg atom.

The main aim of our studies is to develop an optical frequency standard with ultra cold Mg atoms [11]. As a first stage, we realized laser cooling and trapping of  $^{24}\text{Mg}$  atoms into a MOT using strong  $^1\text{S}_0 - ^1\text{P}_1$

transition. This “singlet MOT” with  $10^6 - 10^7$  atoms at temperature of  $\sim 3$  mK was used for high precision spectroscopy of the  $^1S_0 - ^3P_1$  clock transition. Fig. 2 shows our experimental setup for high resolution spectroscopy of cooled Mg atoms. AOMs were used to form a four-pulse Ramsey-Bordé interferometer in the time domain [12] to probe the clock transition. Narrow resonances (Ramsey fringes) were detected in a luminescence signal of an atom cloud when interacting with a probe laser pulses. Fig. 3 shows Ramsey fringes detected with the 3 values of a time delay between pulses. The best spectral resolution of 2-3 KHz in this experiment was limited by a width of laser line. Optical frequency standard at 655.7 THz with relative uncertainty of  $10^{-14}$  could be realized by laser frequency stabilization to a central Ramsey fringe. The main limitation of this stage is a residual Doppler and recoil effects of free atoms. For further frequency uncertainty level of  $10^{-16}$  we plan to realize a second cooling stage. Mg atoms trapping into 1D an optical lattice is the aim of our studies to reach this level of accuracy. Sub-Doppler cooling down to  $\sim 10$   $\mu$ K is an obligatory requirement for effective loading of an optical lattice The  $^3P_2 - ^3D_3$  triplet transition will be used for sub-Doppler cooling of Mg atoms. The level  $^3P_2$  of the transition is degenerate and a sub-Doppler cooling by polarization gradients is possible [13]. The theoretical analysis of sub-Doppler 1D cooling in our case[14] demonstrate that with a proper choice of a laser radiation parameters a large part (up to 60%) of atoms will be cooled down to temperature  $\sim 10$   $\mu$ K. The experimental realization of sub-Doppler cooling is in progress now.

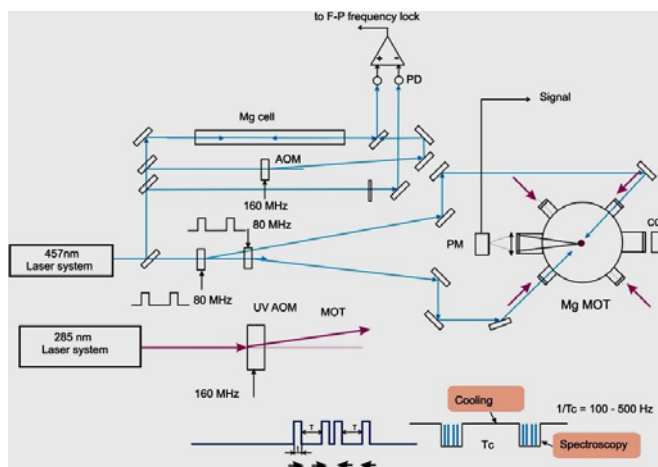


Fig. 2 Experimental setup for high precision spectroscopy of Mg atom in MOT.

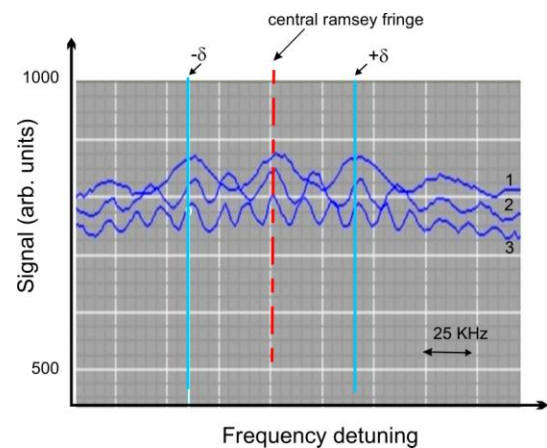


Fig.3 Ramsey fringes detected with the set of delay times  $T$  between pulses of the duration  $\tau=5$   $\mu$ s: 1-  $T=12.5$   $\mu$ s, 2- $T=25$   $\mu$ s, 3-  $T=38$   $\mu$ s. Labels  $-\delta$ ,  $+\delta$  indicate the position of the recoil components,  $\delta=39.6$  KHz.

The work is supported by the Russian Foundation for Basic Research (grants nos. 12-02-00454, 12-02-00403, 11-02-00775, 11-02-01240), by the Russian Academy of Sciences and the Presidium of Siberian Branch of Russian Academy of Sciences, by the Ministry of Education and Science of the Russian Federation in the frame of the Program “Scientific and scientific-pedagogical personnel of innovative Russia” (contract no. 16.740.11.0466 and agreement no. 8387) and the Russian Quantum Center. The young scientists D.V. Brazhnikov, A.M. Shilov also have been supported by the Presidential Grant MK-3372.2912.2 and the RFBR Grant 12-02-31208-“mol\_a”.

- [1] S. Bize *et al*, C. R. Phys. **5**, 829 (2004); T.E. Parker, Metrologia **47**, 1 (2010).
- [2] R.H. Dicke, Phys. Rev. **89**, 472 (1953).
- [3] T. Rosenband *et al*, Science **319**, 1808(2008).
- [4] H. Katori *et al*, PRL**91**, 173005 (2003).
- [5] St. Falke *et al*, Metrologia **48**, 399(2011); H. Katori, Nature Photonics **5**, 203 (2011); P. Lemonde, Eur.J. Special Topics **172**, 81(2009).
- [6] S.G. Porsev *et al*, Phys. Rev. A **74**, 020502 (2006)
- [7] A. V. Taichenachev *et al*, PRL**96**, 083001 (2006).
- [8] T.E. Mehlstäubler *et al*, J. Opt. B: Quantum Semiclass. Opt. **5** (2003) S183(2003); T.E. Mehlstäubler *et al*, Phys. Rev. A **77**, 021402 (2008); N. Rehbein, Phys. Rev. A **76**, 043406(2007).
- [9] W.C. Magno *et al*, Phys. Rev. A **67**, 043407 (2003).
- [10] M. Riedmann *et al*, Phys. Rev. A **86**, 043416 (2012).
- [11] A.N.Goncharov, Science First hand #2(23), 10(2009).
- [12] F. Ruschewitz *et al*, PRL **80**, 3173(1998).
- [13] J. Dalibard and C. Cohen-Tannoudji, J. Opt. Soc. Am. B **6**(11), 2023(1989).
- [14] D.V. Brazhnikov *et al*, Vestnik NSU, Series “Physics”, Vol. **7**, # 4, 6 (2012) [in Russian].

# Deep Laser Cooling of Thulium Atoms

N. Kolachevsky,\* D. Sukachev, E. Kalganova, G. Vishnyakova, A. Savchenkov, A. Sokolov,  
A. Akimov, V. Sorokin

*P.N. Lebedev Physical Institute of the Russian Academy of Sciences, Leninsky prosp. 53, 119991 Moscow, Russia*

*Russian Quantum Center, SKOLKOVO, Moscow region, 143025, Russia*

*\*kolik@lebedev.ru*

**Abstract:** We report on deep two-stage laser cooling and trapping of Thulium atoms. Atoms were loaded in magnetic and optical dipole traps for spectroscopy of the inner-shell transition at 1.14  $\mu\text{m}$ .

Rare-earth elements like Sm, Dy, Er, Tm attract a close interest due to their specific level structure. High magnetic moment of the ground state (up to 10 Bohr magnetons) and corresponding strong anisotropic atom-atom interactions make them favourable species for low-temperature studies. Recent experiments on Bose-Einstein condensation in Dysprosium [1] and Erbium [2] demonstrated tunable dipolar condensation using low-field Feshbach resonances. These experiments become possible due to recent successes in laser cooling and trapping of hollow-shell rare-earth elements with a rich level structure [3].

Another unique feature of hollow  $4f$ -subshell rare-earth elements is the presence of the large ground state fine splitting corresponding to different  $4f$  electronic spin states. The splitting between these states can reach hundreds of therahertz such that corresponding magnetic-dipole transitions can be excited optically. In contrast to transitions by the valence electron from the  $6s$  shell,  $f$ - $f$  transitions are strongly shielded from external electrical fields by the closed outer  $5s^2$  and  $6s^2$  shells. It makes them favorable candidates for applications in highly stable optical clocks. We propose the magnetic-dipole transition between ground state ( $4f^{13}6s^2$ ) multiplet levels  $J=7/2 \rightarrow J=5/2$  ( $J$  – the full electron momentum quantum number) at 1.14  $\mu\text{m}$  as a candidate for the stable clock transition in atomic Thulium [4].

Formerly we demonstrated laser cooling and magneto-optical trapping of Thulium atoms using the strong nearly-closed transition at 410.6 nm [5]. Up to  $10^6$  atoms were loaded in a magneto-optical trap (MOT) with the typical sub-Doppler temperature of 100  $\mu\text{K}$  using a Zeeman slower. Efficient sub-Doppler cooling (Doppler temperature for this transition equals 240  $\mu\text{K}$ ) takes place directly in the MOT because of near-degenerate Landè  $g$ -factors of cooling levels. High ground state magnetic moment of Tm enable magnetic trapping of atoms into a shallow magnetic trap with the axial field gradient of 20 G/cm. We studied the role of binary collisions in the trap containing up to  $4 \times 10^4$  spin-polarized atoms at the temperature of 40  $\mu\text{K}$ . The binary collision rate was estimated as less than  $10^{-11} \text{ cm}^3 \text{ c}^{-1}$  which is compatible with other experiments.

First stage cooling is not enough to reach microkelvin regime which is strongly desirable for efficient loading of atoms in a shallow optical dipole trap or an optical lattice. To reach such temperatures, the second-stage cooling using the weak 530.7 nm transition was implemented. We use 40 mW of the second harmonic of semiconductor laser radiation tuned to  $4f^{13}6s^2 \rightarrow 4f^{12}5d_{5/2}6s^2$  transition for the second stage cooling. The transition turned out to be very convenient for cooling: First, it corresponds to the Doppler limit of only 9  $\mu\text{K}$ , and second, the natural width is still broad enough ( $\Gamma = 300 \text{ kHz}$ ) to allow easy tuning, laser locking and loading of pre-cooled atoms in a molasses.

We have demonstrated efficient re-capture of the first-stage cooled atoms in the second-stage green MOT. The transfer efficiency approaches 100%. Since the 530.7 nm laser line width is of 1 MHz we used large red detunings of 30-50  $\Gamma$  ( $\Gamma$  - the natural line width). We reached temperature of 20  $\mu\text{K}$  in the green MOT which well corresponds to the Doppler theory. As expected, no repumper laser was necessary. The life time in the green MOT was limited by the background gas collisions indicating the absence of leak channels. To lower the temperature further, we plan to lock the laser to high-finesse optical cavity. Narrowing the laser line width to sub-kilohertz level will allow for smaller red detuning and, correspondingly, lower temperatures.

For precision spectroscopy of 1.14  $\mu\text{m}$  transition atoms should be loaded into an optical dipole trap or, preferably, an optical lattice which provides a Doppler-free Lamb-Dicke regime. To reduce photon scattering and corresponding heating we proposed far-off-resonance dipole trap (FORT) operating near 530 nm where powerful multi-watt laser sources are available. We carefully overlapped tightly focussed beam of Verdi G12 laser (Coherent) operating at 530.60 nm with the Thulium atomic cloud and observed re-capture of approximately 10% of atoms in the dipole trap (Fig.1). The trapping beam intensity of 10 W was focussed into a spot with 30  $\mu\text{m}$  waist radius which corresponds to the trap depth of 1 mK. Relatively low recapture efficiency is due to the small spatial overlap between the atomic cloud and the FORT. Although the FORT was blue-detuned from 530.7 nm resonance transition, it was still possible to trap atoms in the intensity maximum. It indicates, that the major contribution for the ground state polarizability is due to 6s electrons and should be nearly the same for both fine structure levels ( $J=7/2$ ,  $5/2$ ). The latter is very encouraging for optical clock applications and should facilitate reduction of the lattice-induced ac Stark shift. Optical trapping in crossed light beams (Fig. 1) as well as in optical lattice was demonstrated. We have also observed the dipole trap robustly operating at 532 nm in the focus of Verdi V8 (Coherent) laser.

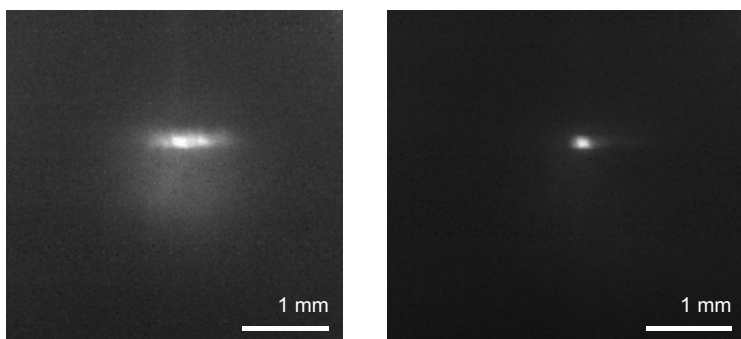


Fig. 1. Images of laser-cooled Thulium atoms trapped in an optical dipole trap at 530.6 nm at 15 ms after switching off the MOT trapping beams. Left: axial trapping in a single focused laser beam. Right: trapping in two crossed focused laser beams.

The experiments open way both for studying the 1.14  $\mu\text{m}$  clock transition and for further cooling Thulium atoms to quantum degeneracy. As next steps we plan deeper cooling of atoms in the green MOT, implementation of a shallower optical lattice and an increase of number of atoms. Ultra-stable laser system for 1.14  $\mu\text{m}$  for spectroscopy of the narrow  $J=7/2 \rightarrow J=5/2$  transition (the natural line width equals 1 Hz) is under development.

## References:

- [1] M. Lu, N.Q. Burdick, S.H. Youn, and B.L. Lev, Phys. Rev. Lett. **107**, 190401 (2011).
- [2] K. Aikawa et al., Phys. Rev. Lett. **108**, 210401 (2012).
- [3] J. J. McClelland and J. L. Hanssen, Phys. Rev. Lett. **96**, 143005 (2006).
- [4] N.N. Kolachevsky, Usp. Phys. Nauk **54**, 863–870 (2011).
- [5] D. Sukachev et al., Phys. Rev. A **82**, 011405 (2010).

# Few-Photon Spectroscopy of a Trapped Ion Through Sensitive Recoil Detection

Y. Wan, F. Gebert, B. Hemmerling<sup>§</sup>, K. Hammerer<sup>†</sup>, P. O. Schmidt

*QUEST Institute for Experimental Quantum Metrology, PTB Braunschweig and Leibniz Universität Hannover, Germany*

*<sup>§</sup>present Address: Physics Department, Harvard University, Cambridge (MA), USA*

*<sup>†</sup>Institute for Theoretical Physics, Leibniz Universität Hannover, Germany*

*Piet.Schmidt@quantummetrology.de*

**Abstract:** We present a novel spectroscopy technique for trapped ions which combines the high detection efficiency of the electron shelving technique with background-free spectroscopy of short-lived excited states.

## 1. Introduction

Precision laser spectroscopy of trapped ions typically comes in two flavors: Laser induced fluorescence of short-lived excited states and laser excitation of long-lived states followed by internal state detection via electron shelving. Whereas the latter offers detection efficiencies close to the quantum-projection noise limit, the former suffers from poor photon collection efficiency and additional noise due to stray light and dark counts. In both cases, the ion needs to provide a suitable transition for laser cooling to reduce Doppler shifts.

## 2. Photon recoil spectroscopy

We present a novel spectroscopy technique overcoming these limitations by combining the high detection efficiency of the electron shelving technique with background-free spectroscopy of short-lived excited states. This is accomplished by detecting photon recoil during laser induced fluorescence of a single ion through a co-trapped ion, which also provides sympathetic laser cooling.

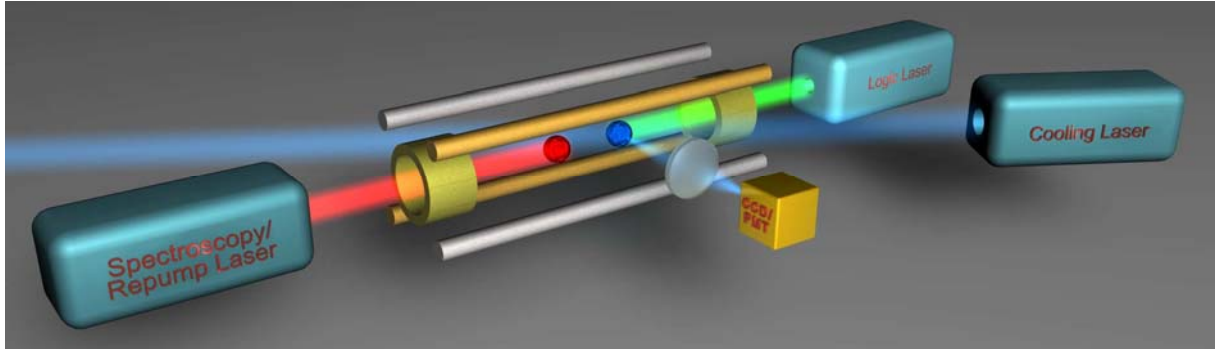


Fig. 1 Sketch of the experimental setup showing the linear Paul trap with the spectroscopy and cooling ions, the lasers and the detection system.

We trap a  $^{40}\text{Ca}^+$  spectroscopy and  $^{25}\text{Mg}^+$  cooling ion simultaneously in a linear Paul trap (see Fig. 1). Using stimulated Raman sideband pulses, we cool the ion crystal into the motional ground state of the two axial normal modes [1,2]. Photon recoil from probing the spectroscopy transition results in motional excitation of the two-ion crystal. This motional excitation is mapped onto two long-lived internal states ( $|\downarrow\rangle, |\uparrow\rangle$ ) of the cooling ion using a stimulated rapid adiabatic passage (STIRAP) pulse on a motional sideband of the cooling ion. High fidelity internal state discrimination of the cooling ion using the electron shelving technique [3] provides the spectroscopy signal (see Fig. 2).

Spectroscopy pulses on the  $\text{Ca}^+$   $S_{1/2}$ - $P_{1/2}$  transition (397 nm) are synchronized with the motion of the ions in the trap to enhance the sensitivity through resonant driving while reducing systematic frequency shifts of the technique. The branching ratio of 16:1 between the  $P_{1/2}$ - $S_{1/2}$  and  $P_{1/2}$ - $D_{3/2}$  transitions, limits the number of scattered photons in the absence of a repump laser. Using this technique, we are able to detect the scattering of around 16 photons with a SNR of 1 on the  $\text{Ca}^+$   $S_{1/2}$ - $P_{1/2}$  spectroscopy transition using a  $\text{Mg}^+$  cooling ion. Typical laser induced fluorescence spectroscopy requires more than an order of magnitude more scattered photons for the same SNR considering only photon shot noise. We present a theoretical description of the technique and discuss possibilities to further enhance its sensitivity.

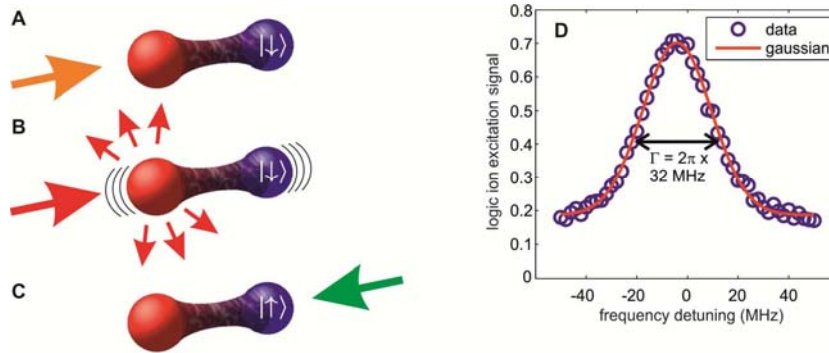


Fig. 2. Principle of photon recoil spectroscopy. (A) Off-resonant probing of the spectroscopy transition does not excite any motion. (B) Photon scattering near the resonance excites the normal motional mode of the 2-ion crystal. (C) A laser pulse maps the motional excitation to an internal state excitation of the cooling ion. (D) Excitation profile of the cooling ion after the motional mapping pulse as a function of spectroscopy laser detuning.

We have performed an absolute frequency measurement by scanning the spectroscopy laser (referenced to PTB's Cs fountain clocks) across the  $\text{Ca}^+ S_{1/2}\text{-}P_{1/2}$  resonance. To allow scattering of more than 16 photons and thus enhance the signal strength, the spectroscopy pulses are interleaved with repump pulses on the  $P_{1/2}\text{-}D_{3/2}$  transition. This allows us to resolve the center of the resonance line to better than 1 part in 100, corresponding to less than 200 kHz. This is an improvement by more than an order of magnitude over previous results using  $\sim 100$   $\text{Ca}^+$  ions [4]. We present results of this absolute frequency measurement, including a discussion of systematic frequency shifts and a comparison with laser induced fluorescence spectroscopy.

### 3. Perspectives

The presented spectroscopy technique is an extension of the quantum logic spectroscopy technique implemented for the aluminum clock [5, 6] to broad spectroscopy transitions. Sympathetic cooling through the cooling ion enables high precision spectroscopy of ion species that do not possess a suitable transition for laser cooling. Furthermore, the large SNR per scattered photon with only a single ion makes this spectroscopy technique particularly useful if either the number of scattered photons or the number of atoms is a valuable resource. Possible applications include spectroscopy of rare isotopes and atoms or molecules with a complex level structure that do not possess fully closed cycling transitions, limiting the number of scattered photons.

### 4. References:

- [1] D. J. Larson, J. C. Bergquist, J. J. Bollinger, W. M. Itano, and D. J. Wineland, *Phys. Rev. Lett.* **57**, 70 (1986).
- [2] B. Hemmerling, F. Gebert, Y. Wan, D. Nigg, I. V. Sherstov, and P. O. Schmidt, *Appl. Phys. B* **104**, 583–590 (2011).
- [3] B. Hemmerling, F. Gebert, Y. Wan, and P. O. Schmidt, *New J. Phys.* **14**, 023043 (2012).
- [4] A. Wolf, S. van den Berg, C. Gohle, E. Salumbides, W. Ubachs, and K. Eikema, *Phys. Rev. A* **78**, 032511 (2008).
- [5] P. O. Schmidt, T. Rosenband, C. Langer, W. M. Itano, J. C. Bergquist, and D. J. Wineland, *Science* **309**, 749–752 (2005).
- [6] T. Rosenband, D. B. Hume, P. O. Schmidt, C. W. Chou, A. Brusch, L. Lorini, W. H. Oskay, R. E. Drullinger, T. M. Fortier, J. E. Stalnaker, S. A. Diddams, W. C. Swann, N. R. Newbury, W. M. Itano, D. J. Wineland, and J. C. Bergquist, *Science* **319**, 1808–1812 (2008).

# Optical control of coherent and squeezed phonons: major differences and similarities

Misochko O.V.

*Institute of Solid State Physics, Russian Academy of Sciences*

*142432 Chernogolovka, Russia*

*misochko@issp.ac.ru*

Coherent and squeezed phonon oscillations can be excited in solids impulsively by a single femtosecond pulse whose duration is shorter than a phonon period. By applying the second ultrafast pump pulse these oscillations can be significantly, but differently modified.

Progress in femtosecond lasers and ultrafast spectroscopy has enabled us to generate and observe the coherent and squeezed lattice oscillations in which atomic motions are excited with light through a nonlinear process and the resulting dynamics is directly observed in the time domain [1]. The process of generation of coherent and squeezed phonons by using ultrashort light pulses has provided a unique tool for time-domain studies of optical and acoustic modes and their coupling to electronic and other excitations in solids. To date such phonons have been observed in time-resolved optical pump-probe experiments as periodic modulations of reflectivity or transmission with increasing attention being turned towards not only observation but also understanding of physics which occurs at this short time scale. The coherent control of these phonons is one of the key issues in femtosecond technology. Such control is enabled by the full knowledge of the dynamics of crystal lattice concerning its amplitude and phase. It is due to the existence of a well-defined phase, phonons generated by an ultrafast pulse can be easily manipulated. Thus, providing well-defined quanta of energy in a well-defined temporal sequence, the lattice can be driven into an artificial quantum-mechanical state, which cannot be achieved by other means of optical excitation. Although interference due to which such control is achieved is intrinsically a classical phenomenon, the superposition principle which underlies it is also at the heart of quantum mechanics. Indeed, in some interference experiments we encounter the idea of quantum entanglement, which became clear after the famous paper by Einstein, Podolsky and Rosen singled out some startling features of the quantum mechanics. Schrödinger emphasized that these unusual features are due to the existence of what he called "entangled states", which are two-particle states that cannot be factored into products of two single-particle states in any representation. "Entanglement" is just Schrödinger's name for superposition in a composite system. Therefore, in this work we have attempted to compare coherent control of one- (coherent) and two-

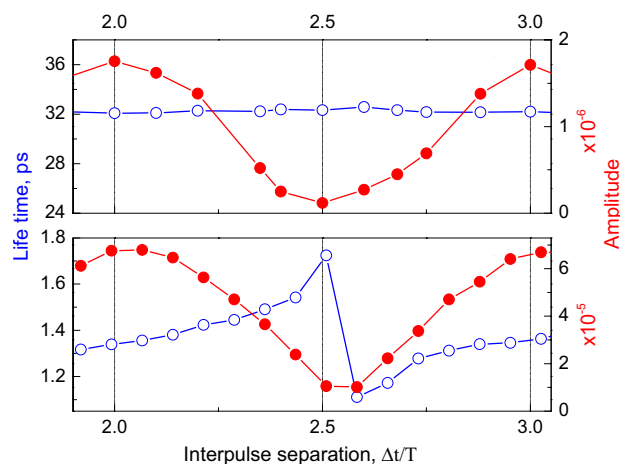


Fig.1. Lifetime (open symbols, left scale) and amplitude (filled symbols, right scale) as a function of control parameter for coherent phonons in Bi (top) and squeezed biphonons in ZnTe (bottom).

phonon (squeezed) lattice states created by ultrafast laser pulse. In particular, we report on the control of coherent  $A_{1g}$  optical phonons in Bi and of squeezed acoustical biphonons in ZnTe using two pump pulse technique.

To study the optical control over coherent phonons, we performed two pump–single probe reflectivity experiments on Bi crystal at helium temperature. It was observed that the reflectivity oscillations due to coherent  $A_{1g}$  phonons can be modified by a second pump pulse [2]. Namely, a time delay of  $nT$  between the two pump pulses, where  $n$  is an integer and  $T=331\text{fs}$  is the phonon period, resulted in enhancement while a time delay of  $(n+1/2)T$  resulted in cancellation of the oscillations, see Fig.1. Even though there was a singularity in the phase behavior at  $(n+1/2)T$ , lifetime of the coherent phonons was unaffected by the second pump pulse, as shown in Fig.1. The latter is compatible with the results of passive control [4] at low excitation strength, where the coherent amplitude grows linearly, while the lifetime remains unchanged for the pump fluences not exceeding  $100\mu\text{J}/\text{cm}^2$ . Given that the  $A_{1g}$  coherent phonons in bismuth are driven by photoexcited carriers (displacive mechanism), the process of coherent control can be thought of in the following way: The first pump pulse creates a new potential surface on which the atoms move. Initially displaced from the newly established equilibrium configuration, the lattice achieves this configuration in approximately one quarter of a phonon period, but the atoms have momentum at that point. When the atoms reach the classical turning point of their motion, a second pump pulse can excite the precise density of carriers to shift the equilibrium position to the current position of the atoms, stopping the oscillatory motion. Because photoexcitation of additional electrons can displace the potential only in one direction, the vibrations can only be stopped at one of the classical turning points.

Having discussed the first-order control of lattice displacements, in which we manipulate interatomic separations, next we turned to second-order control. When ultrafast laser pulse strikes a crystal with van Hove singularity in the phonon density of states, it creates a pair of correlated acoustic phonons running in opposite directions. As a result, the atomic fluctuations in either position or momentum become squeezed below the vacuum level for a quarter of the oscillatory cycle. Because of a correlated behaviour (annihilation operator of one half of the pair is correlated/anticorrelated to creation/annihilation operator of the other half), both halves interfere destructively resulting in two-phonon coherence and a zero net population for the one-phonon mode. Thus, following the impulsive optical excitation, which macroscopically excites lattice vibrations, the transmission in ZnTe starts to oscillate [3]. The oscillation lifetime and frequency at room temperature are 1.4 ps and 3.67 THz, the latter being close to but slightly higher than that of  $2TA(X)$  overtone. Coherent amplification and suppression of the two-phonon oscillations is achieved by two-pump, single-probe technique which, in this case, is an acoustical analogue of two-photon interference for parametrically downconverted photons. Here instead of overlapping pair-correlated photons, we overlap two ensembles of pair-correlated phonons created at different times. The whole control process can be described as the sum of two ensembles of phonons whose motion was initiated at different times and that now interfere. The relative timing of pump pulses determines whether the oscillations add constructively or destructively. As shown in Fig.1, depending on the interpulse separation, the lifetime, as well as the amplitude of two-phonon oscillations, is modulated. The modulation of lifetime, which was absent for coherent phonons, suggests that we are dealing with quantum interference as for its classical counterpart the change of lifetime is impossible: classical coherent states are always transformed into different coherent states. It should be noted that the change of amplitude can be either correlated or anti-correlated to that of life time. The two-phonon amplitude scales with the real part of squeeze parameter, whereas the oscillation lifetime measures how long the constituents of two-phonon state are correlated, or entangled: the longer the time, the stronger the entanglement [3]. Naively, one might think that a larger squeezing results in a stronger entanglement since quantum entanglement is closely related to quantum squeezing. However, as follows from the data presented in Fig.1, the extreme life times come about near *minimum* of the amplitudes, or when the sign of resulting biphonon amplitude changes from positive to negative. Moreover, the decrease in lifetime occurs over a shorter time scale as compared to its increase. This suggests that the relationship between phonon squeezing and entanglement may be more complicated because these effects are of different orders. The squeezing is the second order effect relying on the amplitude-amplitude correlations controlled by one-phonon interference. The entanglement, in contrast, belongs to a class of the forth order effects governed by intensity-intensity correlations (the same class as bunching/anibunching phenomena dictated by field statistics).

In conclusion, we have demonstrated that coherent and squeezed phonon oscillations can be excited in solids impulsively by a single femtosecond pulse whose duration is shorter than a phonon period. By applying the second ultrafast pump pulse these oscillations can be significantly, but differently modified. Thus, the ultrafast laser pulses provide a flexible and powerful tool not only to create and observe but also to control phonon amplitude, squeezing and entanglement. First-order control allows manipulating interatomic separations, whereas second-order control provides the possibility to modify uncertainty contours for the lattice atoms keeping their separations intact.

1. K. Ishioka, and O.V. Misochko, in Progress in Ultrafast Intense Laser Science V, Eds. K.Yamanouchi, A. Giullietti, and K. Ledingham, 23-64, Springer Series in Chemical Physics, Berlin (2010).
2. O.V. Misochko, and M.V. Lebedev, JETP Letters **90**, 284 (2009).
3. O.V. Misochko, J. Hu, and K.G. Nakamura, Physics Letters A 375, 4141 (2011).
4. O.V. Misochko, and M.V. Lebedev, JETP 109, 805 (2009).

# Electromagnetic Coupling of Atoms with Nanostructures: Modification of Atomic States and Excitation of Optical Modes

V. G. Minogin

*Institute of Spectroscopy Russ. Ac. of Sci., Fizicheskaya st. 5, 142190 Troitsk, Moscow  
minogin@isan.troitsk.ru*

**Abstract:** We describe radiative decay rates of the excited atoms into dielectric nanostructures, shifts of the atomic energy states and the shape of the laser-excited fluorescence line for the atoms located near nanostructures.

Over the past decade there has been an increasing interest in the interactions between optically excited atoms and dielectric nanostructures, such as optical nanofibers, nanospheres and nanodisks. On one hand, this is mostly due to the potential such systems offer for controlling and manipulating single atoms and, on the other hand, due to the potential the systems can offer for controlling the light propagating inside the optical nanostructures. From somewhat more general point of view optical nanostructures can be considered as interfaces allowing one to connect the atoms located near nanostructures with the electromagnetic fields propagating inside the nanostructures and accordingly control the states of both the atoms and photons guided inside the nanostructures [1-5].

In this paper, we describe basic spectroscopic features of the electromagnetic coupling of atoms with nanostructures: modified radiative decay rates into nanostructures, shifts of atomic levels due to the Van der Waals or Casimir-Polder interaction of atoms with nanostructures and asymmetric shapes of the spontaneous emission lines for the atoms located near nanostructures.

First, we analyze spontaneous decay of the excited states of an atom located inside hollow nanocylinder (Fig. 1a) or near nanofiber (Fig. 1b) and corresponding excitation of the guided optical modes of a nanostructure. This analysis is based on the Hamiltonian for a system “two-level atom+vacuum field”. In case of a nanofiber, considering probability amplitudes for the states which include the internal atomic states and the states of the vacuum field in the optical nanofiber we derive the spontaneous decay rates into the guided modes with a specific propagation direction and specific polarization. As an example Fig. 2 shows spontaneous decay rate of a two-level atom into the lowest guided modes including modes  $HE_{11}$  (solid line),  $TE_{01}$  (dotted line),  $TM_{01}$  (dashed line) and fundamental mode  $HE_{21}$  (dot-dashed line) as a function of a distance between the atom and the axis of the optical nanofiber with core refractive index  $n_1 = 1.45$  and radius  $a=450$  nm. Emission wavelength  $\lambda=780$  nm is taken for 5S-5P dipole transition in  $^{85}\text{Rb}$  atom. Decay rate  $W_{\text{guid}}$  is normalized on the decay rate  $W_0$  for free space. According to Fig. 2 excitation efficiency of the lowest optical modes of a nanofiber pumped by spontaneous emission can differ by 2 orders of magnitude.

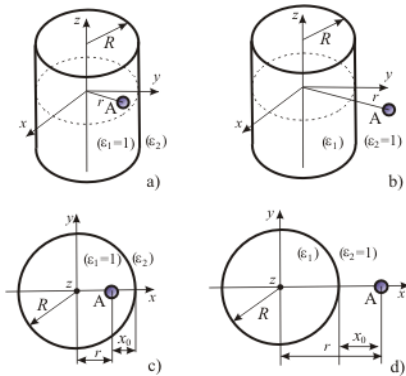


Figure 1

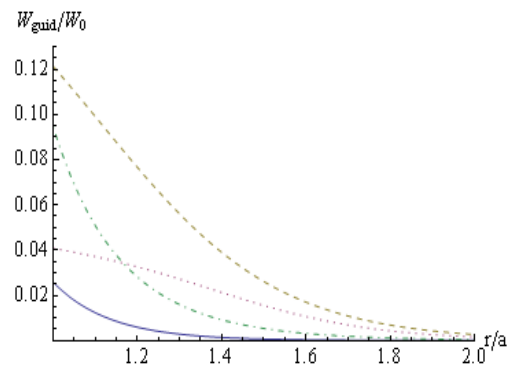


Figure 2

Next, we consider shifts of the atomic energy levels due to the Van der Waals and Casimir-Polder interaction of an atom with concave or convex nanocylinder (Fig. 1a,b) and concave or convex nanosphere (Fig. 1c,d). Basically, we evaluate the effect of the surface curvature on the strength of the van der Waals interaction by considering, in the electrostatic approximation, the interaction of a ground-state atom with a metal or dielectric nanocylinder or nanosphere. We consider two cases: (i) the atom is surrounded by a spherical metal or dielectric medium, i.e. a concave surface and (ii) the atom interacts with the outer surface of the metal or dielectric

nanosphere, i.e. a convex surface. For the validity of the electrostatic approximation we assume that both the radius,  $R$ , of the nanosphere and the distance,  $x_0$ , between the atom and the surface satisfy the condition  $R, x_0 \leq \lambda/2\pi \approx 100$  nm, where  $\lambda$  is a characteristic optical wavelength defined by the lowest optical transition of the atom. We derive closed analytical expressions for the Van der Waals interaction energy for both these cases and compare it with that obtained for a flat surface. These estimations, presented in simple closed form, are useful for a comparison between theoretical predictions and experimental measurements of the Van der Waals constant,  $C_3$ , and for evaluation of the strength of the Van der Waals interaction in experiments dealing with the control of cold atomic clouds or slow atomic beams located at, or propagating near, curved surfaces. As an example, Fig. 3 shows the van der Waals interaction energy for a concave surface (dashed line), flat surface (solid line) and convex surface (dotted line) as a function of the atom's distance from the surface,  $x_0$ . The distance from the surface is normalized to the radius of the sphere,  $R$ , and the interaction energy is normalized to the energy  $U_R = C_3/R^3$ . Figure 4 shows dependence of the spherical surface factors, defined by the equation  $U = -(C_3/x_0^3)\mu$ , on the distance  $x_0$  between the atom and the spherical surface. This figure shows that the difference between surface factors for a concave shaped surface (dashed line) and a convex shaped surface (dotted line) can be as high as 6.

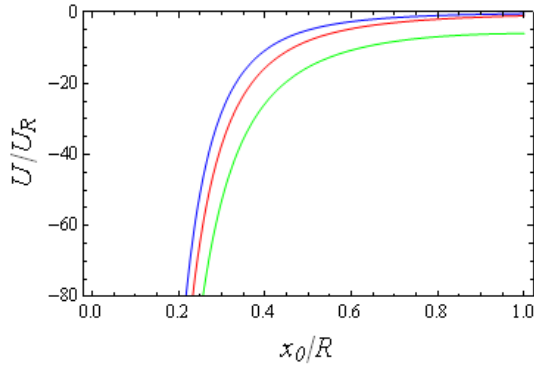


Figure 3

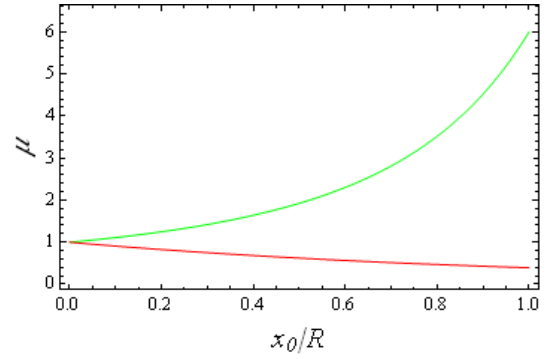


Figure 4

Finally, we discuss the shape of the fluorescence line emitted by optically excited atoms near nanostructures. Specifically, we show that Van der Waals interaction of atoms with the surface of an optical nanofiber can produce well-pronounced asymmetry in the frequency dependence of spontaneous emission coupled into the guided mode of an optical nanofiber. As an example Fig. 5 shows frequency dependence of the spontaneous emission power from  $^{85}\text{Rb}$  cloud coupled into the optical nanofiber with core radius  $a=200$  nm and atomic cloud radius  $R=400$  nm (solid line) and 1000 nm (dashed line). The dotted line shows, for comparison, the lineshape for the artificial case where the Van der Waals shift is absent. This example shows that interaction of the atoms with the surface of the optical nanofiber causes the asymmetry of the lineshapes with well pronounced redshifts.

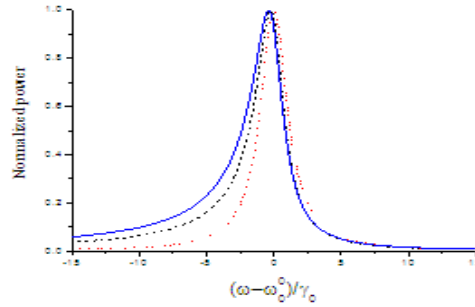


Figure 5

In conclusion, results from our study show that interaction of atoms with nanostructures can considerably alter radiative decay rates of excited atomic states, produce considerable shifts of atomic levels and modify shapes of the atomic spectral lines. All this can be important in experiments on manipulating cold atoms both freely moving and confined near nanostructures. In particular, measurement of the lineshape of the coupled fluorescence could be used to characterize the strength of the interaction of atoms with dielectric surfaces and for detection of atoms using nanofibers.

This work was supported in part by Russian Foundation for Basic Research, Project No. 12-02-00867-a.

1. H. Nha and W. Jhe, Phys. Rev. A 56, 2213 (1997).
2. T. Søndergaard and B. Tromborg, Phys. Rev. A 64, 033812 (2001).
3. V. V. Klimov and M. Ducloy, Phys. Rev. A 69, 013812 (2004).
4. F. Le Kien et al., Phys. Rev. A 72, 032509 (2005).
5. L. Russell et al., J. Phys. B 42, 185006 (2009).

# Generalized Ramsey Method in Precision Spectroscopy of Ultracold Atoms and Ions

K. S. Tabatchikova, A. V. Taichenachev, V. I. Yudin

*Institute of Laser Physics SB RAS, Ac. Lavrentyev Prospect, 13/3, Novosibirsk, 630090 Russia*

*Novosibirsk State Technical University, K. Marksa Prospect, 20, Novosibirsk, 630073, Russia*

*Novosibirsk State University, Pirogova Street, 2, Novosibirsk, 630090, Russia*

*k.tabatchikova@gmail.com*

**Abstract:** We analyze the Hyper-Ramsey excitation scheme with account for the spontaneous relaxation of atomic levels and finite width of laser line. It is shown that for efficient cancelation of the light shift both effects should be considered.

Presently, laser spectroscopy and fundamental metrology are among the most important and actively developed directions in modern physics. Ramsey's method of separated oscillatory fields was crucial for the progress in precision spectroscopy and the development of atomic clocks [1] and is an important tool in quantum information processing [2]. In the case of optical spectroscopy the high probe light intensities required to drive these transitions will unavoidably lead to level shifts through the dynamical Stark effect. This so-called light shift appears through the nonresonant coupling to other energy levels by the probe light and is usually proportional to its intensity.

Several methods were investigated to compensate this shift, for example, linear extrapolation to zero intensity or the use of an additional inversely shifting field [3]. Nevertheless, a wide range of precise frequency measurements presently suffer from significant uncertainties due to light shift. Here, two-photon [4], higher order multipole [5,6], and magnetic-field induced transitions [7,8] are good examples. In work [9] a generalized Ramsey excitation scheme recently proposed by Yudin et al. (fig. 1), which cancels the light shift and efficiently suppresses the sensitivity of the spectroscopic signal to variations of the probe light intensity. The dominating dependence of signal frequency shift on atomic transition shift is cubic on certain ratio of pulse durations. First experiments on a laser-cooled single  $^{171}\text{Yb}$  ion corroborated high efficiency of given method [10].

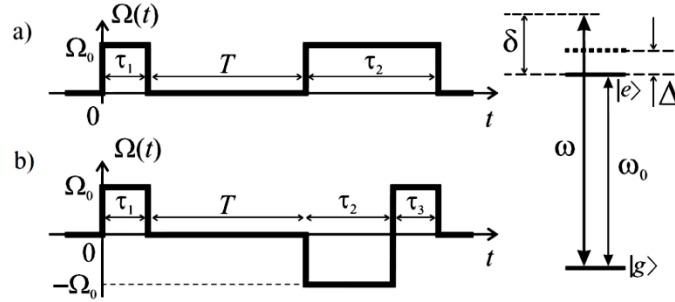


Fig. 1. Ramsey pulses with Rabi frequency  $\Omega_0$  of different duration  $\tau_1$ ,  $\tau_2$  and  $\tau_3$  and with phase step in the second pulse.

Also shown is a two-level atom with splitting  $\omega_0$ , detuning  $\delta$  of the laser with frequency  $\omega$  during dark time  $T$  and excitation-related shift  $\Delta$  during pulses.

In work [9] authors consider idealized case, which ignores spontaneous relaxation of atomic level and finite width of laser line. In this work we investigate the proposed scheme (fig. 1) with account for the spontaneous relaxation of atomic levels and finite width of laser line. The analysis is executed by numerical solution of system of quantum kinetic equations.

Theoretical analysis of excitation scheme indicates that the suppression efficiency of the field shift diminishes for scheme represented on figure 1a in the presence of typical experimental Rabi frequency fluctuation. The phase step in the second pulse (fig. 1b) provides the robust suppression of the field shift.

Therefore, we consider the scheme presented in figure 1b. Suppose that the spontaneous relaxation of atomic levels and the width of laser line are equal to zero. In this case, the effective suppression of the field shift and maximum amplitude of resonance are achieved when  $\Omega_0\tau_1 = \pi/2$ ,  $\Omega_0\tau_2 = \pi$  and  $\Omega_0\tau_3 = \pi/2$ . Dependence of signal frequency shift on atomic transition shift for calculated value is represented in figure 2a (solid line). The analogous dependence for calculated value of pulse durations has form represented on figure 2a (dashed line) when spontaneous relaxation of atomic level and finite width of laser line are taken into account. Influences of the spontaneous relaxation of atomic level and finite width of laser line lead to significant decrease of field shift suppression efficiency.

Further, we calculate optimal values of pulse durations canceling the field shift when spontaneous relaxation of atomic level and finite width of laser line are taken into account. Dependence of signal frequency shift on atomic transition shift is represented on figure 2b. When comparing dependences (fig. 2a,b) we summarize that spontaneous relaxation of atomic level and finite width of laser line must be considered. Spontaneous relaxation for forbidden transition is insignificant, so spectral line width has major influence on calculation results.

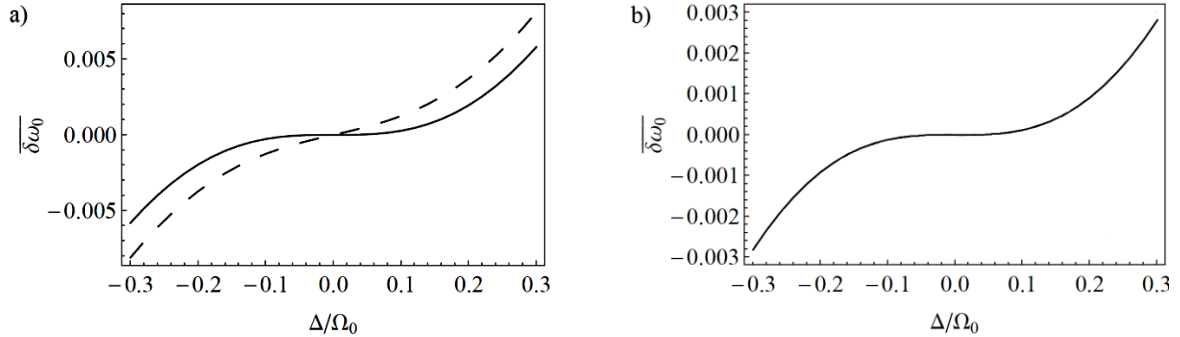


Fig. 2. Dependence of signal frequency shift on atomic transition shift a)  $\Omega_0\tau_1 = \pi/2$ ,  $\Omega_0\tau_2 = \pi$  and  $\Omega_0\tau_3 = \pi/2$  to both case b) for optimal pulses  $\Omega_0\tau_1 = 1.6$ ,  $\Omega_0\tau_2 = 3.25$  and  $\Omega_0\tau_3 = 1.65$  in the presence spontaneous relaxation of atomic level  $\gamma/\Omega_0 = 0.01$  and the finite width of laser line  $\gamma_d/\Omega_0 = 0.01$ .

Thus, the theoretical analysis of the Ramsey scheme with pulses of different duration and with a phase step in the second pulse with account for the spontaneous relaxation of atomic level and the finite width of laser line. We define optimum features of pulses that correspond to maximum suppression of the field shift and maximum amplitude of resonance for both schemes. Ramsey scheme with a phase step in the second pulse provides effective suppression of the field shift and it is less sensitive to the Rabi frequency fluctuations in comparison with Ramsey scheme with pulses of different duration.

The work is supported by the Ministry of Education and Science of the Russian Federation in the frame of the Program “Scientific and scientific-pedagogical personnel of innovative Russia” (contract no. 16.740.11.0466 and agreement no. 8387), by the Russian Foundation for Basic Research (grants nos. 12-02-00454, 12-02-00403, 11-02-00775, 11-02-01240), by the Russian Academy of Sciences and the Presidium of Siberian Branch of Russian Academy of Sciences, and the Russian Quantum Center. The young scientist K.S. Tabatchikova is supported by the Presidential Grant MK-3372.2912.2 and the RFBR Grant 12-02-31208-“mol\_a”.

- [1] N. F. Ramsey, “Experiments with separated oscillatory fields and hydrogen masers,” *Rev. Mod. Phys.* **62**, 541-552 (1990).
- [2] H. Häffner, “Quantum computing with trapped ions,” C. Roos, and R. Blatt, *Phys. Rep.* **469**, 155-203 (2008).
- [3] H. Häffner, S. Gulde, M. Riebe, G. Lancaster, C. Becher, J. Eschner, F. Schmidt-Kaler, and R. Blatt, “Precision measurement and compensation of optical Stark shifts for an ion-trap quantum processor,” *Phys. Rev. Lett.* **90**, 143602 (2003).
- [4] C. G. Parthey, A. Matveev, J. Alnis, B. Bernhardt, A. Beyer, R. Holzwarth, A. Maistrou, R. Pohl, K. Predehl, T. Udem, T. Wilken, N. Kolachevsky, M. Abgrall, D. Rovera, C. Salomon, P. Laurent, and T.W. Hänsch, “Improved measurement of the Hydrogen  $1S-2S$  transition frequency,” *Phys. Rev. Lett.* **107**, 203001 (2011).
- [5] S. A. King, R. M. Godun, S. A. Webster, H. S. Margolis, L. A. M. Johnson, K. Szymaniec, P. E. G. Baird, and P. Gill, “Absolute frequency measurement of the  $^2S_{1/2} - ^2F_{7/2}$  electric octupole transition in a single ion of  $^{171}\text{Yb}^+$  with 10-15 fractional uncertainty,” *New J. Phys.* **14**, 013045 (2012).
- [6] N. Huntemann, M. Okhapkin, B. Lipphardt, S. Weyers, Chr. Tamm, and E. Peik, “High-accuracy optical clock based on the octupole transition in  $^{171}\text{Yb}^+$ ,” *Phys. Rev. Lett.* **108**, 090801 (2012).
- [7] A.V. Taichenachev, V. I. Yudin, C.W. Oates, C.W. Hoyt, Z.W. Barber, and L. Hollberg, “Magnetic field-induced spectroscopy of forbidden optical transitions with application to lattice-based optical atomic clocks,” *Phys. Rev. Lett.* **96**, 083001 (2006).
- [8] T. Akatsuka, M. Takamoto, and H. Katori, “Three-dimensional optical lattice clock with bosonic  $^{88}\text{Sr}$  atoms,” *Phys. Rev. A* **81**, 023402 (2010).
- [9] V. I. Yudin, A.V. Taichenachev, C.W. Oates, Z.W. Barber, N. D. Lemke, A. D. Ludlow, U. Sterr, C. Lisdat, and F. Riehle, “Hyper-Ramsey spectroscopy of optical clock transitions,” *Phys. Rev. A* **82**, 011804(R) (2010).
- [10] N. Huntemann, B. Lipphardt, M. Okhapkin, Chr. Tamm, E. Peik, A.V. Taichenachev, V. I. Yudin, “Generalized Ramsey excitation scheme with suppressed light shift,” *Phys. Rev. Lett.* **109**, 213002 (2012).

# Atomic slower *via* dispersive optical interactions

M. Hamamda, M. Boustimi\*, F. Correia, J. Baudon, T. Taillandier-Loize, G. Dutier,  
F. Perales and M. Ducloy

Laboratoire de Physique des Lasers, CNRS-UMR 7538, Université Paris 13  
99, Avenue J.B. Clément, 93430-Villetaneuse, France

(\*)Department of Physics, Umm Al-Qura University, Makkah, Saudi Arabia  
Corresponding author: [jacques.baudon@univ-paris13.fr](mailto:jacques.baudon@univ-paris13.fr)

**Abstract:** The dispersive interaction of atoms with optical potential pulses generated by a time-modulated standing wave lowers the velocity from several hundreds m/s down to almost zero, over a path shorter than 20 cm.

A well-known method to slow down alkalis or rare-gas metastable atoms, in most cases in view of trapping them, is to use a so-called *Zeeman slower* [1]. This slower is based on the radiation pressure exerted on an atom beam, by a counter-propagating light beam, the velocity-dependent frequency tuning being controlled thanks to a spatially inhomogeneous magnetic field. This slower works satisfactorily for what concerns the access to low velocities and trapping, but it has the disadvantage to produce poorly collimated beams of slow atoms (angular aperture of 0.1 rad, velocity dispersion of a few 10%) because of spontaneous emission. We propose here to use the *dispersive* interaction of atoms with “co-moving” optical pulses generated *via* far-off resonance time-modulated standing waves. In this approach, each optical pulse reduces the atomic velocity by a small amount. Repeating the process thousand of times, the velocity can be lowered from several hundreds m/s down to nearly zero, over a very short path of a few tens of cm. Because of the absence of random recoil processes, the initial characteristics of the atomic beam as angular aperture, velocity dispersion, etc. should be preserved. One indeed shows that at the end of the slowing process the phase space density is maintained, contrary to what happens in free space propagation due to vacuum dispersion. In “adiabatic slowing” [2, 3] methods, an external magnetic or electric field, periodic in space, is pulsed in time in such a way that the atom (or molecule) experiences a slowing gradient and nothing else. Low final velocities (a few 10 m/s) are accessible, but at the price of rather strong fields (*e.g.* B = 5.2 T in ref. [4]).

In the method proposed here, the nature of the force is quite different, since it derives from a special potential depending on both space and time, so-called “comoving” potential, of the form [5]:  $V(x, t) = S(t) \cos[2\pi x/\Lambda]$ , where  $S(t)$  is a limited-range ( $[0, \tau_1]$ ) function of time, *e.g.*  $S(t)\exp(-t/\tau)$ , and  $\Lambda$  a spatial period. Experimental demonstration of this kind of forces acting on atoms has been achieved on metastable hydrogen in a Stern-Gerlach interferometer [6]. This potential transforms the initial atomic wave function (for a given value of  $k$ )  $\psi_0$  into  $\psi = \exp[i\varphi(k, t)]\psi_0$ , where the phase shift, in the WKB approximation, is given by

$$\varphi(k, t) = -\hbar^{-1} \int_0^{(t)} dt' S(t') \cos[2\pi\hbar k t'/(m\Lambda)] - \hbar^{-1} S(\tau_1) \Theta(t - \tau_1) (t - \tau_1) \cos[2\pi\hbar k \tau_1/(m\Lambda)] \quad (1)$$

$\hbar k$  is the momentum along  $x$ ,  $m$  the atomic mass,  $(t) = \min\{t, \tau_1\}$ ,  $\Theta$  is the Heaviside function. The centre motion of a synchronized wave packet is altered: the group velocity becomes  $v = k_0/m - [\partial_t \partial_k \varphi]_{k_0}$ ,  $k_0$  being the central momentum. This effect has been theoretically investigated at low velocities with metastable argon atoms  $\text{Ar}^*(^3P_2)$  to create *de facto* a negative-index “meta-medium” for matter waves [7]. It should be noted that in general, the total energy is not conserved. In particular, for pulses of a short duration, the final velocity is smaller than the initial one. This is the basic idea to conceive our slower.

For our purpose, the use of co-moving optical potentials in place of conventional magnetic or electric potentials provides us with a spatial period reduced by a huge factor ( $\sim 10^3$ ) relatively to values (a few mm) used with standard fields [8]. In principle such a potential is generated by a linearly polarized, far off-resonance standing light wave modulated in time and generated inside an interferometer. For a Rabi frequency  $\Omega$  and a sufficiently large detuning  $\delta\omega$  with respect to the atomic frequency  $\omega_0$ , the optical potential takes the simple form [9 - 11]:

$$V_{\text{opt}}(t, x) = \frac{\hbar\Omega^2}{2\delta\omega} \exp(-t/\tau) [1 + \cos(4\pi x/\lambda_{\text{opt}})] \quad (2)$$

where  $\lambda_{\text{opt}}$  is the optical wavelength. In order to operate “far from resonance”, to avoid spontaneous emission, we need that the difference between the laser frequency and the frequencies of the two Doppler-shifted resonances

$(\omega_0 \pm \Delta\omega)$  be large compared to the power-broadened line width. Actually, we have in view to get a magnitude  $S(0)$  of the potential, sufficiently high to achieve the complete slowing over a distance shorter than *e.g.* 20 cm. To use a reasonable laser power, we shall take a moderately large negative detuning  $\delta\omega = \omega_L - \omega_0 = -5 \Delta\omega(560) = 2\pi \cdot 3.45 \cdot 10^9$  rd/s (3.45 GHz). For the simulation, one assumes a laser intensity of 32 mW/mm<sup>2</sup>. Then the saturation parameter  $s = I / I_{\text{sat}}$ , with  $I_{\text{sat}} = 14$  W/m<sup>2</sup>, is equal to 2267.3. The natural width of the transition being  $\gamma = 2\pi \cdot 5.8 \cdot 10^6$  rd/s, the power-broadened width is  $\gamma' = 2\pi \cdot 2.762 \cdot 10^8$  rd/s, which leads to a ratio  $R = \delta\omega / \gamma' = 12.49$ , large compared to 1. As the velocity  $v$  is lowered,  $\Delta\omega$  decreases, tending to zero at  $v = 0$ . Then either  $\delta\omega$  is kept constant and the condition  $R \gg 1$  is better and better verified, or  $\delta\omega$  is kept equal to  $5 \Delta\omega(v)$  allowing us to reduce the intensity (as  $v$ ) as well as  $\gamma'$  (as  $v^{1/2}$ ), but then the ratio  $R$  decreases as  $v^{1/2}$ , which implies a lower limit for  $v$  ( $R = 1$  at  $v = 3.59$  m/s).

A series of many pulses separated from each other by a small amount of time is applied, each of them (numbered  $n$ ) providing a small decrease  $\delta v(n)$  of the velocity (a few mm/s). The duration  $\tau_1(n)$  of each pulse is adjusted in such a way that the first maximum value of  $|\delta v|$  is reached at the end of the pulse. The path  $v \tau_1$  covered by the atom during successive pulses is roughly a constant ( $\approx 0.12$   $\mu\text{m}$ ).  $|\delta v|$  increases quasi exponentially from 0.2 mm/s at  $v = 560$  m/s to 2.9 mm/s at  $v \approx 0$ . To get a complete stopping, a large number of pulses, namely  $N = 1987500$ , is needed (see figure 1). Nevertheless this does not mean a very long distance since the velocity is lowered from 560 m/s down to “zero” (*cf.* the limits defined previously) over a distance of about 19.3 cm, shorter than that needed in a Zeeman slower. It is worth to note that the density in phase space of the slowed beam,  $\rho = (\delta k \delta x)^{-1}$ , first decrease then increase up to its initial value. This is an important property for atom optics.

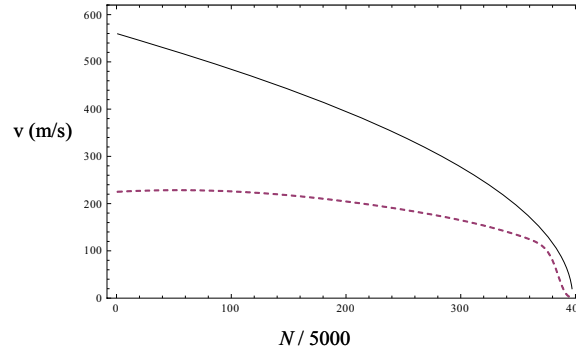


Fig. 1. Full line: velocity as a function of the pulse number  $N$  ;  
dashed line: statistical velocity width ( $\times 100$ )

## References

- [1] W.D. Phillips and H.J. Metcalf, Phys. Rev. Lett. **48** (9), 596 (1982)
- [2] H.L. Bethlem, F.M.H. Crompvoets, R.T. Jongma, S.Y.T. van de Meerakker, G. Meijer, Phys. Rev. A, **65**, 053416 (2002)
- [3] H.L. Bethlem, G. Berden, G. Meijer, Phys. Rev. Lett. **83**, 1558 (1999)
- [4] E. Narevicius, A. Libson, Ch. G. Parthey, I. Chavez, J. Narevicius, U. Even and M. G. Raizen, Phys. Rev. Lett. **100**, 093003 (2008)
- [5] R. Mathevet, K. Brodsky, J.B. Lawson-Daku, Ch. Miniatura, J. Robert, J. Baudon, Phys.Rev.A **56** (4), 2954 (1998)
- [6] K. Brodsky, R. Mathevet, B. J. Lawson-Daku, J. Baudon and J. Robert, Europhys. Lett. **44**, 137 (1998)
- [7] J. Baudon, M. Hamamda, J. Grucker, M. Boustimi, F. Perales, G. Dutier, M. Ducloy, Phys. Rev. Lett. **102**, 140403 (2009)
- [8] M. Hamamda *et al.* Phys. Rev. A **85**, 023417 (2012)
- [9] M. Partlow, X. Miao, J. Bochmann, M. Cashen, H. Metcalf, Phys. Rev. Lett. **93**, 213004 (2004)
- [10] V.I. Balykin, V.G. Minogin, V.S. Letokhov, in *Electromagnetic trapping of cold atoms*, Rep. Prog. Phys., **63**, 1429 (2000)
- [11] H.J. Metcalf and P. van der Straten, *Optical cooling and trapping*, Springer Verlag, New-York (revised edition, 2001)

# **From nonlinear optics with single photons to nanoscale quantum sensors: new frontiers of optical science**

Mikhail Lukin

*Department of Physics, Harvard University  
Lyman Laboratory, 17 Oxford St.  
Cambridge, MA 02138, USA*

We will discuss recent developments involving a new scientific interface between quantum optics, many body physics, nanoscience and quantum information science. Specific examples include the use of quantum optical techniques for manipulation of individual spins using atom-like impurities in diamond and for controlling individual optical photons using strongly interacting atoms. Novel applications of these techniques ranging from quantum networks to strongly interacting photonic systems and nanoscale sensing in biology will be discussed.

# Quantum limits of optical super-resolution and a priori information

Mikhail I. Kolobov

*Laboratoire PHLAM, Université Lille 1, F-59655 Villeneuve d'Ascq, France\**

We shall give an overview of the quantum theory of optical resolution and show that super-resolution crucially depends on the amount of a priori information about the object. We shall demonstrate that the standard quantum limit of super-resolution for discrete objects is much higher than that for continuous objects due to higher amount of a priori information. We shall present the latest results for the quantum limits of super-resolution for sparse optical images using the Compressed Sensing approach.

Quantum Imaging [1, 2] is nowadays an established branch of quantum optics studying the ultimate performance limits of optical imaging allowed by the quantum nature of the light. One of the most important limits for any optical imaging scheme is that of its resolving capabilities. The classical diffraction limit established by Abbe and Rayleigh at the end of the 19th century, is nowadays recognized as a useful practical criterion but not a fundamental physical limit like, for example, the Heisenberg uncertainty relation. Numerous publications have demonstrated possibilities to improve the resolution beyond the Rayleigh limit. A natural question arises about the “real” quantum limit of optical super-resolution, i. e. resolution beyond the Rayleigh limit.

During the last ten years series of papers [3–6] have addressed the question of quantum limits of optical super-resolution in one- and two-dimensional coherent imaging for both continuous [3–5] and discrete [6] objects. In this talk we shall give an overview of the quantum theory of super-resolution and demonstrate that the super-resolution factor crucially depends on the amount of a priori information about the object. We shall formulate the standard quantum limit of super-resolution and show that one can go beyond this limit using spatially multimode squeezed light. Then we shall prove that the standard quantum limit of super-resolution for discrete objects is much higher than that for continuous objects due to higher amount of a priori information. We shall present the latest results for the quantum limits of super-resolution for sparse optical images using the Compressed Sensing approach.

Compressed Sensing (CS) is a new method of signal and image processing which allows for exact recovery of a signal from a number of samples much smaller than required by the Nyquist/Shannon theorem [7]. Compressed Sensing uses a priori information about the object called “sparsity”, which means that in some appropriate basis the signal has only a small number of nonzero components. Recent publications [8, 9] have shown that CS can be used to achieve super-resolution in optical imaging. In this talk we address the question of quantum limits of super-resolution of sparse optical objects using the CS technique. Our analysis allows to determine the ultimate performance capabilities of CS imposed by the quantum nature of the light.

Compressed Sensing employs a powerful recovery algorithm from linear programming known as basis pursuit [7] in order to reconstruct the object. This algorithm uses two different bases for decomposing the original object, known as sensing and representation bases. The first one is the basis in which the object is observed, while the second is the basis in which the object is sparse. A typical example of such a pair is the canonical or spike basis and the Fourier basis.

Recently [10] we have proposed to use *discrete prolate spheroidal sequences* (DPSS) as the sensing basis in the algorithm of CS. The DPSS were used previously for formulating the quantum theory of super-resolution of discrete optical objects [6]. In this talk we shall prove using both analytical calculations and numerical simulations that DPSS are an ideal tool for achieving super-resolution in reconstruction of sparse optical objects via the CS method.

In our numerical simulations we consider a simple sparse discrete object composed of  $K = 51$  components with only  $P = 5$  nonzero ones having both positive and negative values. This corresponds to the objects that carry both amplitude and phase information. Our imaging system is a simple one-dimensional diffraction-limited scheme with a diaphragm of varying size which determines the optical resolution of the scheme. Figure 1 shows the results of reconstruction of such a sparse object using the CS algorithm based on spike-Fourier basis (third panel) and spike-DPSS basis (forth panel) for three different sizes of the diaphragm. In both cases we neglect the quantum fluctuations. One can clearly see that while the spike-Fourier basis produces errors in recovery of the object even in the noiseless case, the spike-DPSS pair provides perfect recovery for all three sizes of the diaphragm.

In order to study the role of the quantum fluctuations, we have simulated numerically the quantum fluctuations of a coherent state for nonzero components of the object, and that of the vacuum state for the zero components. In this talk we shall provide the results of our simulations.

---

\*Electronic address: [Mikhail.Kolobov@univ-lille1.fr](mailto:Mikhail.Kolobov@univ-lille1.fr)

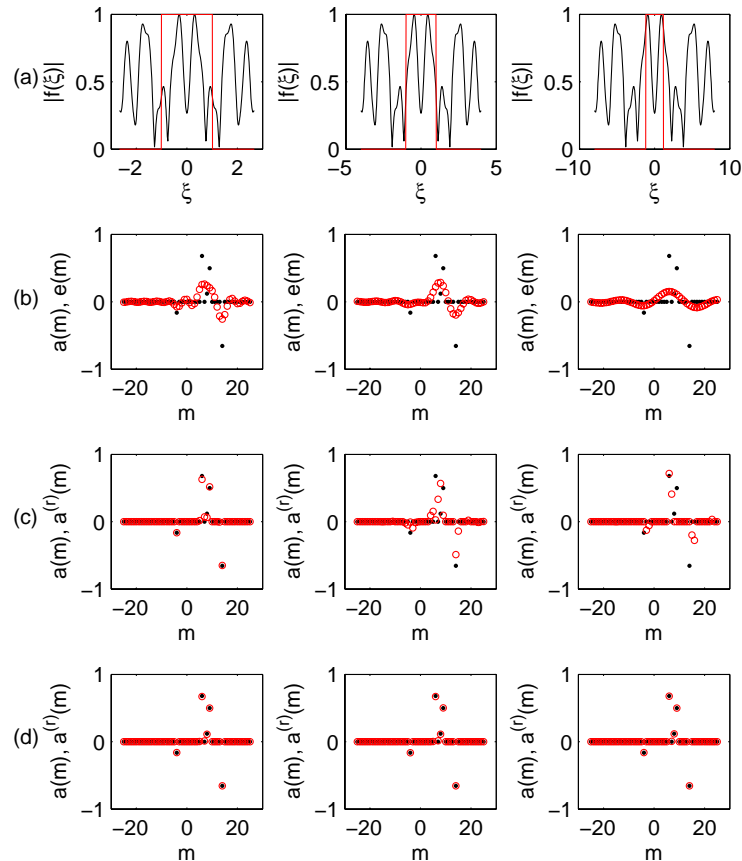


FIG. 1: Reconstruction of an original sparse object with superresolution via CS method: (a) modulus of the spatial Fourier spectrum of the object and the size of the transmitting diaphragm; (b) original object (dots) and its diffraction-limited image (circles); (c) original object (dots) and its reconstruction (circles) using the CS algorithm and the spike-Fourier pair; (d) original object (dots) and its reconstruction (circles) using the CS algorithm and the spike-DPSS pair.

- 
- [1] M. I. Kolobov (Ed.), “*Quantum Imaging*,” (Springer, NY, 2006).
  - [2] S. J. Bentley, “*Principles of Quantum Imaging: Ghost Imaging, Ghost Diffraction, and Quantum Lithography*,” (Taylor & Francis, Boca Raton, 2010).
  - [3] M. I. Kolobov and C. Fabre, “Quantum limits on optical resolution,” *Phys. Rev. Lett.* **85**, 3789-3792 (2000).
  - [4] V. N. Beskrovnyy and M. I. Kolobov, “Quantum limits of super-resolution in reconstruction of optical objects,” *Phys. Rev. A* **71**, 043802(1-10) (2005).
  - [5] V. N. Beskrovnyy and M. I. Kolobov, “Quantum-statistical analysis of superresolution for optical systems with circular symmetry,” *Phys. Rev. A* **78**, 043824(1-11) (2008).
  - [6] M. I. Kolobov, “Quantum limits of superresolution for imaging discrete subwavelength structures,” *Opt. Express* **16**, 58-66 (2008).
  - [7] E. J. Candès and M. B. Wakin, “An introduction to compressive sampling,” *IEEE Signal Process. Mag.* **25**, 21 (2008).
  - [8] S. Gazit, A. Szameit, Y. C. Eldar, and M. Segev, “Super-resolution and reconstruction of sparse sub-wavelength images”, *Opt. Express* **17**, 23920 (2009).
  - [9] Y. Shechtman, S. Gazit, A. Szameit, Y. C. Eldar, and M. Segev, “Super-resolution and reconstruction of sparse images carried by incoherent light”, *Opt. Lett.* **35**, 1148 (2010).
  - [10] H. Wang, S. Han, and M. I. Kolobov, “Quantum limits of super-resolution of optical sparse objects via sparsity constraint”, *Opt. Express* **20**, 23235 (2012).

# Long-distance quantum networks built from spin registers in diamond

**Ronald Hanson**

*Department of Quantum Nanoscience, Kavli Institute of Nanoscience, Delft University of Technology*

*P.O. Box 5046, 2600 GA Delft, The Netherlands*

*r.hanson@tudelft.nl*

**Abstract:** We present our most recent results towards realization of scalable quantum networks with spins in diamond, including universal control of a local nuclear spin register and heralded entanglement of electron spins separated by 3 meters.

Entanglement of spatially separated objects is one of the most intriguing phenomena that can occur in physics. Besides being of fundamental interest, entanglement is also a valuable resource in quantum information technology enabling secure quantum communication networks and distributed quantum computing.

Here we present our most recent results towards the realization of scalable quantum networks with solid-state qubits. We have entangled two spin qubits in diamond, each associated with a nitrogen vacancy center in diamond [1]. The two diamonds reside in separate setups three meters apart from each other. With no direct interaction between the two spins to mediate the entanglement, we make use of a scheme based on quantum measurements: we perform a joint measurement on photons emitted by the NV centers that are entangled with the electron spins. The detection of the photons projects the spins into an entangled state. We verify the generated entanglement by single-shot readout of the spin qubits in different bases and correlating the results.

These results open the door to a range of exciting opportunities. For instance, the remote entanglement can be extended to nuclear spins near the NV center. Our recent experiments demonstrate robust methods for initializing, controlling and entangling nuclear spins by using the electron spin as an ancilla [2,3,4]. Entanglement of remote quantum registers will enable deterministic quantum teleportation, distributed quantum computing tasks and the implementation of an elementary quantum repeater.

## References

- [1] H. Bernien et al., *Nature* (2013, in press).
- [2] T. van der Sar et al., *Nature* **484**, 82 (2012).
- [3] T. H. Taminiau et al., *Phys. Rev. Lett.* **109**, 137602 (2012).
- [4] W. Pfaff et al., *Nature Physics* **9**, 29 (2013).

# Complete quantum theory of nondegenerate optical parametric amplification at low frequency pumping

A.S. Chirkin<sup>1</sup>, A.M. Chebotarev<sup>2,3</sup>, T.V. Tlyachev<sup>1</sup>

<sup>1</sup> Faculty of Physics and International Laser Center, M.V. Lomonosov Moscow State University, Leninskie Gory,  
Moscow 119991, Russia;

FAX: +7 495/939-3113; email: [aschirkin@rambler.ru](mailto:aschirkin@rambler.ru)

<sup>2</sup> Faculty of Physics, M.V.Lomonosov Moscow State University, Leninskie Gory, Moscow 119991, Russia;

<sup>3</sup> Moscow Institute for Electronics and Mathematics of National Science University Higher School of Economics,  
Moscow 109028, Russia

**Abstract:** We develop quantum theory of three coupled parametric processes including one parametric down-conversion followed by two up-conversion. To find the density operator for this interaction the approach, elaborated by us earlier, is applied.

Coupled optical parametric interactions are of interest as a method of obtaining multipartite quantum entanglement. Application of multipartite entangled quantum states in quantum information and quantum computations have a number of advantages compared with two-partite entangled states. Therefore, recently multipartite (multimode) entangled quantum states draws considerable attention.

We elaborate complete quantum theory of generation of entangled four-mode state. Such a process consists of parametric down-conversion related to two parametric up-conversion. The process under consideration is described by the interaction Hamiltonian

$$H_{\text{int}} = i\hbar(\beta a_1^+ a_2^+ + \gamma_1 a_3^+ a_1 + \gamma_2 a_4^+ a_2) + h.c. \quad (1)$$

and can be implemented in aperiodical nonlinear photon crystal [1] and gases [2]. Here  $a_j^+$  ( $a_j$ ) is the creation (annihilation) operators with the standard commutation relationships, the index  $j$  refers to the corresponding mode.

In (1)  $\beta$  is the nonlinear coupling coefficient responsible for parametric down-conversion, and coefficients  $\gamma_{1,2}$  are responsible for parametric up-conversion. Conventional approach to determining the density operator of system is based on the Wei-Norman method [3] including the so-called normal ordering procedure that leads to a set of coupled nonlinear equations. In the case of two coupled parametric processes in which entangled three-mode state is generated, these equations are solved [4]. However, in the case of three coupled parametric processes such equations cannot be solved analytically already. At the same time, the approach developed in [5-7], allowed to avoid these difficulties and to find a state vector corresponding dynamics of the system described by the Hamiltonian (1). The basis of this approach are formed by the canonical transformation of Bose operators, which define the evolution of the system in the Heisenberg picture, and a specific ordered formula for the unitary operator of the system. Note that our approach is applicable for any number of coupled parametric processes.

As result for the interaction under study we have obtained the following explicit formula for the system state:

$$|\psi\rangle = C \sum_{m,n,k,l=0}^{\infty} Q_{12}^m Q_{34}^n Q_{14}^k Q_{23}^l \sqrt{C_{m+n}^m C_{n+k}^n C_{n+l}^n C_{m+l}^m} |m+k\rangle_1 |m+l\rangle_2 |n+k\rangle_3 |n+k\rangle_4 \quad (2)$$

The vector (2) corresponds to the initial vacuum state, and  $Q_{pq}$  is the matrix element determined by elements of the canonical transformation matrix. The vector (2) allows one to calculate any statistical characteristics of the quantum state.

## Reference

- [1] A.S. Chirkin, I.V. Shutov, *JETP Lett.* **86**, 693 (2007), *JETP* **109** 547 (2009).
- [2] X.Liang, X. Hu, Ch.He, *Phys.Rev. A*, **85** 032329 (2012).
- [3] J. Wei and E.Norman *J. Math. Phys.* **4** 575 (1963).
- [4] A.V. Rodionov, A. S. Chirkin *JETP Lett.* **79** 253 (2004).
- [5] T.V. Tlyachev, A.M. Chebotarev, A. S. Chirkin *Physica Scripta* **T 153** xxx (2013).
- [6] A.M. Chebotarev, T.V. Tlyachev, A.A. Radionov, *Mathematical Notes* **92** 700 (2012)
- [7] A.M. Chebotarev, T.V. Tlyachev, A.A. Radionov **89** 577 (2011)

# Quantum electrodynamics of atoms and molecules in nanoenvironment

Vasily Klimov

In this talk I will discuss influence of nanoparticles and nanostructures (including metamaterials) on optical properties of atoms and molecules. In the first part of lecture I will present history and general principles of QED in nanoenvironment. Here I will touch both weak and strong regimes of light-matter interaction. Special attention will be paid to quantization of electromagnetic field near nanoparticles and nanostructures and relation between classical and quantum descriptions. Notion of local density of photon states will be also discussed here. In second part of lecture I will present our results on radiation of atoms and molecules for different specific geometries and materials. In final part of talk I will outline main challenges in this area.

# Second Stage Laser Cooling and Optical Trapping of $^{169}\text{Tm}$ Atoms

G. Vishnyakova,\* D. Sukachev, E. Kalganova, A. Savchenkov, A. Sokolov, A. Akimov,  
N. Kolachevsky, V. Sorokin

*P.N. Lebedev Physical Institute of the Russian Academy of Sciences, Leninsky prosp. 53, 119991 Moscow, Russia*  
*Moscow Institute of Physics and Technology, Dolgoprudny, 141700, Russia*  
*Russian Quantum Center, SKOLKOVO, Moscow region, 143025, Russia*  
*\*gulnarav7@gmail.com*

**Abstract:** We have demonstrated second-stage laser cooling of  $^{169}\text{Tm}$  atoms on the weak transition (wavelength  $\lambda=530.7$  nm, natural line width  $\gamma=360$  kHz). Laser cooled atoms have been trapped in an optical dipole trap operating near 532 nm.

Laser cooling and trapping of neutral atoms is one of the most powerful tools for studying atomic ensembles at ultralow temperatures [1]. It has opened a new era in precision laser spectroscopy [2], the study of collisions, atomic interferometry, and the study of quantum condensates. During the last decade laser cooling of rare-earth elements with the hollow inner shell (Er, Dy, Tm) attract close interest. These elements possess high ground state magnetic moments which make them attractive for studying atom-atom interactions at ultralow temperatures. Inner shell transition can also be considered as promising candidates for applications in ultra-stable optical clocks. Laser cooling and trapping of rare-earths is a challenging task due to their rich level structure. Recently, laser cooling was demonstrated for Er, Dy and Tm – rare earths with the hollow  $4f$  subshell.

We propose to use the transition at the wavelength 1.14  $\mu\text{m}$  between two fine-structure components of Thulium ground-state as a “clock transition” in optical lattice clock. Narrow natural line width (1.2 Hz) and strong shielding by closed  $6s^2$  and  $5s^2$  shells provide high frequency stability of Thulium-based optical clocks. To load atoms in a shallow optical dipole trap or optical lattice, they should be laser cooled to temperatures as low as 1-10  $\mu\text{K}$ .

Thulium atoms were successfully laser cooled in our laboratory at LPI in 2010 [3]. We used a strong nearly closed transition with the wavelength of  $\lambda=410.6$  nm and the natural line width of  $\gamma=9.4$  MHz for Zeeman slowing and trapping of laser-cooled atoms in a magneto-optical trap (MOT). Due to similar magnetic sensitivity of the upper and lower cooling levels, sub-Doppler cooling mechanisms happened to be very efficient which allowed us to reach temperatures down to 25  $\mu\text{K}$  directly in the MOT, which is much smaller than Doppler limit of 240  $\mu\text{K}$ . In principle, such temperatures already allow loading atoms in a deep optical dipole trap formed by a strongly focused few-watt laser beam. Such regime would be unfavorable for optical clock applications due to a strong dynamic Stark shifts from the trap field and low re-capturing efficiency due to tight focusing. To reach more favorable regime further cooling is required.

We have demonstrated second stage laser cooling of Tm atoms on the closed transition  $4f^3 6s^2 (J=7/2) \rightarrow 4f^2 5d_{5/2} 6s^2 (J'=9/2)$  with the wavelength of  $\lambda=530.7$  nm and the natural line width of  $\gamma=360$  kHz. Compared to the first stage cooling transition it has much lower Doppler limit of 9  $\mu\text{K}$  which should allow to easily load atoms in the optical dipole trap. For the second stage cooling we use a frequency doubled semiconductor laser providing a spectral line width of  $\sim 1$  MHz. Such line width allows to cool atoms only using large red frequency detuning ( $30-50\gamma$ ) which increases the velocity capture range, but, in turn, results in temperatures much higher than the Doppler limit. In our case the temperature of atoms in the green 530.7 nm MOT was in the range 20-30  $\mu\text{K}$ . We demonstrated re-capturing of atoms from the blue MOT with nearly 100% efficiency, as well as direct capturing of atoms from decelerated atomic beam. To further reduce the temperature we plan to narrow the laser spectral line width by locking it to external optical cavity.

Laser cooled atoms were successfully loaded from the MOT into the optical dipole trap (Fig.1a) operating near 532 nm. Radiation of frequency doubled  $\text{Nd}^{3+}$ -doped laser was tightly focused into an atomic cloud (up to 10 W in the 30  $\mu\text{m}$  beam waist) which forms an optical trap with an estimated depth of 1 mK. To observe the optical dipole trap we switch off the cooling beams in the presence of trapping laser and after a few ms (typical time-of-flight of MOT) we illuminate cold atoms to make them visible and make a picture. Successful optical trapping of atoms in the beam waist was observed both in a trap formed by one beam and in two crossed beams. We also demonstrated trapping in the optical lattice (optical standing wave) (Fig.1b) by retro-reflecting the trapping beam. The life time of atoms in the trap corresponds to 200 ms which indicates low heating rates well suiting for further precision experiments. Relatively low re-capture efficiency (1.5%) is due to small spatial overlap between the initial atomic cloud and optical trap beams.

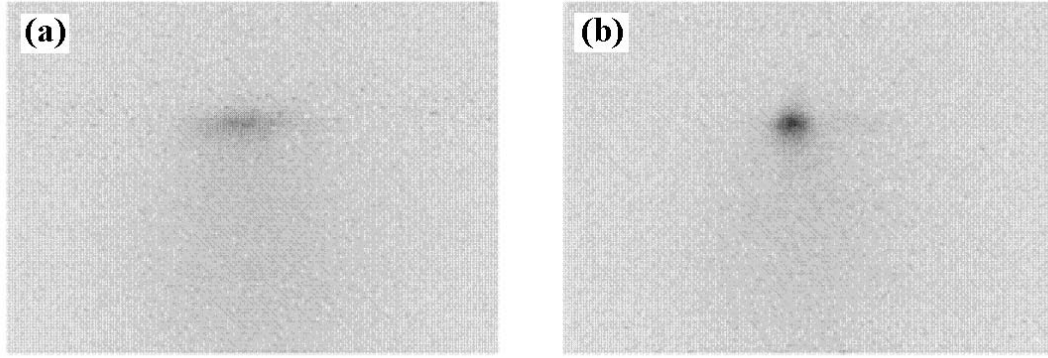


Fig.1. Optical dipole trap (a) and optical lattice (b). The wavelength of trapping laser is 532 nm, the power is 10 W, the beam waist is 30  $\mu\text{m}$ . Time-of-flight (see the text) is 15 ms. The dipole trap is stretched because of the long size of the beam waist (about few cm).

- [1] W. D. Phillips, *Rev. Mod. Phys.* 70, 721 (1998).
- [2] F. Riehle, *Frequency Standards. Basics and Applications* (Wiley-VCH, Weinheim, 2004).
- [3] D. Sukachev et al., *Phys. Rev. A* 82, 011405 (2010).

# High-efficiency object identification using multi-dimensional correlated orbital angular momentum (OAM) states

A. V. Sergienko,<sup>1,4</sup> N. Uribe-Patarroyo,<sup>1</sup> A. Fraine,<sup>1</sup> D. S. Simon,<sup>1,2</sup> and O. Minaeva<sup>3</sup>

<sup>1</sup>Dept. of Electrical & Computer Engineering, Boston University, Boston, Massachusetts 02215

<sup>2</sup>Dept. of Physics and Astronomy, Stonehill College, 320 Washington Street, Easton, MA 02357

<sup>3</sup>Dept. of Biomedical Engineering, Boston University, Boston, MA 02215, USA<sup>3</sup>

<sup>4</sup>Dept. of Physics, Boston University, Boston, Massachusetts 02215  
e-mail:alexserg@bu.edu

**Abstract:** We present a novel approach that allows object identification using fewer resources than in conventional pixel-by-pixel imaging by exploiting the enhanced sensitivity of correlated orbital angular momentum states to multiple azimuthal Fourier coefficients.

**OCIS codes:** (270.0270) Quantum Optics; (270.1670) Coherent optical effects

## SUMMARY

Using spontaneous parametric down conversion as a source of entangled photon pairs, correlations are measured between the orbital angular momentum (OAM) in a target beam (which contains an unknown object) and that in an empty reference beam. Unlike previous studies, the effects of the object on *off-diagonal* elements of the OAM correlation matrix are examined. Due to the presence of the object, terms appear in which the signal and idler OAM do not add up to that of the pump. Using these off-diagonal correlations, the potential for high-efficiency object identification by means of correlated OAM states is experimentally demonstrated for the first time. The higher-dimensional OAM Hilbert space enhances the information capacity of this approach, while the presence of the off-diagonal correlations allows for recognition of specific spatial signatures present in the object. In particular, this allows the detection of discrete rotational symmetries and the efficient evaluation of multiple azimuthal Fourier coefficients using fewer resources than in conventional pixel-by-pixel imaging. This represents a demonstration of sparse sensing using OAM states, as well as being the first correlated OAM experiment to measure properties of a real, stand-alone object, a necessary first step toward correlated OAM-based remote sensing.

Correlated optical sensing uses various types of correlations between pairs of photons or pairs of classical light beams to form an image or to detect specific object features. This includes techniques such as ghost imaging [1,2] and compressive ghost imaging [3,4]. In ghost imaging, correlated light is sent through two different paths, one of which contains the target object and a bucket detector, and the other has a spatially resolving detector but no object. Correlation between the outputs of each detector allows reconstruction of an image or sensing of particular features of the object [4]. In compressive sensing [5], the illumination of the target object is modulated by a number of known (usually random) spatially varying transmission masks and an estimation of the object or its features can be found by correlating the intensity of the detected light with the mask profile. Compressive ghost imaging uses the techniques of compressive sensing in a ghost imaging setup to attain more efficient imaging [6].

The use of orbital angular momentum (OAM) states in classical and quantum imaging techniques has been shown to provide additional effects that enhance the sensitivity to particular features of an object. For example, it has been shown that the use of OAM modes in phase imaging configurations increases edge contrast by using a spiral phase distribution as a filter [7]. In addition, digital spiral imaging [8] has been proposed as a technique in which the OAM basis is used to illuminate the object and to analyze the transmitted or reflected light. The two-dimensional spatial structure of the mode along with the high dimension of the OAM basis set leads to the probing of two-dimensional objects without obtaining a pixel-by-pixel reconstruction, analogous to the approach of compressive sensing.

It has been shown that this high dimensionality combined with the use of correlated two-photon states gives rise to an improved version of digital spiral imaging which exploits the full two-dimensional OAM joint spectrum [9]. Our current result [10] presents, to the best of our knowledge, the first experimental demonstration of a sparse sensing technique based on OAM states (see Fig. 1 and Fig. 2). It expands states generated by spontaneous parametric down conversion (SPDC) in terms of the OAM basis in order to identify objects without attempting image reconstruction. Significant information from the object has become available by measuring the *joint* OAM spectrum of two-photon states, giving rise to novel features *outside the main OAM-conserving diagonal* [11] of correlation matrix, due to the interaction with the object (Fig. 2(d)).

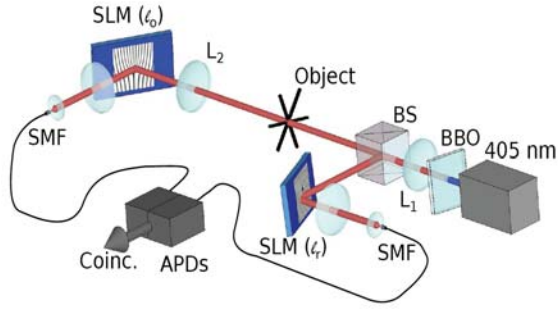


Fig. 1. Setup for the sensing of the object via orbital angular momentum of correlated photons.

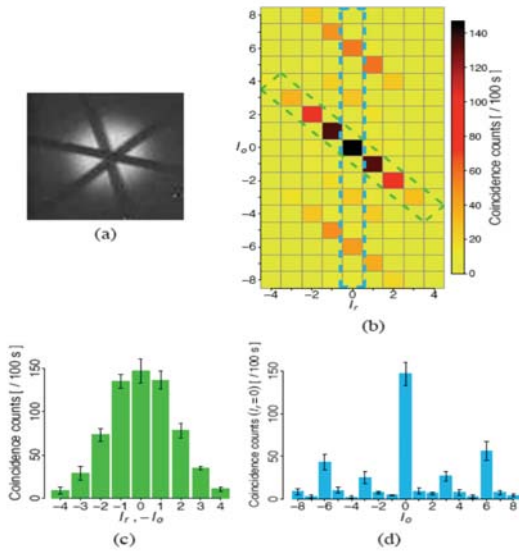


Fig. 2. (a) Image of the three-arm cross used as target, (b) the experimental joint spectrum, (c) a histogram of the joint spectrum main diagonal and (d)  $P(l_o|l_r = 0)$  cross section of the joint spectrum.

symmetry components. This represents a realistic remote sensing application using physical objects detached from any optical components. Although the experiment was conducted with a transmissive object, a trivial modification of the optical setup (simply changing the position of the lens, SLM, and object arm detector) makes it suitable for remote sensing of reflective targets at arbitrarily large distances.

## References:

- [1] T. B. Pittman, Y. H. Shih, D. V. Strekalov, and A. V. Sergienko, Phys. Rev. A **52**, R3429–R3432 (1995).
- [2] Ryan S. Bennink, Sean J. Bentley, and Robert W. Boyd, Phys. Rev. Lett. **89**, 113601 (2002).
- [3] Ori Katz, Yaron Bromberg, and Yaron Silberberg, Applied Physics Letters **95**, 131110 (2009).
- [4] Vladimir Katkovnik and Jaakko Astola, J. Opt. Soc. Am. A **29**, 1556–1567 (2012).
- [5] E.J. Candes and M.B. Wakin, Signal Processing Magazine, IEEE **25**, 21–30 (2008).
- [6] Wenlin Gong and Shensheng Han, J. Opt. Soc. Am. A **29**, 1571–1579 (2012).
- [7] B. Jack, J. Leach, J. Romero, S. Franke-Arnold, M. Ritsch-Marte, S. M. Barnett, and M. J. Padgett, Phys. Rev. Lett. **103**, 083602 (2009).
- [8] Lluís Torner, Juan Torres, and Silvia Carrasco, Opt. Express **13**, 873–881 (2005); Gabriel Molina-Terriza, Liis Rebane, Juan P. Torres, Lluís Torner, and Silvia Carrasco, Journal of the European Optical Society: Rapid Publications **2**, 10.2971 (2007).
- [9] David S. Simon and Alexander V. Sergienko, Phys. Rev. A **85**, 043825 (2012).
- [10] Nestor Uribe-Patarroyo, Andrew Fraine, David S. Simon, Olga Minaeva, Alexander V. Sergienko, Phys. Rev. Lett. **110**, 043601 (2013).
- [11] Alois Mair, Alipasha Vaziri, Gregor Weihs, and Anton Zeilinger, Nature **412**, 313–316 (2001).

**Discussion.** More insight about the structure of each object is acquired by analyzing specific non-diagonal cross sections such as in Fig. 2(d). Previous works regarding the OAM joint spectrum of SPDC (see for example [11]) have considered only the main diagonal elements corresponding to the conservation of OAM with respect to the pump (Fig.2(c)). In the current case, there is an interaction between the OAM from SPDC and the spatial features of the object resulting in contributions that require analysis of the complete two-dimensional joint spectrum *outside the main OAM-conserving diagonal*.

The non-diagonal cross section  $P(l_o|l_r = 0)$  shown in Fig.2(d) indicates significant six-fold symmetry as the dominant feature of the object. This feature can be uniquely attributed to the object because it is outside the diagonal that corresponds to the conservation of OAM in SPDC. Fig.2(d) also exhibits richer features associated with the higher complexity of the object. Specifically, apart from the dominant six-fold symmetric contribution, a three-fold contribution is observed. At the center of the object (Fig.2(a)), the three stripes are displaced with respect to the center. This forms a triangular shape in a small region with three-fold rotational symmetry. This small deviation from a strict six-fold symmetry is readily observed in the non-diagonal cross section by the appearance of significant contributions at  $l_o = \pm 3$ .

A practical demonstration of high-efficiency sensing using OAM states has been presented that allows recognition of objects using a smaller number of measurements. These results demonstrate that an object imprints its own characteristic symmetry features onto the joint OAM joint spectrum of SPDC. New elements arise that do not fulfill the OAM conservation condition required by SPDC alone, but which are affected by the object as well. The capability of correlated spiral imaging (CSI) for object recognition is demonstrated by these results including high sensitivity to the presence of small

# Structure and optical control of the spectrum of resonance fluorescence at x-ray energies

Stefano M. Cavaletto<sup>1,\*</sup>, Zoltán Harman<sup>1,2</sup>, Christian Buth<sup>1</sup>, and Christoph H. Keitel<sup>1</sup>

<sup>1</sup>Max-Planck-Institut für Kernphysik, Saupfercheckweg 1, 69117 Heidelberg, Germany

<sup>2</sup>ExtreMe Matter Institute (EMMI), Planckstraße 1, 64291 Darmstadt, Germany

\*Corresponding author: Tel: +49 (0)6221 / 516-174, Fax: +49 (0)6221 / 516-601, Email: [stefano.cavaletto@mpi-hd.mpg.de](mailto:stefano.cavaletto@mpi-hd.mpg.de)

**Abstract:** The spectrum of x-ray resonance fluorescence is studied with the aim of (i) observing Rabi flopping induced by intense XFEL pulses and (ii) generating an x-ray frequency comb from coherent pulse shaping.

The spectrum of resonance fluorescence, i.e., the frequency properties of the photons spontaneously emitted by an ensemble of particles driven by an external field, represents a cornerstone in quantum optics. At low intensities the atoms elastically scatter photons with the same spectral properties, i.e., frequency and bandwidth, as the driving field. For high intensities, though, the field can induce *Rabi flopping* of the atomic properties of the system, i.e., cycles of population and depopulation of the levels to which the field is tuned at a *Rabi frequency* which is proportional to the square root of the intensity of the driving field.

Other effects determining the time evolution of the light-matter interaction are spontaneous and Auger decay, detuning and bandwidth of the driving field. When the intensity, i.e., the Rabi frequency, is high enough to make up for these decoherence and decay effects, Rabi flopping can dominate the time evolution of the system and manifest itself in the spectrum of resonance fluorescence, e.g., in the observed Mollow triplet [1].

The lack of coherent and sufficiently intense x-ray light sources has for long time obstructed analogous investigations at x-ray frequencies. On the one hand, the ultrafast decay times of inner-shell x-ray transitions require very high intensities to induce Rabi oscillations within the lifetime of the system. On the other hand, the large bandwidth provided by synchrotron sources negatively influences the appearance of coherent effects.

The advent of x-ray free-electron lasers (XFELs) [2] is revolutionizing such a scenario, encouraging the investigation of x-ray quantum optical phenomena [3]. XFELs based on self-amplified spontaneous emission (SASE) provide chaotic light with large bandwidth, but self- and laser-seeding methods [4] are already used to significantly improve the coherence of emitted x rays.

Our investigations are driven by and take advantage of state-of-the-art and anticipated near-future advances in intense x-ray sources. In Sec. I we focus on the appearance of Rabi flopping at x-ray frequencies for fast Auger decaying, inner-shell transitions driven by SASE and seeded XFEL light. In Sec. II, we augment this x-ray-only scheme of two additional optical transitions and use an optical frequency comb to manipulate the emitted x-ray spectrum. We highlight the presence of an x-ray frequency comb in the emitted spectrum, which might eventually make such a scheme a valid alternative to present x-ray comb-generation methods based on high-order harmonic generation (HHG).

## I. Rabi flopping in XFEL x rays

We first investigate the possibility to induce Rabi oscillations in  $\text{Ne}^+$  ions driven by an XFEL-like field tuned to the  $1s\ 2p^{-1} \rightarrow 1s^{-1}\ 2p$  transition at 848 eV and evidence its signature in the resonance fluorescence spectrum [5].

We use a two-level system to model the transition, because this is well isolated, by more than 70 natural linewidths, from the next  $1s \rightarrow 1s^{-1}\ 3p$  Rydberg excitation at 867 eV. The Auger decay rate is 0.27 eV; present SASE pulses have a bandwidth of 6 eV, wherefore previous experimental investigations of the Auger electron spectra are still not conclusive [6, 7].

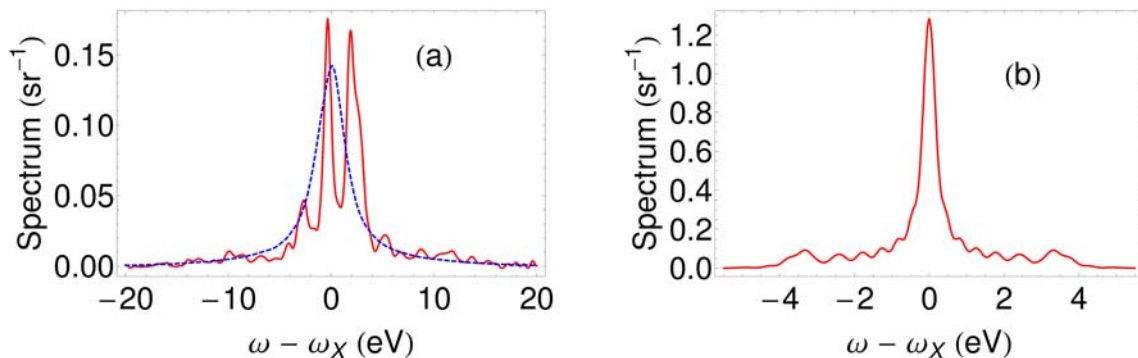


**Figure 1.** Resonance fluorescence spectrum of the two-level system used to model the  $1s\ 2p^{-1} \rightarrow 1s^{-1}\ 2p$  transition at 848 eV in  $\text{Ne}^+$  ions. (a) SASE pulses, simulated with the partial-coherence method described in [5], drive the transition: the blue, dashed line is the arithmetic mean over 1,000 SASE pulses with average peak intensity  $3.8 \times 10^{18}$  W/cm<sup>2</sup>, FWHM of 6.5 fs, and a bandwidth of 6 eV; the red, continuous line is for a single SASE pulse with the same parameters. (b) A Gaussian x-ray pulse of peak intensity  $2.6 \times 10^{17}$  W/cm<sup>2</sup> and FWHM 5 fs is used to drive the transition.

The spiky shape and the short coherence time of present SASE XFEL pulses limit the observability of nonlinear interactions of matter and x rays. Nonetheless, in Fig. 1(a) one can already predict a nontrivial enlargement of the width of the emitted spectrum [5], mostly due to the width of the driving x rays, which would not appear at low intensities. However, in the foreseeable future, use of self- or laser-seeding methods at XFELs providing approximately Gaussian pulses [4] can allow, as predicted in [5], the observation of a clear signature of Rabi oscillations in the resonance fluorescence spectrum at x-ray frequencies, shown here in Fig. 1(b).

## II. X-ray frequency combs

When the x-ray-only system of the previous section is augmented with additional optical transitions, one can drive them with an auxiliary optical field, aiming at controlling the properties of the emitted x rays. Similar control schemes have been developed [8], and used, e.g., to describe phenomena such as electromagnetically induced transparency in x rays [9].

In our case, we use a four-level system to model the ground state and the first excited states of He-like ions [10] such as  $\text{Be}^{2+}$  and  $\text{Ne}^{8+}$ . Three of the four electric-dipole-allowed transitions are driven by external fields tuned to them: the x-ray transition  $1s^2\ ^1S_0 \rightarrow 1s\ 2p\ ^3P_1$  is driven by x rays of small bandwidth, as underdevelopment techniques are expected to make available in the near future; the  $1s\ 2p\ ^3P_1 \rightarrow 1s\ 2s\ ^1S_0$  optical transition is driven by an auxiliary optical laser; finally, an optical frequency comb drives the remaining  $1s\ 2s\ ^1S_0 \rightarrow 1s\ 2p\ ^1P_1$  optical transition. This scheme is used to manipulate the photons spontaneously emitted on the  $1s\ 2p\ ^1P_1 \rightarrow 1s^2\ ^1S_0$  transition at the x-ray energy  $\omega_x$ . In [11] we compute the coherent spectrum of resonance fluorescence on the  $1s\ 2p\ ^1P_1 \rightarrow 1s^2\ ^1S_0$  transition that an ensemble of ions emits in the forward direction. The driving optical comb can imprint its structure on the emitted x rays: a frequency comb with its same spacing and centered on the x-ray energy  $\omega_x$  appears in the resonance fluorescence spectrum [11], as displayed in Fig. 2.

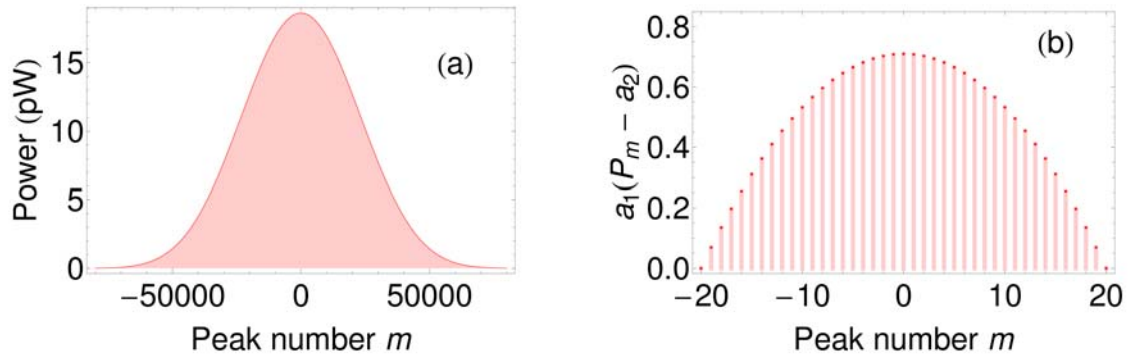


**Figure 2.** Coherent spectrum of resonance fluorescence emitted on the  $1s\ 2p\ ^1P_1 \rightarrow 1s^2\ ^1S_0$  transition of  $\text{Be}^{2+}$  ions, centered on the x-ray transition energy  $\omega_x = 123.7$  eV [10]. The power of each peak in the spectrum is displayed (a) for the whole comb and (b) around the maximum. In panel (b),  $a_1 = 10^5\ \text{pW}^{-1}$ ,  $a_2 = 18.64\ \text{pW}$ .

By properly tuning the peak intensities of the three driving fields one can maximize the intensity of the emitted x-ray comb and the number of peaks it contains [11]. We show that such a method requires a peak intensity of the incoming optical frequency comb of  $\sim 10^{11}\ \text{W/cm}^2$ , which is lower than that needed for presently used extreme-ultraviolet comb-generation methods based on HHG [12]. In addition, the scheme that we propose can be used to drive x-ray transitions ranging from hundreds of eV up to the keV range. Though relying on small-bandwidth x rays driving the  $1s^2\ ^1S_0 \rightarrow 1s\ 2p\ ^3P_1$  transition, our scheme predicts output intensities comparable with those produced with HHG-based methods and used for direct-comb spectroscopy [11, 12]. Anticipated developments of small-bandwidth x-ray sources will make this scheme feasible for the generation of x-ray frequency combs with energies up to the keV range.

## III. References

- [1] B. R. Mollow, *Phys. Rev.* **188**, 1969 (1969); F. Y. Wu, R. E. Grove, and S. Ezekiel, *Phys. Rev. Lett.* **35**, 1426 (1975).
- [2] P. Emma *et al.*, *Nature Photon.* **4**, 641 (2010); W. Ackermann *et al.*, *Nature Photon.* **1**, 336 (2007); D. Pile, *Nature Photon.* **5**, 456 (2011); M. Altarelli *et al.*, *The European X-Ray Free-Electron Laser*, Technical Design Report (DESY, Hamburg, Germany, 2006).
- [3] B. W. Adams, C. Buth, S. M. Cavaletto, J. Evers, Z. Harman, C. H. Keitel, A. Pálffy, A. Picón, R. Röhlsberger, Y. Rostovtsev, K. Tamasaku, *J. Mod. Opt.*, DOI:10.1080/09500340.2012.752113 (2013).
- [4] J. Amann *et al.*, *Nature Photon.* **6**, 693 (2012).
- [5] S. M. Cavaletto, C. Buth, Z. Harman, E. P. Kanter, S. H. Southworth, L. Young, C. H. Keitel, *Phys. Rev. A* **86**, 033402 (2012).
- [6] N. Röhringer and R. Santra, *Phys. Rev. A* **77**, 053404 (2008).
- [7] E. P. Kanter *et al.*, *Phys. Rev. Lett.* **107**, 233001 (2011).
- [8] L. M. Narducci *et al.*, *Phys. Rev. A* **42**, 1630 (1990); A. Manka *et al.*, *Phys. Rev. A* **43**, 3748 (1991); S. Y. Zhu and M. O. Scully, *Phys. Rev. Lett.* **76**, 388 (1996); C. H. Keitel, *Phys. Rev. Lett.* **83**, 1307 (1999); M. Macovei and C. H. Keitel, *Phys. Rev. Lett.* **91**, 123601 (2003); O. Postavaru, Z. Harman, and C. H. Keitel, *Phys. Rev. Lett.* **106**, 033001 (2011).
- [9] C. Buth, R. Santra, and L. Young, *Phys. Rev. Lett.* **98**, 253001 (2007); T. E. Glover *et al.*, *Nature Phys.* **6**, 69 (2010).
- [10] V. A. Yerokhin and K. Pachucki, *Phys. Rev. A* **81**, 022507 (2010).
- [11] S. M. Cavaletto, Z. Harman, C. Buth, and C. H. Keitel, submitted, arXiv:1302.3141, (2013).
- [12] A. Cingöz *et al.*, *Nature* **482**, 68 (2012).

# Single-emitter nanolaser — Heisenberg-Langevin and density operator approach

<sup>1</sup>Nikolay V. Larionov, <sup>2</sup>Mikhail I. Kolobov

<sup>1</sup>*Department of Theoretical Physics, St. Petersburg State Polytechnical University, 195251, St. Petersburg, Russia, larionov.nikolay@gmail.com*

<sup>2</sup>*Laboratoire de Physique des Lasers, Atomes et Molécules, Université Lille 1, F-59655 Villeneuve d'Ascq Cedex, France*

**Abstract:** Using Heisenberg-Langevin and density operator approaches we investigate properties of incoherently pumped single-emitter nanolaser. We provide analytical results in good- and bad-cavity regimes and also specify conditions needed for thresholdless behaviour.

## 1. Introduction

Nowadays a single-emitter laser is realized in experiments where the role of emitter can play the single atom [1], or ion [2] or quantum dot [3]. In most of theoretical works devoted to such nanolaser problem the different type of numerical methods are used. In this connection, the purpose of our paper is to provide analytical results which can be considered as a tools for experimenter. Thus in our previous Brief Report [4] with the help of the Heisenberg-Langevin (H-L) approach we obtained analytical expressions for linewidth, amplitude fluctuation spectrum and Mandel Q parameter which describe the behaviour of a single-emitter nanolaser in the case of good cavity regime. We also improved the condition required for thresholdless regime. Here we continue our calculations based on H-L approach and extend it to bad-cavity regime. Using the master equation written in terms of the coherent states, in stationary regime we obtain approximated expression for Glauber-Sudarshan P function. The latter proves our previous results and gives us possibility to analyze some limited cases and threshold behaviour of the nanolaser.

## 2. Model and results

The simplest model of a single-emitter nanolaser is the single two-level system placed inside the single-mode cavity and incoherently pumped to its upper level. Just four constants characterize this nanolaser:  $\Gamma$  – the incoherent pumping rate, pumping process associated with the transition from lower to upper level;  $\gamma/2$  – the decay rate of polarization due to spontaneous emission to modes other than the laser mode;  $\kappa/2$  – the field decay rate in the cavity;  $g$  – the coupling constant between the field and the two-level system.

This type of nanolaser relates to so called self-quenching laser [5] which has the following semiclassical stationary intracavity intensity  $I_0 = \frac{I_s}{2} [(r-1) - (r+1)^2/c]$ . Here we introduce new dimensionless parameters: the dimensionless pumping rate  $r = \Gamma/\gamma$ ; the dimensionless saturation intensity  $I_s = \gamma/\kappa$ ; the dimensionless coupling strength  $c = 4g^2/\kappa\gamma$ .  $I_0$  has a physical interpretation when  $c > 8$  and when the value of the pump rate lying in the domain between two points, so called threshold  $r_{th}$  and self-quenching  $r_q$  points. The maximum of intensity  $I_m = I_s(c/8 - 1)$  reaches in maximum point  $r_m = c/2 - 1$ .

Using linearization procedure applied to the H-L equations [6] we investigated small fluctuations of nanolaser field near the dominant stationary semiclassical mean value  $I_0$ . We managed to obtain analytical expression for amplitude fluctuation spectrum [7] which allowed us to estimate nanolaser behaviour in the bad-cavity regime  $I_s \ll 1$ . Here we observed two different situations: when the pump rate  $r$  is close to its maximum value  $r_m$  then laser generates as in a good-cavity regime (see Fig.1 a, curve 1); when  $r$  is close to threshold  $r_{th}$  then high peak in the amplitude fluctuations spectrum appears which indicates on the relaxation oscillation phenomenon (see Fig.1 a, curve 2).

With the help of the master equation for density matrix written in terms of coherent states  $|z\rangle$  we derived stationary equation for the Glauber-Sudarshan P function which is only function of  $|z|^2$  (accurately obtained phase independence of the equation is a result of phase diffusion process). A detailed analysis of the latter equation allowed us to obtain approximated solution for P function [7], which works good when  $cI_s \gg 1$ . We analyzed obtained solution in some special cases. In the good-cavity regime, for the pump parameter centered around  $r_m$  P function can be written as Gaussian distribution (see Fig.1 b) with mean value coincided with the semiclassical intracavity intensity  $I_0$  and with width expressed as a product  $I_0 Q(r, c)$ , where  $Q(r, c)$  is the analytical formula for the Mandel Q parameter obtained by us in [4]. For the values of pump rate lying far below threshold and far above self-quenching points P function behaviour is similar to thermal distribution (P representation for the thermal distribution) converged to delta function when  $r \rightarrow 0$  or  $r \rightarrow \infty$ .

More precise analysis of the approximated solution showed that the region  $r_{th} < r < r_q$  can be split into two subregions according to nanolaser behaviour. In the first subregion  $r < r_m$  the nanolaser behaviour is similar to that of conventional laser. Also in this subregion in strong coupling regime  $c \gg I_s$  and for  $r$  centered around  $r = c/5$  the

P function manifests oscillating behaviour (Fig.1 c). Namely for such parameters early obtained  $Q(r, c)$  reaches small negative values [4]. Probably, this is manifestation of the well-known antibunching phenomenon for a single-emitter. In the second subregion  $r > r_m$  the P function does not have any nonclassical features.

We also investigated the behaviour of P function in the threshold point  $r_{th}$  for three different regimes 1)  $c \ll I_s$  (weak coupling), 2)  $c \approx I_s$  ("intermediate"), 3)  $c \gg I_s$  (strong coupling). In the weak coupling regime the P function has a typical plateau (Fig.1 d, curve 1, plateau is marked by solid straight line), which indicates transition to lasing: from thermal to Gaussian type distribution. As saturation intensity is decreased and the strong coupling regime occurs the maximum of P function moves from zero value of variable  $I$  and the semiclassical threshold behaviour disappears (Fig.1 d, curve 3).

Dynamics of the threshold pump rate in above considered regimes can be approximated by formula  $\tilde{r} = 1 + 4/c - 2/I_s$ . In the weak-coupling regime the last term can be neglected what implies the semiclassical threshold  $\tilde{r} = r_{th} \approx 1 + 4/c$ . When strong-coupling regime occurs then  $\tilde{r} < r_{th}$  what indicates on the transition to thresholdless regime.

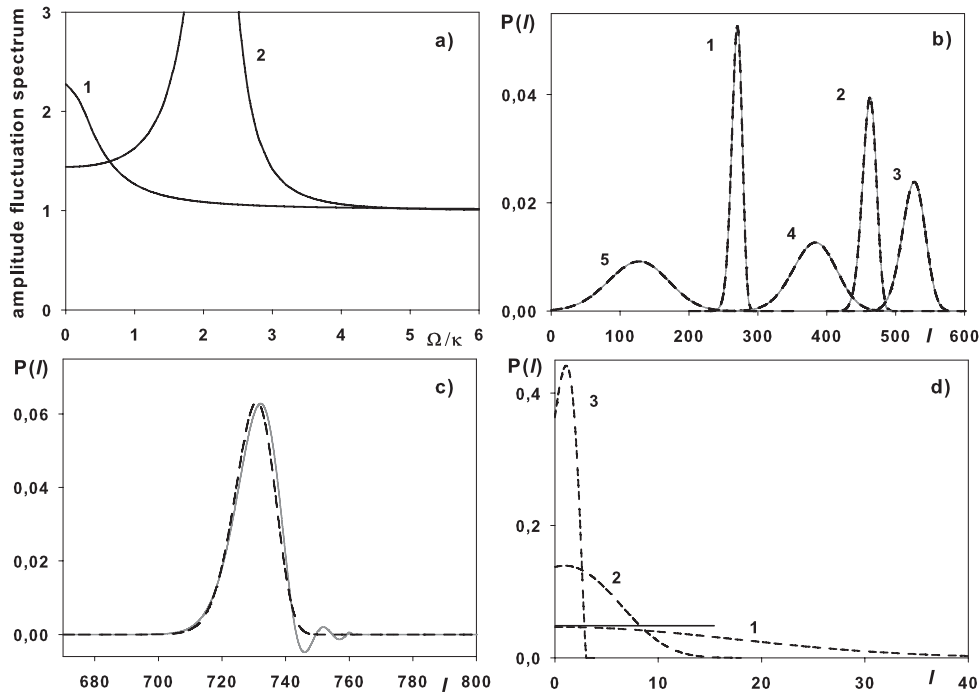


**Fig. 1** a) The amplitude fluctuation spectrum vs dimensionless frequency  $\Omega/\kappa$ : 1)  $r = r_m = 199$ , 2)  $r = 3$ . For all curves  $I_s = 0.2$ ,  $c = 400$ . b) P function vs  $I = |z|^2$  for different pump parameter  $r$ . 1)  $r = 8$ , 2)  $r = 16$ , 3)  $r = 24$ , 4)  $r = 36$ , 5)  $r = 44$ . For all curves  $I_s = 100$ ,  $c = 50$ ; c) Oscillation behaviour of the P function,  $I_s = c = 100$ ,  $r = c/5 = 20$ . d) Transition to thresholdless regime. 1)  $I_s = 600$ , 2)  $I_s = 60$ , 3)  $I_s = 6$ . For all curves  $c = 100$ ,  $r = r_{th} = 1.04$ . Dashed line - obtained approximated solution for P function, solid gray line - numerical simulation of the master equation.

## References

- [1] J. McKeever, A. Boca, A. D. Boozer, J. R. Buck, and H. J. Kimble, "Experimental realization of a one-atom laser in the regime of strong coupling", *Nature* 425, 268-271 (2003).
- [2] F. Dubin, C. Russo, H. G. Barros A. Stute, C. Becher, P. O. Schmidt, and R. Blatt, "Quantum to classical transition in a single-ion laser" *Nature Physics*, Published Online: 28 March 2010.
- [3] M. Nomura, N. Kumagai, S. Iwamoto, Y. Ota, and Y. Arakawa, "Photonic crystal nanocavity laser with a single quantum dot gain", *Optics Express*, 17, 15975 (2009).
- [4] N. Larionov, M. Kolobov, "Analytical results from the quantum theory of a single-emitter nanolaser", *Phys. Rev. A*, 84, 055801 (2011).
- [5] Yi Mu, C.M. Savage, "One-atom lasers", *Phys. Rev. A*. 46, 9, 5944 (1992).
- [6] F. Haake, M. Kolobov, C. Seeger, C. Fabre, E. Giacobino, S. Reynaud, "Quantum noise reduction in stationary superradiance", *Phys. Rev. A*. 54, 2, 1625 (1996).
- [7] N. Larionov, M. Kolobov, "Analytical results from the quantum theory of a single-emitter nanolaser II", <http://arxiv.org/abs/1301.5652>, (2013).

# Capture and Cooling of Atoms in an Optical Trap Formed by Sequences of Counterpropagating Light Pulses

L.P. Yatsenko<sup>1</sup>, V.I. Romanenko<sup>1</sup>, Ye.G. Udovitskaya<sup>1</sup>, A.V. Romanenko<sup>2</sup>, G.A. Kazakov<sup>3</sup>, A.N. Litvinov<sup>3</sup>

<sup>1</sup>*Institute of Physics, Nat. Acad. Sci. of Ukraine (46, Nauka Ave., Kyiv 03028, Ukraine)*

<sup>2</sup>*Taras Shevchenko National University of Kyiv (4, Academician Glushkov Ave., Kyiv 03022, Ukraine)*

<sup>3</sup>*State Polytechnical University of St. Petersburg, (29, Polytechnicheskaya st., St. Petersburg 195251, Russia)*  
yatsenko@iop.kiev.ua

**Abstract:** The motion of atoms in a trap formed by sequences of counter-propagating light pulses has been analyzed. We use Monte-Carlo wave function approach for description of the atomic state, whereas the atomic motion is described by classical mechanics. The motion of trapped atom was shown to be slowed down for properly chosen parameters of the field.

## 1. Introduction

Mechanical action of light on atoms [1–3] is a cornerstone of modern atomic optics. In most cases, the required strengths of light pressure are attained making use of continuous laser radiation, which may be an additional factor that decreases the accuracy of physical experiments owing to light shifts induced by laser radiation. The control of atomic motion with the help of light pulses can be a promising alternative, which would enable the interaction between the atom and the field to be so organized that the atom would be subjected to the action of laser radiation only within a short time intervals [4–7].

The optical trap for atoms proposed in [4] is based of the interaction between atoms and sequences of counter-propagating  $\pi$ -pulses. Figure 1 illustrates the mechanism of trap action. Let light pulses propagate along the  $z$ -axis. An atom at point A has just undergone the action of pulse R propagating from left to right, and soon it will be subjected to the action of pulse L propagating from right to left. If this atom was in the ground state before the action of pulse R, the interaction with the latter transforms it into the excited state with the momentum  $\hbar k$  directed along the  $z$ -axis. After being subjected to the action of pulse L, the atom emits a photon, and its momentum changes by another  $\hbar k$  in the same direction. A similar reasoning for an atom at point B bring us to a conclusion that, owing to the interaction with a pair of counter-propagating pulses, its momentum changes by  $-2\hbar k$ , directed towards point C. Hence, counter-propagating light  $\pi$ -pulses can form a trap for an atom. As was marked in works [4,5], pulses with areas different from  $\pi$  can also be used for this purpose.

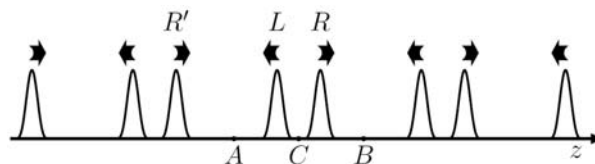


Fig. 1. Sequences of counterpropagating pulses form the trap near C

The frequency detuning of monochromatic counter-propagating waves from the resonance with the frequency of atomic transition is known [8] to bring about the so-called Doppler cooling of atomic ensemble, if the field frequency is lower than the transition one. In work [9], it was shown for the case of low-intensity fields that atoms can also be cooled down in the field of counter-propagating pulses. At the same time, for the analysis of the light trap in the field of counter-propagating pulses, the high intensities of field are required, when the areas of light pulses are close to  $\pi$ .

## 2. Model of atom-field interaction

In this work, we analyze the motion of an atom in a trap formed by light  $\pi$ -pulses. We show that the resonance interaction between the atom and the leads to momentum diffusion of the atoms in the trap. If the carrier frequency of light pulses is detuned from that of atomic transition, a decelerating force emerges under certain conditions, and its influence can prevail over the influence of momentum diffusion. As a result, the amplitude of atom's oscillations in the trap becomes smaller than the wavelengths. At the same time, owing to the momentum diffusion, the equilibrium position of the atom, around which it oscillates (at field antinodes), occasionally changes by half a wavelength. To describe the evolution of atomic state, we use a wave function constructed with the help of the Monte Carlo method [10]. The atom's motion is described in the framework of classical mechanics, which corresponds to a narrow, in comparison with the wavelength, atomic wave packet.

### 3. Results and discussion

Numerical simulation of the atoms motion in a trap formed by sequences of counter-propagating  $\pi$ -pulses with the carrier frequency  $\nu$  coinciding with that of transition in the atom  $\nu_0$  showed that the field heats the atoms due to momentum diffusion. This is expected result, as far as the atom interacts with resonant pulsed standing wave near the center of the trap. When the carrier frequency of the pulses differs from the transition frequency in the atom, heating or cooling of atoms can be observed, depending on the sign and value of the detuning  $\delta = \nu - \nu_0$ . For example, in the case  $\delta=1/T$ , where  $T$  is the pulse repetition period, momentum diffusion is observed. Near  $\delta=1/(2T)$  the transition from heating ( $\delta<1/(2T)$ ) to cooling regime is observed. The parameters of simulation (wavelength and spontaneous emission time) correspond to cooling transitions in Na and Cs [3]. Figure 2 illustrates a time dependence of the coordinate of Na atom for  $\delta = -10$  MHz for one of the random sequences of spontaneous transitions of the excited atom to the ground state. The initial conditions are  $z = 0$  and  $v = 20$  m/s, the pulse duration is 1ps.

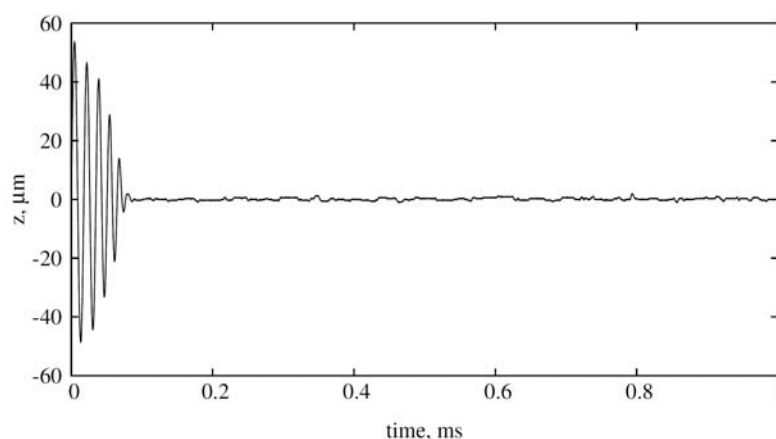


Fig. 2. An example of the time dependence of Na atom coordinate for  $\delta = -10$  MHz

The atom velocity drops to 0.5 m/s approximately after 100  $\mu$ s that corresponds to cooling from 1.1K to 0.7mK, close to Doppler limit 0.5mK. The atom oscillates near the antinodes of light wave, at a short distance from the coordinate origin, much shorter than the light pulse extension in the space.

Besides atoms trapping, possible application of the trap on the basis of counter-propagating light pulses can be trapping of nanoparticles containing a small fraction of atoms (of about 0.1% or smaller) with the transition frequency close to the carrier frequency of light pulses. The laser cooling and trapping of molecules that have closed electronic transitions with diagonal Franck–Condon factors in the analyzed trap may be a new important research area.

- [1] V. G. Minogin and V. S. Letokhov, *Laser Light Pressure on Atoms* (Gordon and Breach, New York, 1987).
- [2] A. P. Kazantsev, G. I. Surdutovich, and V. P. Yakovlev, *Mechanical Action of Light on Atoms* (World Scientific, Singapore, 1990).
- [3] H. J. Metcalf and P. van der Stratten, *Laser Cooling and Trapping* (Springer-Verlag, New York, Berlin, Heidelberg, 1999).
- [4] T. G. M. Freegarde, J. Waltz, and W. Hänsch, “Confinement and manipulation of atoms using short laser pulses”, *Opt. Commun.* **117**, 262–267 (1995).
- [5] A. Goepfert, I. Bloch, D. Haubrich, F. Lison, R. Schütze, R. Wynands, and D. Meshede, “Stimulated focusing and deflection of an atomic beam using picosecond laser pulses”, *Phys. Rev. A* **56**, R3345–3357 (1997).
- [6] V. I. Balykin, “Motion of an atom under the effect of femtosecond laser pulses: from chaos to spatial localization”, *JETP Lett.* **81**, 206–213 (2005).
- [7] V. I. Romanenko and L. P. Yatsenko, “Theory of one-dimensional trapping of atoms by counterpropagating short pulse trains”, *J. Phys. B* **44**, 115305 (2011).
- [8] V. S. Letokhov, V. G. Minogin, B. D. Pavlik, “Cooling and trapping of atoms and molecules by a resonant laser field”, *Opt. Commun.* **19**, 72–76 (1976).
- [9] K. Mølmer, “Limits of Doppler cooling in pulsed laser fields”, *Phys. Rev. Lett.* **66**, 2301–2304 (1991).
- [10] C. Mølmer, Y. Castin, and J. Dalibard, “Monte-Carlo wave function method in quantum optics”, *J. Opt. Soc. Am. B* **10**, 524–538 (1993).

# Quantum Fluctuations of 1D-Dark Dissipative Solitons in a Driven Nonlinear Interferometer

L.A. Nesterov<sup>1,2</sup>, N.A. Veretenov<sup>1,2</sup>, N.N. Rosanov<sup>1-3</sup>

<sup>1</sup>St.-Petersburg National Research University of Information Technologies, Mechanics and Optics, Kronverkskiy pr. 49, St.-Petersburg, 197101, Russia;

<sup>2</sup>Vavilov State Optical Institute, Kadetskaya liniya 5/2, St.-Petersburg, 199053, Russia;

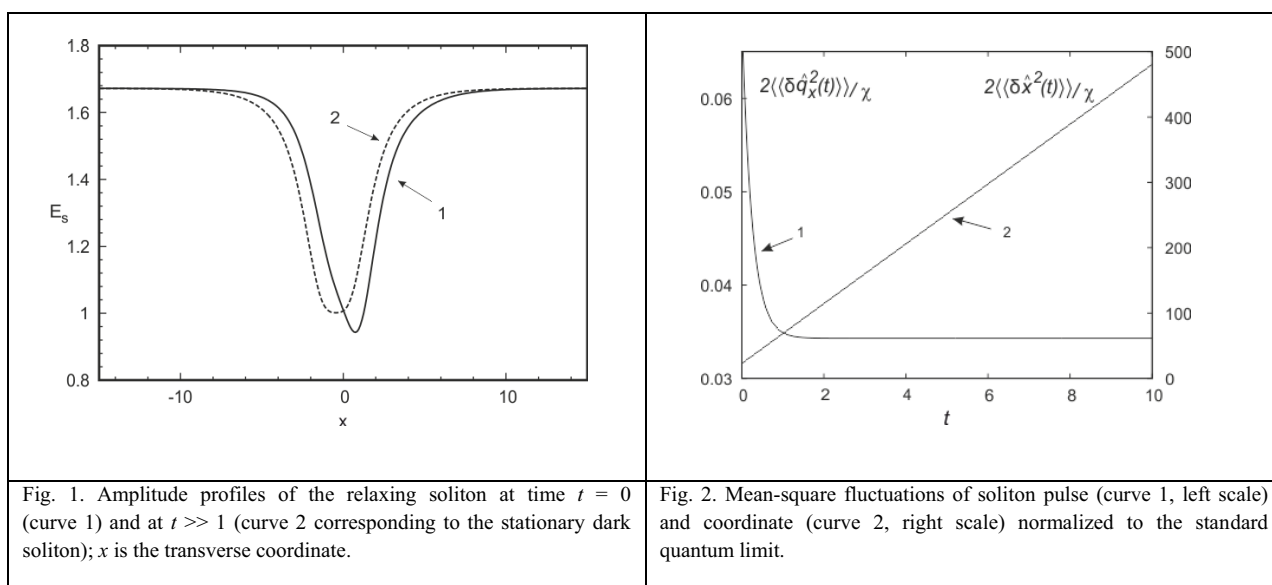
<sup>3</sup>Ioffe Physical Technical Institute, Politekhnicheskaya ul. 26, 194021, Saint-Petersburg, Russia  
e-mail: [nrosanov@yahoo.com](mailto:nrosanov@yahoo.com)

**Abstract:** The theory of quantum fluctuations of spatial dark dissipative solitons in a driven nonlinear interferometer is developed. The formation of soliton states squeezed in pulse is predicted and possible experiments with large squeezing are discussed.

Proposed is the theory of quantum fluctuations of spatial dark dissipative solitons in a wide-aperture driven interferometer with Kerr nonlinearity in the approximation of weak deviations from the classical state of the field in the soliton regime, similarly to the case of bright solitons [1]. In the classical limit, there is a wide variety of dissipative soliton types with different number of intensity oscillations in their central part, and we have found first the parameter domains where these types of solitons exist.

For quantum fluctuation characterization, the quantum Langevin equation was derived, see also [1], which was after that linearized in the vicinity of the stable stationary soliton solution. The eigenvalues spectrum of the linearized equation was studied, and the theory of spectral expansion of arbitrary fluctuations in series of its eigenfunctions was developed. The developed theory allows one to investigate the excitation spectrum of the system considered and to obtain rigorous and unambiguous definition of coordinate operator for dissipative solitons with constant background at infinity. One class of eigenfunctions corresponds to “relaxing solitons” describing dynamics of approach of perturbed solitons to the stationary dark soliton at time  $t \gg 1$ , as illustrated in Fig. 1; relaxing bright solitons have been found earlier in [1].

The mean-square quantum fluctuations of dark soliton coordinate and pulse have been also calculated, and the existence of states squeezed in soliton pulse has been predicted. The parameter region was found where soliton states with the squeezing large with respect to the standard quantum limit (Fig. 2). This squeezing can exceed significantly that for the case of bright solitons. The possibility of squeezed states observation is discussed.



[1] L. A. Nesterov, Al. S. Kiselev, An. S. Kiselev, and N. N. Rosanov, “Quantum fluctuations of spatial dissipative solitons in a nonlinear interferometer,” *Opt. Spectros.* **106**, 570-578 (2009).

# Asymptotic analytical formulas for the static polarizabilities of Rydberg atom or ion

A A Kamenski and V D Ovsianikov

Department of Physics, Voronezh State University, 394006 Voronezh, Russia

Email: san40@bk.ru

The approximation model for describing single-electron Rydberg states of atom or ion are proposed on the basis of method of the Fues' model potential. Scalar and tensor static polarizabilities are presented as asymptotic series with coefficients derived analytically.

Optical lattices present a unique opportunity to create Rydberg-atom traps with suppressed collisions, long storage times, and minimal trap-induced shifts. Microwave spectroscopy of Rydberg atoms trapped in an optical lattice will also allow for high precision spectroscopy of quantum defects and the Rydberg constant. This makes the highly excited atoms attractive for generating entanglement in experiments on quantum computing [1–3].

So while quantum device designing, the simple approximation formulas for lifetimes, polarizabilities etc. are preferred. Evaluating of asymptotic series and corresponding coefficients for the static characteristics of atoms and ions keeps actuality in present time (see, for example, [4]).

The static electric dipole polarizability of  $|nLJM\rangle$ -state atom or ion reads as follows:

$$\alpha_{nLJM} = \alpha_{nLJ}^s + \alpha_{nLJ}^t \frac{3M^2 - J(J+1)}{J(2J-1)}.$$

If the dependence of radial integrals on the fine structure (momentum  $J$ ) is negligible, the scalar and tensor parts may be presented as

$$\alpha_{nL}^s = \frac{2}{3(2L+1)} [LR_{L-1} + (L+1)R_{L+1}], \quad \alpha_{nL}^t = -\frac{2L}{3(2L+1)} \left[ R_{L-1} + \frac{2L-1}{2L+3} R_{L+1} \right], \quad (1)$$

where second-order radial matrix elements contain the radial Green function  $g_{L'}$  with the mean multiplet energy in the subspace of states with angular momentum  $L' = L \pm 1$ :

$$R_{L'} = \langle nL | r g_{L'} r | nL \rangle. \quad (2)$$

The method of the Fues' model potential is used here for evaluating Rydberg-state wave functions in atom or ion. So the radial matrix element (2) may be presented in the form [5], containing  $\Gamma$ -functions, Pochhammer symbols and generalized hypergeometric function  $F_2$  (Appel function) of five parameters:

$$R_{L'} = \frac{\nu^3 (2\lambda_L + 2)_{n_r} [\Gamma(\lambda_L + \lambda_{L'} + 4)]^2}{16Z^4 \Gamma(2\lambda_L + 2) \Gamma(2\lambda_{L'} + 2) n_r!} \times \sum_{k=0}^{\infty} \frac{(2\lambda_{L'} + 2)_k}{k! (k + \lambda_{L'} + 1 - \nu)} [F_2(\lambda_L + \lambda_{L'} + 4; -n_r, -k; 2\lambda_L + 2, 2\lambda_{L'} + 2; 1, 1)]^2. \quad (3)$$

Here the effective principle quantum number  $\nu = \lambda_L + n_r + 1$  is determined by the energy

$$E_{nL} = -\frac{Z^2}{2\nu^2}.$$

It should be taken into account, that the main contribution to the matrix element (3) is given by terms with small difference  $|k - n_r|$ . After complicated transformations of gamma- and hypergeometric function  $F_2$  we present the radial matrix elements (3) in an approximate form. The most suitable is the following asymptotic polynomial in powers of  $1/n$ :

$$R_{L',J'} = B_{L'} n^7 \left( 1 + \frac{b_{L'1}}{n} + \frac{b_{L'2}}{n^2} \right). \quad (4)$$

Here

$$B_{L'} = \frac{9\pi}{4Z^4} \text{ctg}(\pi \xi_{LL'}), \quad b_{L'1} = \frac{35}{36\pi} (\xi_{LL'} \eta_{LL'} + 4) \text{tg}(\pi \xi_{LL'}) - 7\delta_{L'0},$$

$$b_{L'2} = \frac{1}{2} \left( 1 + \frac{\pi(\delta_{L'2} - \delta_{L'2})}{\sin(2\pi\xi_{LL'})} \right) - \frac{1}{12} (\xi_{LL'}^2 + 2)(\eta_{LL'}^2 + 2) - 21\delta_{L'0}^2 - 6\delta_{L'0} b_{L'1};$$

where  $\xi_{LL'} = n_{L'} - n_L - \delta_{L'0} + \delta_{L'0}$ ,  $\eta_{LL'} = n_{L'} + n_L - \delta_{L'0} - \delta_{L'0} - 1$ . The quantum defect parameters  $\delta_{L'0}$ ,  $\delta_{L'2}$  are taken from the Ritz formulae [6].

The analytical form of static polarizability

$$\alpha_{nLJ}^{s,t} = A_{LJ}^{s,t} n^7 \left( 1 + \frac{a_{L1}^{s,t}}{n} + \frac{a_{L2}^{s,t}}{n^2} \right) \quad (5)$$

follows from the matrix element (4). So, in  $L$ -presentation (1) the values  $A_{LJ}^{s,t}$ ,  $a_{Li}^{s,t}$  are combinations of coefficients  $B_{L'}$ ,  $b_{L'i}$ . For example, the scalar polarizability coefficients for s-state (the simplest case) reads:

$$A_0^s = \frac{2}{3} B_1, \quad a_{0i}^s = b_{11}, \quad a_{02}^s = b_{12}.$$

The formulae (4) and corresponding coefficients hold also for the  $J$ -dependent radial matrix elements, with account of  $J$ -dependence of the parameter  $\lambda_L$ .

The presented scheme for evaluating analytically coefficients of static polarizability (5) is general, as it may be used for Rydberg state of every monovalent atom or ion, except for the hydrogen atom due to its degeneration of spectra. Our formulas for such coefficients gives the numerical results in good agreement with corresponding data for helium [7] and alkali metal atoms [4].

[1] Igor I Ryabtsev, Denis B Tretyakov and Ilya I Beterov, " Stark-switching technique for fast quantum gates in Rydberg atoms", *J. Phys. B: At. Mol. Opt. Phys.* **36** 297-306 (2003).

[2] M. Saffman and T. G. Walker, "Analysis of a quantum logic device based on dipole-dipole interactions of optically trapped Rydberg atoms", *Phys.Rev. A* **72**, 022347 (2005).

[3] Markus Muller, Linmei Liang, Igor Lesanovsky and Peter Zoller, "Trapped Rydberg ions: from spin chains to fast quantum gates", *New J. Phys.* **10**, 093009 (2008).

[4] E. Yu. Il'inova, A. A. Kamenski and V. D. Ovsianikov, "Hyperpolarizabilities of Rydberg states in helium and alkali-metal atoms", *J. Phys. B: At. Mol. Opt. Phys.* **42**, 145004 (16pp) (2009).

[5] A.A. Kamenski and V.D. Ovsianikov, "Electric-field-induced redistribution of radiation transition probabilities in atomic multiplet lines", *J. Phys B: At. Mol. Opt. Phys.* **39**, № 9, 2247 – 2265 (2006).

[6] Mohamed Tahar Djerad, "Atomic parameters for transitions involving Rydberg states of singly ionized alkaline earths", *J.Phys. II* **1**, 1 – 9 (1991)[8] Zong-Chao Yan, "Polarizabilities of the Rydberg states of helium", *Physical Review A* **62**, 052502 (5pp) (2000).

[7] Zong-Chao Yan, "Polarizabilities of the Rydberg states of helium", *Physical Review A* **62**, 052502 (5pp) (2000).

# Dynamic back action in imbalanced Michelson interferometer

S.P. Vyatchanin and N.A. Vostrosablin<sup>1</sup>

<sup>1</sup>Physics Department, Moscow State University, Moscow, Russia  
svyatchanin@phys.msu.ru

We consider Michelson interferometer with movable north and east mirrors (Fig. 1) which may demonstrate optical rigidity. For balanced interferometer optical rigidity is unstable. We show that in imbalanced case this model allows to get stable optical spring.

As simplified model of laser gravitational wave antenna we consider Michelson interferometer with power and signal recycling mirrors as shown on Fig. 1 (below we use notations on it). The mirrors in east and north arms may move as free masses, where as power and signal recycling mirror in west and south arms are assumed to be unmovable. The interferometer is pumped through west port.

In case of complete balance optical paths in north and east arms are tuned so that hole output power returns through power recycling mirror in west arm and no mean power goes through signal recycling mirror in south port. In this case one can analyze common and differential modes separately, in particular, common mode interact with sum mechanical mode  $x_+ \equiv x_e + x_n$  and differential one — with  $x_- \equiv x_e - x_n$ . Recall, gravitational wave signal produces change of differential position and analysis of interferometer may be reduced to analysis of Fabry-Perot cavity [1]. If differential optical mode is detuned the circulated light introduces optical rigidity into movement of  $x_-$  [2–4] — it is dynamic back action. Usage of optical rigidity allows dramatically improve the sensitivity of laser gravitational wave antennas [5–8]. The drawback is *instability* (dynamic back action introduces negative damping with rigidity), which has to be compensated by low noise feedback. Another possibility to avoid instability is to use additional pump on detuned frequency [9–11].

Here we show that in the non-balanced case it is possible to introduce *stable* rigidity with *single* pump.

Important, that in non-balanced case common and differential modes are coupled with each other. One may show that equation of movement slow amplitudes  $a_w$ ,  $a_s$  and positions  $x_{\pm}$  may be derived from Hamiltonian

$$\mathcal{H} = \mathcal{H}_e + \mathcal{H}_m + \mathcal{H}_{\text{int}}, \quad \mathcal{H}_e \equiv \hbar\delta_w a_w^\dagger a_w + \hbar\delta_s a_s^\dagger a_s + \hbar\delta(a_s^\dagger a_w + a_s a_w^\dagger), \quad (0.1)$$

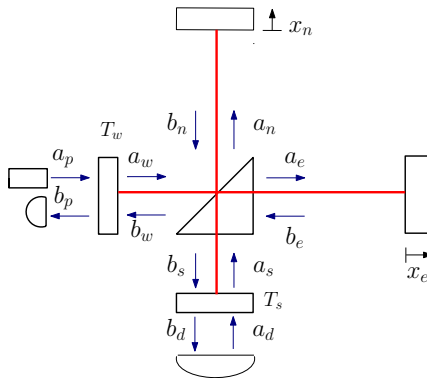


FIG. 1: Michelson interferometer with Power and Signal recycling mirrors.

$$\mathcal{H}_m \equiv \frac{p_+^2 + p_-^2}{2m}, \quad \mathcal{H}_{\text{int}} = \frac{\hbar k}{\tau} [(a_s^\dagger a_s + a_w^\dagger a_w) \chi_+ + (a_w^\dagger a_s + a_s^\dagger a_w) \chi_-]. \quad (0.2)$$

Here  $\delta_w$ ,  $\delta_s$  are detunings introduced into optical sum and differential modes by displacements of power and signal recycling mirrors correspondingly,  $\delta$  is coupling proportional to imbalance between arms (for balance case  $\delta = 0$ ),  $p_\pm$  are momentums corresponding to coordinates  $\chi_\pm$ ,  $m$  are masses of end mirrors (we assume that they are equal to each others).

It is convenient to use transformation from amplitudes  $a_{w,s}$  and detunings  $\delta_{w,s}$  to normal amplitudes  $q_{w,s}$  and detunings  $\tilde{\delta}_{w,s}$  by usual way in order to eliminate ‘‘cross term’’ in  $\mathcal{H}_e$ . The detailed analysis shows that one may choose set of detunings  $\delta_w$ ,  $\delta_s$ ,  $\delta$  by a special way in order to avoid instability.

It may be demonstrated for particular case when movement, for example, of position  $\chi_+$  is fixed (i.e.  $\chi_+ = 0$ ). Then one may obtain equation for  $\chi_-$  in frequency domain (fluctuative forces is omitted):

$$(-m\Omega^2 + K_-)\chi_- = 0, \quad K_- = \text{const} \left\{ \frac{|\tilde{Q}_s|^2 \tilde{\delta}_w}{(\Gamma - i\Omega)^2 + \tilde{\delta}_w^2} + \frac{|\tilde{Q}_w|^2 \tilde{\delta}_s}{(\Gamma - i\Omega)^2 + \tilde{\delta}_s^2} \right\} \quad (0.3)$$

Here  $\tilde{Q}_{w,s}$  are mean amplitudes depending on detuning  $\delta$ ,  $\tilde{\delta}_w$ ,  $\tilde{\delta}_s$  and pump. For simplicity we assume that relaxation rates of normal coordinate are equal to each other and equal to  $\Gamma$ .

Important that form of rigidity  $K_-$  is the same as for the case of double pump [9–11]. Each term in (0.3) is similar to rigidity created by each pump in case of double pump. Hence, we may conclude that rigidity  $K_-$  may be done stable by choosing parameters as for double pump case.

- 
- [1] A. Buonanno, Y. Chen, ‘‘Scaling law in signal recycled laser-interferometer gravitational-wave detectors’’, *Phys. Rev.* **D67**, 062002 (2003).
  - [2] V.B. Braginsky, I.I. Minakova, ‘‘Dynamic back action of position meter on behavior of mechanical oscillator’’, *Vestnik Moskovskogo Universiteta, Seria 3: Fizika i Astronomiya*, No. 1, 83 (1964).
  - [3] V. B. Braginsky, A. B. Manukin, ‘‘About ponderomotive effects of ‘electromagnetic radiation’’, *Sov. Phys. JETP* **25**, 653 (1967).
  - [4] V. B. Braginsky, A. B. Manukin, M. Yu. Tikhonov, ‘‘Investigation of dissipative ponderomotive effects of electromagnetic radiation’’, *Sov. Phys. JETP* **31**, 829 (1970).
  - [5] V.B.Braginsky, F.Ya.Khalili, Low-noise rigidity in quantum measurements, *Physics Letters* **A257**, 241-246 (1999).
  - [6] F.Ya.Khalili, Frequency-dependent rigidity in large-scale interferometric gravitational-wave detectors, *Physics Letters* **A288**, 251-256 (2001).
  - [7] V.I. Lazebny, S.P. Vyatchanin, ‘‘Optical rigidity in signal-recycled configurations of laser gravitational-wave detectors’’, *Physics Letter* **A344**, 7 (2005).
  - [8] F.Y. Khalili, V.I. Lazebny, S.P. Vyatchanin, ‘‘Sub-standard-quantum-limit sensitivity via optical rigidity in the advanced LIGO interferometer with optical losses’’, *Physical Review* **D73**, 062002 (2006).
  - [9] H. Rehbein, H. Mueller-Ebhardt, K. Somiya, S. L. Danilishin, R. Schnabel, K. Danzmann, Y. Chen, ‘‘Double optical spring enhancement for gravitational-wave detectors’’, *Phys. Rev.* **D78**, 062003 (2008).
  - [10] A.A. Rakhubovsky, S. Hild, S.P. Vyatchanin, ‘‘Stable double-resonance optical spring in laser gravitational-wave detectors’’, *Phys. Rev.* **D84**, 062002 (2011).
  - [11] A.A. Rakhubovsky, S.P. Vyatchanin, ‘‘Sensitivity of laser gravitational-wave detectors with stable double-pumped optical spring’’, *Physics Letters* **A376**, 1405 (2012).

# Semiclassical Study of Sub-Doppler Laser Cooling of Magnesium Atoms Using $3^3P_2 \rightarrow 3^3D_3$ Dipole Transition

D.V. Brazhnikov, A.E. Bonert, A.N. Goncharov, A.M. Shilov,  
A.V. Taichenachev, A.M. Tumaikin, V.I. Yudin, K.S. Tabatchikova  
*Institute of Laser Physics SB RAS, pr. Lavrent'eva 13/3, 630090 Novosibirsk, Russia*  
*Novosibirsk State University, ul. Pirogova 2, 630090 Novosibirsk, Russia*  
*Novosibirsk State Technical University, pr. Karla Marksa 20, 630092 Novosibirsk, Russia*  
LLF@laser.nsc.ru

**Abstract:** Theoretical analysis of laser cooling of  $^{24}\text{Mg}$  atoms using  $3^3P_2 \rightarrow 3^3D_3$  transition out of limits of slow atoms approximation and for arbitrary field intensity is presented. The temperature as low as several microkelvins can be achieved.

Frequency standards play significant role in many fundamental and applied investigations. At present, microwave frequency standards, based on the cold cesium atoms, have relative uncertainty of the order of  $10^{-16}$  [1]. These types of standards, most likely, have reached their limit of potential accuracy. Major hopes for significantly enhancing metrological properties of frequency standards are connected with the optical spectral band. In this direction in the past few years an increased attention have been being paid to optical clocks based on a laser-cooled single ion confined in an electromagnetic trap [2] or on large number of atoms trapped in an optical lattice [3]. The relative frequency uncertainty of these standards of the orders of  $10^{-17}$ - $10^{-18}$  is expected.

For a few reasons, ones of the main candidates for producing the new-generation frequency standards are alkaline earth and alkaline-earth-like atoms: Yb, Ca, Sr, Hg and Mg. To date, atoms of the first four elements can be effectively cooled down to the recoil energy limit [4,5] and even below to obtain the Bose-Einstein condensate [6]. But long time researchers have not been able to reach the same success with Mg atoms [7]. Recently some good experimental results have been achieved in the Hannover University [8]. In the experiments small number of ultracold atoms ( $N=5000$ ,  $T=5 \mu\text{K}$ ) was confined in a dipole trap.

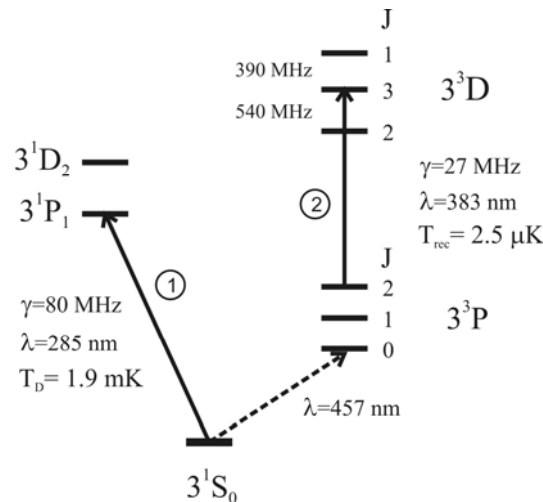


Fig. 1. Relevant energy levels of  $^{24}\text{Mg}$ : solid lines denote the cooling transitions (the 1<sup>st</sup> and the 2<sup>nd</sup> stages with corresponding temperature limits), dashed line corresponds to the highly-forbidden transition that can be used for the laser stabilization (“clock” transition). The distances between the levels are not in scale

The present research is aimed to theoretical analysis of deep laser cooling of magnesium atoms, using electro-dipole transition  $3^3P_2 \rightarrow 3^3D_3$  (see Fig.1) and to make recommendations for maximizing the fraction of cold atoms in a cloud. The energy levels of the transition are degenerate, what allows one to realize the sub-Doppler laser cooling by polarization levels of the transition [9]. The regular semiclassical approach, based on the Fokker-Planck equation for the momentum distribution function, is exploited. At that, the problem is solved out of limits of the slow atoms approximation. By overcoming this limit we are able to investigate kinetic properties of the atomic cloud in a wide range by intensity and frequency detuning of the light field. Here, without going into mathematical details, we present a number of graphical results. The one-dimensional light field configuration, composed of two counterpropagating plane waves with opposite circular polarizations, is considered.

Figures 2a and 2b represent the dependences of average atomic kinetic energy on the laser field intensity (or more exactly on the ratio  $R^2/\gamma^2$ , with  $R$  the Rabi frequency and  $\gamma$  the spontaneous decay rate) and on the frequency detuning  $\delta$  in  $\gamma$  units. By analyzing such plots for different intensities one can figure out that the

lowest achievable kinetic energy is about  $20 \times E_{\text{rec}}$  [10], where  $E_{\text{rec}}$  is the recoil energy. This value is sufficiently large for further applications of cooled atoms (e.g. for loading an optical lattice). In the present work we suggest the way for overcoming this problem with keeping of essential part of cold atoms in a cloud. Let us consider the momentum distribution of cold atoms in various cases of the light field intensity. As it follows from Fig.2c, the distribution profile can be quite “nonmaxwellian” with narrow and high-contrast spike at the center (solid line). This spike corresponds to the coldest atoms, while the wide base characterizes “hot” ones. The new task hereby arises: what conditions do maximize the relative area under the spike? Assume the atoms to name “cold” if their momentum is less than, for example,  $3 \times \hbar k$ . Fig.2d shows that the relative number of cold atoms has maximum at the certain intensity. In other words, the relative number of cold atoms in a cloud can be maximized by proper choice of the field parameters. After the sub-Doppler laser cooling the atoms can be loaded into a dipole trap. Its depth can be selected so that the only cold atoms (corresponding to the spike) will be confined in it. In that case an effective temperature of the cloud will be defined by the width of the narrow spike (just several  $\mu\text{K}$ ).

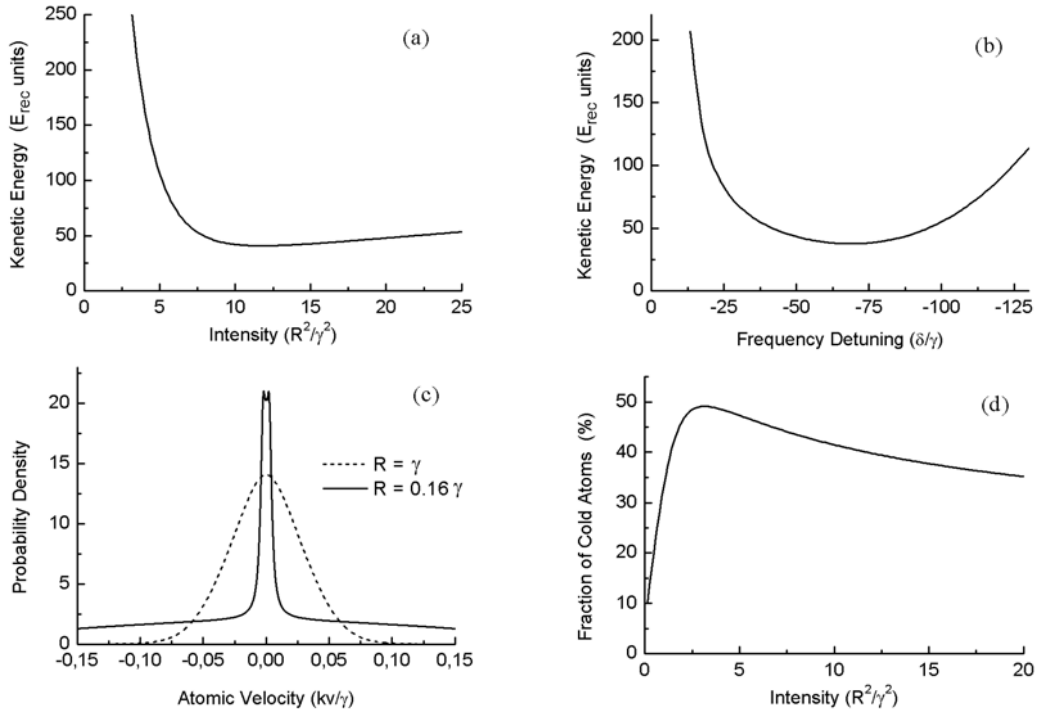


Fig. 2. Average kinetic energy of atom in a cloud as the functions of *a*) light intensity (proportional to the Rabi frequency in a square) and *b*) frequency detuning at  $R=0.7\gamma$ . *c*) The examples of momentum atomic distributions in various light-field intensity regimes. *d*) Relative fraction of cold atoms in a cloud as the function of the light intensity. For the figures *a*), *c*) and *d*) frequency detuning equals to  $-2\gamma$

The work is supported by the Ministry of Education and Science of the Russian Federation in the frame of the Program “Scientific and scientific-pedagogical personnel of innovative Russia” (the Contract no. 16.740.11.0466 and the Agreement no. 8387), by RFBR (grants nos. 12-02-00454, 12-02-00403, 11-02-00775, 11-02-01240), by the Presidium of Siberian Branch of Russian Academy of Sciences and the Russian Quantum Center. The young scientists D.V. Brazhnikov, A.M. Shilov and K.S. Tabatchikova are also supported by the Presidential Grant MK-3372.2912.2 and the RFBR Grant 12-02-31208-“mol\_a”.

- [1] T.E. Parker, “Long-term comparison of caesium fountain primary frequency standards”, *Metrologia* **47**, 1-10 (2010).
- [2] T. Rosenband, D.B. Hume, P.O. Schmidt et al., “Frequency ratio of  $\text{Al}^+$  and  $\text{Hg}^+$  single-ion optical clocks. Metrology at the 17th decimal place”, *Science* **319**, 1808-1812 (2008).
- [3] H. Katori, “Optical lattice clocks and quantum metrology”, *Nature Photonics* **5**, 203-210 (2011).
- [4] C. Degenhardt, H. Stoehr, Ch. Lisdat et al., “Calcium optical frequency standard with ultracold atoms: Approaching  $10^{-15}$  relative uncertainty”, *Phys. Rev. A* **72**, 062111 (2005).
- [5] S. Mejri, J.J. McFerran, L. Yi et al., “Ultraviolet laser spectroscopy of neutral mercury in a one-dimensional optical lattice”, *Phys. Rev. A* **84**, 032507 (2011).
- [6] S. Sugawa et al., “Bose-Einstein condensate in gases of rare atomic species”, *Phys. Rev. A* **84**, 011610 (2011).
- [7] T.E. Mehlstäubler, K. Moldenhauer, M. Riedmann et al., “Observation of sub-Doppler temperatures in bosonic magnesium”, *Phys. Rev. A* **77**, 021402 (2008).
- [8] M. Riedmann, H. Kelkar, T. Wübena et al., “Beating the density limit by continuously loading a dipole trap from millikelvin-hot magnesium atoms”, *Phys. Rev. A* **86**, 043416 (2012).
- [9] J. Dalibard and C. Cohen-Tannoudji, “Laser cooling below the Doppler limit by polarization gradients: simple theoretical models”, *J. Opt. Soc. Am. B* **6**(11), 2023-2045 (1989).
- [10] D.V. Brazhnikov, A.E. Bonert, A.N. Goncharov et al., “Study of a possibility of deep laser cooling of magnesium atoms for designing the new-generation frequency standard”, *Vestnik NSU, Series “Physics”*, Vol. **7**, Is. 4, 6-18 (2012) [in Russian].

# Advanced LIGO imbalanced scheme

Vostrosablin N.A.\*, Vyatchanin S.P.

*Physics Faculty, Moscow State University  
Leninskie gori, Moscow, 119991 Russia  
\*E-mail: vostrosablin@physics.msu.ru*

**Abstract:** Laser interferometer gravitational-wave observatory (LIGO) is designed to detect gravitational waves and to become a tool in the study of their sources [1]. We consider a DC readout scheme which will be applied in Advanced LIGO. We analyze such scheme in terms of quantum noise and we calculate its spectral density.

Existence of gravitational waves was predicted by Einstein in his general theory of relativity. Soon new generation of antennas will be launched (Advanced LIGO). These antennas will be significantly upgraded. One of the modifications will be the transition from heterodyne to DC readout scheme. This scheme has a number of advantages: reduction of influence of technical noise sources is expected, noise which is brought by the heterodyne scheme is completely eliminated. Besides DC readout scheme is a particular case of homodyne detection and we want to emphasize that so-called local oscillator wave will be automatically stabilized using the filtering properties of Fabry-Pero cavities in interferometer arms.

Technical implementation of such scheme is also simpler than in homodyne and heterodyne detections [2]. The main idea is to produce an imbalance in interferometer scheme in order to obtain a small constant power on a photo detector that will play a role of a local oscillator. In this case only one photo detector is necessary instead of two identical detectors in homodyne detection. Laser gravitational-wave antenna consist of Michelson interferometer with Fabry-Pero resonators in its north and east arms as shown on Fig. 1. There are two ways to produce such imbalance: to vary distance between resonator Fabry-Pero and beam splitter holding arm length constant; to displace a distant mirror in each resonator in opposite sides, without varying distance between beam splitter and interferometer. We consider the second way.

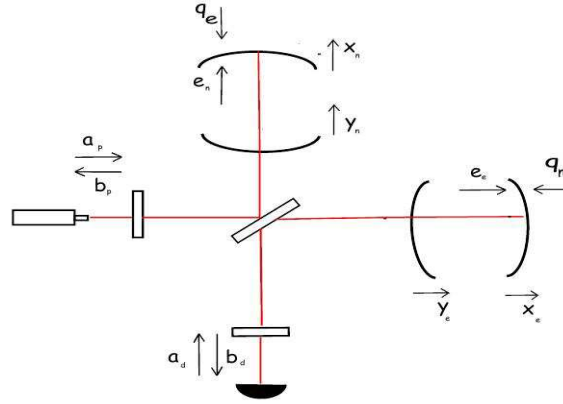


Fig 1: Advanced LIGO scheme

A well known effect of so-called optical rigidity exist in such optomechanical systems [3-8]. It means that the back-action force acting on mirrors depends on coordinate of mirror. Complex coefficient in this relation will be the mentioned optical rigidity  $K$ . In LIGO system two mechanical modes exist – differential and common modes. Differential mode keeps information about signal. For both modes we can write down two independent equations of motion in spectral representation:

$$-\mu \Omega^2 z_+ + K_+ z_+ = 0, \quad (1)$$

$$-\mu \Omega^2 z_- + K_- z_- = 0, \quad (2)$$

where  $\mu$  – is the mirrors' reduced mass,  $K_{+,-}$  – optical rigidities,  $\Omega$  – signal frequency.

In the case of detuned system situation changes: additional cross-rigidities appear. Then we can rewrite equations of motion (they won't be independent any more):

$$-\mu \Omega^2 z_+ + K_{++} z_+ + K_{+-} z_- = 0, \quad (3)$$

$$-\mu \Omega^2 z_- + K_{--} z_- + K_{-+} z_+ = 0, \quad (4)$$

It resembles a system of coupled oscillators with couple coefficients  $K_{+-}$  and  $K_{-+}$ . In this case in the output additional quantum noise relied with laser fluctuations appears because of coupling of modes. We give a theoretical description of fields circulating in such system and forces acting on mirrors. We consider small power in the output is 80 mW while power circulating in both east and north arms is 800 MW. To realize this situation we have to detune distant mirrors in Fabry-Pero resonators by the small value of  $0.06 \text{ sec}^{-1}$ . For this case we calculate spectral densities of current fluctuations on the photo detector. We consider this value in terms of space-time metric  $h$  and we normalize it on a standard quantum limit:  $\sqrt{\frac{S_h}{h_{SQL}}}$ . Results of numerical analysis

are represented in Fig.2. As we can see influence of additional quantum noise will not very significant. So we can conclude that using of DC readout scheme is appropriate despite additional noise introduced into the system.

We also consider an asymmetry in arms when transition coefficients and losses differ in east and north arms:  $\frac{\delta T_{ITM}}{T_{ITM}} \sim \pm 1\%$ ,  $T_{BS} - R_{BS} \sim [0.5 \dots 1\%]$ ,  $\frac{\delta A_{loss}}{A_{loss}} \sim [30 \dots 50\%]$ ,  $A_{loss} \sim 50 \text{ ppm}$ . Here  $T_{ITM}$  - transition coefficient of input mirror of resonator Fabry-Pero,  $T_{BS}$  and  $R_{BS}$  - transition and reflection coefficients of beam splitter,  $A_{loss}$  - losses in distant mirrors of resonators in arms. We show that such asymmetry will not greatly affect on the sensitivity of detector.

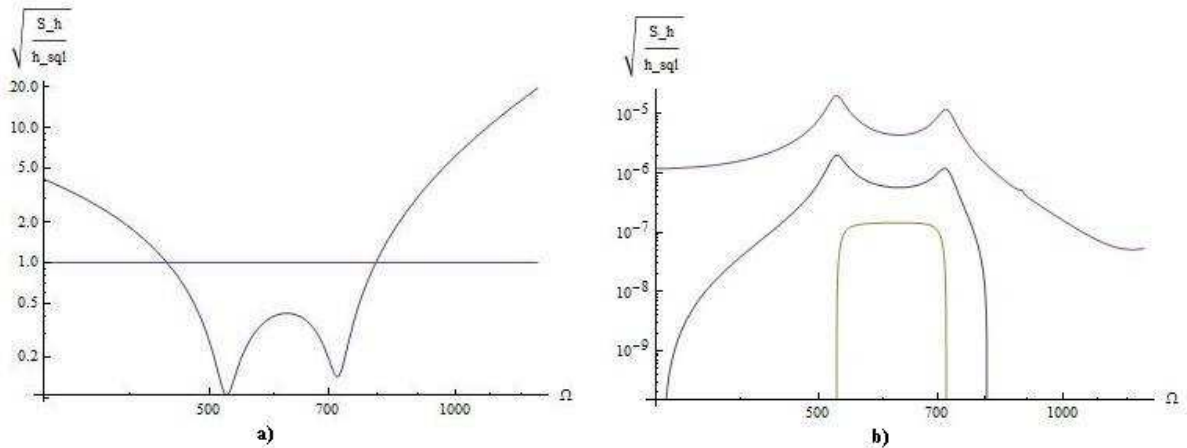


Figure 2: a) spectral density of quantum noise of imbalanced aLIGO scheme b) difference between imbalanced and balanced scheme spectral densities for different levels of laser noise relatively zero quantum fluctuations

## References:

- [1] Abbot B.P. (et al.), "LIGO: the Laser Interferometer Gravitational-wave Observatory," Reports on Progress in Physics. – 2009. – V.72. –P.0769
- [2] McKenzie K., Gray M.B., Lam P.G., McClelland D.E., "Technical limitations to homodyne detection at audio frequencies," Appl. Opt. – 2007.-V.46.-P.3389-3395
- [3] V.B. Braginsky, I.I. Minakova, "Dynamic back action of position meter on behavior of mechanical oscillator", Vestnik Moskovskogo Universiteta, Seria 3: fizika I Astronomiya, No. 1, 83 (1964)
- [4] V.B. Braginsky, A.B. Manukin, "About ponderomotive effects of electromagnetic radiation", Sov. Phys. JETP 25, 653 (1967)
- [5] V.B. Braginsky, A.B. Manukin, M. Yu. Tikhonov, "Investigation of dissipative ponderomotive effects of electromagnetic radiation", Sov. Phys. JETP 31, 829 (1970)
- [6] V.B. Braginsky, F.Ya. Khalili, "Low-noise rigidity in quantum measurements", Physics Letters A 257, 241-246 (1999)
- [7] F.Ya. Khalili, Frequency-dependent rigidity in large-scale interferometric gravitational-wave detectors, Physics Letters A 288, 251-256 (2001).
- [8] Lazeby V.I., Vyatchanin S.P., "Optical rigidity in signal-recycled configurations of laser gravitational-wave detectors," Physics Letters. – 2005. – V.344, N 1. – P.7-1

# Adaptive Quantum Measurement in Gravitational-Wave Detectors

Korobko Mikhail\*, Kiriukhin Oleg\*\*

Faculty of Physics, M.V. Lomonosov Moscow State University, Russia, Moscow, 119991, GSP-1, Leninskie Gory, 1, bld. 2

\*korobko@physics.msu.ru

\*\*kiryukhin@physics.msu.ru

**Abstract:** Second-generation gravitational-wave detectors will be quantum noise limited. We introduce an original method of overcoming this limit, called Standard Quantum Limit (SQL). Our method – adaptive quantum measurements – allows to overcome SQL without significant modification of experimental scheme.

## 1. Introduction

Contemporary so-called second-generation gravitational-wave detectors (such as Advanced LIGO [1,2], Advanced VIRGO [3], and LCGT [4], which are under construction now) will be quantum noise limited. Two kinds quantum noises will limit the sensitivity: at high gravitational wave frequencies the phase fluctuations of the light inside the interferometer (shot noise) and the random force created by the amplitude fluctuations of the light (radiation-pressure noise) at low gravitational wave frequencies. For a balanced detector the best sensitivity point - where these two noise sources become equal - is known as the Standard Quantum Limit (SQL) [5]. In the linear position meter (the gravitational-wave interferometer is special case of it) the shot noise corresponds to the measurement noise and radiation pressure noise - to the back-action noise. Spectral densities of these noises obey the Heisenberg uncertainty relation [5].

The SQL is not an absolute limit for measurement precision: there are few methods of overcoming it in gravitational-wave detectors. The most well-known examples are: Quantum Non-Demolition (QND) measurements, that suppose using the Hamiltonian of interaction the test body and measurement device, which commutes with operator of measured quantity [5,6], and Back-Action Evading (BAE) measurements [6-9], that use the correlation between the measurement noise and the back-action noise [9,12,13].

The application of these methods is planned for the third generation detectors (like Einstein Telescope gravitational-wave detector) - to provide a sensitivity better than the SQL. However, both of them require sufficient modification of existing experimental schemes and have some technical difficulties (e.g. variational-readout scheme is sensitive to optical losses).

We offer another approach based on non-stationary measurements – so-called adaptive linear measurements in which parameters of the experimental scheme change depending on the result of the previous measurements. In this work we introduce original method of adaptive measurements of the impulse force with unknown arrival time using homodyne detector with homodyne phase that changes depending on previous measurements. We also demonstrate advantages of this approach to conventional measurements. Furthermore, we provide general method for the creation of schemes for quantum adaptive measurement and discuss possible application of this approach.

## 2. Adaptive method

For the introduction of the adaptive method let's consider the following simple two-step procedure. We consider a system of the mechanical oscillator and the linear position meter. We suppose that some impulse force with unknown arrival time acts on the oscillator:  $F(t) = F_0 \delta(t - \tau)$ , where  $\tau$  is arrival time. The goal is to measure the amplitude of this force, but we can't do it without knowing the arrival time. To solve this task we introduce the following adaptive algorithm:

*First Step.* We measure two quadratures of the oscillator with the same precision. These measurements are quite weak, because we want only to get some information about the state of the oscillator without perturbing it significantly.

*Computation.* Knowing these quadratures we can calculate the estimation for the arrival time. Knowing the estimated arrival time we can estimate in which quadrature lies the signal and then measure this quadrature.

*Second step.* We measure the estimated quadrature with maximal precision and obtain value for the force amplitude.

The final precision we get would be better than SQL for this system. To illustrate this, we consider the more complex but realistic system.

## 3. Optomechanical system

We consider the optomechanical system with an optical homodyne detection. The idea of the procedure is almost the same – we measure the combination of two optical quadratures, then we obtain some information about the arrival time, use this information for the next measurement, and continue the procedure until we get good estimation. The measured signal can be written down in terms of quantum optical quadratures  $\hat{a}_{1,2}(t)$  :

$$\hat{y}(t) = \hat{a}_1(t) \cos \zeta(t) + \hat{a}_2 \sin \zeta(t) + \frac{\alpha}{\hbar} \left( \frac{F_0}{m \omega_m} \sin \omega_m(t - \tau) + \alpha \int_0^t dt_1 G(t - t_1) \hat{a}_1(t_1) \right) \sin \zeta(t)$$

where  $\alpha$  is coupling constant,  $G(t)$  is Green function of the the oscillator, and  $\zeta(t)$  is homodyne angle.

We use BLUE (best linear unbiased estimation) to estimate arrival time from this signal and then we apply this information to the second stage. On the second stage we proceed variational measurements in order to evade the back-action. From the signal obtained on the second stage we choose the homodyne angle that allows to evade the back-action (partially) on the next cycle of the measurement. Finally we have the algorithm for changing the homodyne angle at each step of procedure depending on the result of all previous measurements.

We also introduce different adaptive algorithms and discuss their possible application to more complex systems and to macroscopic quantum measurements in general.

#### 4. References

- [1] [www.advancedligo.mit.edu](http://www.advancedligo.mit.edu).
- [2] G.M.Harry (for the LIGO Scientific Collaboration), “Advanced ligo: the next generation of gravitational wave detectors.” *Classical and Quantum Gravity*, 27:084006, 2010.
- [3] <http://www.cascina.virgo.infn.it/advirgo/>.
- [4] <http://www.icrr.u-tokyo.ac.jp/gr/LCGT.html>.
- [5] V.B.Braginsky, F.Ya.Khalili, “Quantum Measurement”, Cambridge University Press, 1992.
- [6] V. B. Braginsky, F. Ya. Khalili, “Gravitational wave antenna with QND speed meter”, *Physics Letters A*, 147:251–256, 1990.
- [7] A. Buonanno, Y. Chen, “Quantum noise in second generation, signal-recycled laser interferometric gravitational-wave detectors”, *Physical Review D*, 64(4):1–21, July 2001.
- [8] F.Ya.Khalili, “Frequency-dependent rigidity in large-scale interferometric gravitational-wave detectors”, *Physics Letters A*, 288:251–256, 2001.
- [9] H.J.Kimble, Yu.Levin, A.B.Matsko, K.S.Thorne and S.P.Vyatchanin, “Conversion of conventional gravitational-wave interferometers into qnd interferometers by modifying their input and/or output optics”, *Physical Review D*, 65:022002, 2001.
- [10] V.B.Braginsky, Yu.I.Vorontsov, F.Ya.Khalili, “Quantum features of the pondermotive meter of electromagnetic energy”, *Sov. Phys. JETP*, 46:705, 1977.
- [11] V. B. Braginsky, F. Ya. Khalili, “Quantum nondemolition measurements: the route from toys to tools”, *Review of Modern Physics*, 68:1–11, 1996.
- [12] W.G.Unruh. In P.Meystre and M.O.Scully, editor, “Quantum Optics, Experimental Gravitation, and Measurement Theory”, page 647. Plenum Press, New York, 1982.
- [13] M.T.Jaekel and S.Reynaud, “Quantum limits in interferometric measurements”, *Euro-physics Letters*, 13:301, 1990.
- [14] S.P.Vyatchanin and A.B.Matsko, “Quantum variation scheme of measurement of force and compensation of back action in intereferometric meter of position”, *Sov. Phys. JETP*, 83:690–697, 1996.

# Collimation of thulium atomic beam by two-dimensional optical molasses

E. Kalganova, D. Sukachev, G. Vishnyakova, A. Sokolov N. Kolachevsky and V. Sorokin

*P. N. Lebedev Physics Institute, Leninsky Prospekt 53, Moscow 119991, Russia  
Moscow Institute of Physics and Technology, Institutskii per. 9, Dolgoprudny 141700, Russia  
Russian Quantum Center, SKOLKOVO, Moscow region, 143025, Russia  
e-mail address: [kalganova.elena@gmail.com](mailto:kalganova.elena@gmail.com)*

**Abstract:** We have increased the number of laser cooled and trapped thulium atoms in a magneto-optical trap (MOT) by a factor of 3 using a two-dimensional optical molasses which collimates an atomic beam before a Zeeman slower. Also we have devised a semiconductor laser amplifier operating at 410.6 nm to form laser beams for optical molasses.

Laser cooling and magneto-optical trapping are well-known methods for cooling neutral atoms which find applications in various spectroscopic and condense-matter studies. An important task is to capture larger amounts of atoms to increase the signal-to-noise ratio and/or number density.

We have achieved threefold increase of the number of thulium atoms trapped in a MOT using two-dimensional optical molasses. The MOT described in our earlier work [1] is loaded from a decelerated atomic beam. Tm vapor is produced in an oven and atoms pass through the diaphragm D1 (Fig. 1) into the Zeeman slower where they are decelerated. To increase the fraction of atoms that pass through the second diaphragm D2 and reach the trapping region the atomic beam has been collimated by two-dimensional optical molasses. The optical molasses are formed before the Zeeman slower in the plane perpendicular to its axis by two orthogonal pairs of antipropagating laser beams.

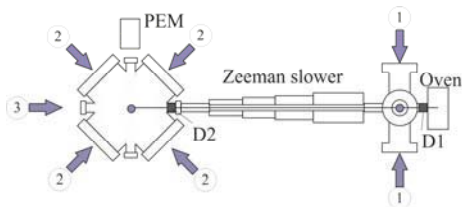


Fig.1 Experimental setup. D1, D2 – diaphragms forming atomic beam, 1- collimating laser beams, 2 – cooling laser beams, 3 – laser beam for the Zeeman slower

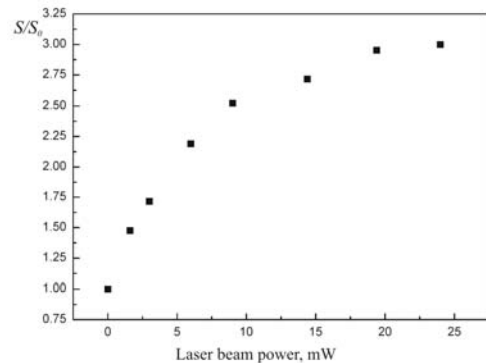


Fig.2 The relative change in the number of atoms in the MOT vs. the cooling laser beam power. The red detuning is 10 MHz ( $1\gamma$ )

Laser cooling of Tm atoms is performed on strong transition at 410.6 nm by the second harmonic of Ti:sapphire laser. The total power of cooling laser light is 100 mW. The major part of this power is used for the MOT and the Zeeman slower, and the rest 4 mW are injected into the specially designed semiconductor laser and amplified up to 200 mW. The amplified radiation is used for two-dimensional molasses. The laser frequency is red detuned from the resonance by acousto-optic modulator.

The number of trapped atoms is measured by the luminescence signal of the atomic cloud that is detected by the photomultiplier tube. The luminescence signal is proportional to the amount of atoms in the trap, so the effect of the atomic beam collimation can be easily characterized. A number of experiments have been carried out with different cooling laser frequency detunings from the resonance. The largest effect was observed with the red detuning of 10 MHz (corresponding to  $1\gamma$ , the natural line width). In this case the number of trapped atoms was increased by a factor of three (Fig.2).

[1] D. Sukachev, A. Sokolov, K. Chebakov, A. Akimov, S. Kanorsky, N. Kolachevsky and V. Sorokin, "Magneto-optical trap for thulium atoms," PHYSICAL REVIEW A **82**, 011405(R) (2010).

# Methods of approximation of whispering gallery modes eigenfrequencies in rotational bodies

Yury A. Demchenko

Moscow State University, 119991, Leninskie Gory, Moscow, Russia

wanderblum@mail.ru

## Abstract

This work is devoted to approximate calculation of eigenfrequencies of WGM in bodies of revolution. The calculations were performed for toroidal cavity and strongly oblate spheroidal cavity. Also approximation have been refined for dielectric cavity.

## 1 Introduction

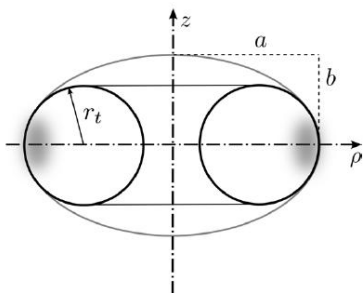
The problem of eigenfrequency's precision for cavity with WGM modes is not only fundamental, but it plays a great role in creation of tiny optical comb based on WGM modes [1].

Since the problem of finding the eigenfrequencies can not be solved in general form for an arbitrary shape of the resonator, it is necessary to resort to approximate methods.

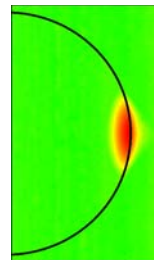
## 2 Calculation

The most accurate result for the eigenfrequencies of WGM is given by the eikonal method. This semi-classical method is used to find the asymptotic solution of the Helmholtz equation, if the refractive index varies slightly compared with the wavelength. If we combine the eikonal method with the modified Bohr-Sommerfeld quantization condition, we can obtain an approximation for the eigenfrequencies.

For WGM we can introduce the concept of the caustic surface. This is a surface that is tangent to rays propagating in the cavity. In this work we consider modes with large azimuthal number and in this case approach that caustic surface lies close to the surface is quite accurate.



Approximation of spheroid with toroid



Field distribution in dielectric resonator

In the papers [2, 3] eigenfrequency were obtained for spheroidal cavities and resonators, which are defined by a quartic surface. These calculations give great accuracy for prolate cavities, but for oblate cavities accuracy of the approximation is very small. This is due to the fact that the caustic surface and the surface of the cavity are no longer close for oblate cavities and caustic surface stops well described nested spheroid.

Using eikonal method new formula was obtained for the eigenfrequency of the toroid (2), which is comparable in accuracy to existing formulas, which were obtained in [3].

Since the resulting formula divergences for large oblate, it was an attempt to approximately solve the Helmholtz equation in spheroidal coordinates, which can be divided into angular and radial. The angular field distribution is well approximated by Gause function. For the radial distribution of the field, we used the method of Olver [4]. It allows us to obtain asymptotic expressions for the solutions

of differential equations with a large parameter. Using this method, we got expressions that do not quite accurately describe the natural frequencies. Also managed to guess the type of solution that fairly accurately approximated the eigenfrequency of the strongly flattened resonator.

If the resonator is dielectric, the resonator field is not equal to 0 at the boundary of the cavity (2). As is known, the total internal reflection occurs not on a dielectric boundary, but on the surface located behind it. In this case, we can use the already obtained formulas for the eigenfrequencies, but for a resonator with effective parameters. Assuming that the caustic surface is located close to the surface of the resonator we obtained a formula for the average distance by which the boundary shifts in reflection. This calculation increase the precision of eigenfrequency's more than 10 times compared to the result in [2].

## References

- [1] Savchenkov A. A., Matsko A. B., Liang W., Ilchenko V. S., Seidel D. and Maleki L., Kerr combs with selectable central frequency, *Nature Photonics* vol. 5 may 2011
- [2] Gorodetsky M. L., Fomin A.E. Geometrical Theory of Whispering-Gallery Modes *IEEE journal of selected topics in quantum electronics*, vol. 12, no. 1, january/february 2006 33
- [3] Gorodetsky M. L., Demchenko Y. A., Accurate analytical estimates of eigenfrequencies and dispersion in whispering-gallery spheroidal resonators, *Proc. SPIE* 8236, 823623 (2012)
- [4] Olver W. F. J., *The Asymptotic Solution of Linear Differential Equations of the Second Order for Large Values of a Parameter*, *Philosophical Transactions of the Royal Society of London. Series A, Mathematical and Physical Sciences*, Vol. 247, No. 930 (Dec. 28, 1954), pp. 307-327

# Thermal Shifts and Broadening of Energy Levels in the Group II Ions

V.V. Chernushkin, I.L. Glukhov, S.N. Mokhnenko, E.A. Nikitina and V. D. Ovsianikov  
 Physics Department, Voronezh State University; University square 1, Voronezh, 394006, Russia  
 e-mail: [ovd@phys.vsu.ru](mailto:ovd@phys.vsu.ru)

**Abstract:** Asymptotic polynomial extrapolation formulas, derived on the basis of calculations in the Fues model potential approach, are presented for natural widths and blackbody-radiation-induced shifts and broadening of energy levels in  $\text{Be}^+$ ,  $\text{Mg}^+$  and  $\text{Ca}^+$  ions.

Ions of alkaline-earth elements attract much attention as worthwhile candidates for designing new optical standards of frequency and quantum processing systems. Singly charged beryllium  $\text{Be}^+$ , magnesium  $\text{Mg}^+$  and calcium  $\text{Ca}^+$  are the lightest ions in the list of group II elements and the best appropriate for handling, both theoretically and experimentally. Rather suitable structure of energy levels makes these ions high-efficiency partners for sympathetic cooling and trapping ions, specifically those of the group III elements, extremely useful for the development of superstable optical clocks [1,2].

The structure of alkaline-earth ions is quite similar to that of the alkali atoms, therefore it is reasonable to use in calculating radiation transition amplitudes the Fues model potential (FMP), which was applied to numerical calculations of electromagnetic transition amplitudes and susceptibilities in alkali vapors [3].

Long-living Rydberg states in neutral atoms and ions take an important place in modern researches on quantum information processing [4] and high-precision measurement of blackbody radiation (BBR) characteristics in atomic clocks [5]. Thermally induced shifts of Rydberg-state energy levels at room temperature reach several kHz and may be measured with a precision of mHz by means of frequency combs [6]. Therefore, transitions to Rydberg states may serve as a BBR thermometer. Alkaline-earth ions are considered as rather suitable objects both for metrology and quantum processing. In this communication we report on theoretical calculations of natural widths and BBR-induced shifts and widths of Rydberg states in  $\text{Be}^+$ ,  $\text{Mg}^+$  and  $\text{Ca}^+$ .

The natural (spontaneous radiation) width  $\Gamma_{nl}^{sp}$  of a Rydberg state  $|nl\rangle$  is determined by the total rate of spontaneous decays into all lower states,

$$\Gamma_{nl}^{sp} = \frac{4}{3c^3(2l+1)} \sum_{n'l'}^{E_{n'l'} < E_{nl}} l_{>} \omega_{m'}^3 |M_{nl \rightarrow n'l'}|^2, \quad (1)$$

where the summation runs over all lower-energy dipole-accessible states,  $l_{>} = (l+l'+1)/2$  is the greater of the angular momenta  $l$  and  $l'$ ,  $\omega_{m'} = E_{nl} - E_{n'l'}$  is the dipole transition frequency. In atomic units  $e = m = \hbar = 1$ , the speed of light is the inverse of the fine-structure constant,  $c = \alpha^{-1} = 137.036$ ;  $M_{nl \rightarrow n'l'} = \langle n'l' | r | nl \rangle$  is the radial matrix element of the dipole transition. In calculating this matrix element, we used the single-electron FMP approach where the radial wave functions are presented in terms of generalized Laguerre polynomials. For determining the FMP parameters we use quantum defects  $\mu$ , extrapolated to Rydberg levels with arbitrary principal quantum numbers:

$$\mu_{nl} = \mu_l^{(0)} + \frac{\mu_l^{(1)}}{m^2} + \frac{\mu_l^{(2)}}{m^4} + \frac{\mu_l^{(3)}}{m^6} \quad (2)$$

where  $m = n - n_0 + 1$ ,  $n_0$  is the principal quantum number of the lowest-energy state in the series of states with orbital momentum  $l$ . The numerical values of coefficients  $\mu_l^{(i)}$ ,  $i = 0, 1, 2, 3$  for  $S$ -,  $P$ -,  $D$ -, and  $F$ -series of states in  $\text{Be}^+$ ,  $\text{Mg}^+$  and  $\text{Ca}^+$  were determined on the basis of the curve fitting polynomial interpolation procedure with available data for energy levels [7].

The width (1) is reciprocal to the energy-level lifetime of a free atom,  $\tau_{nl} = 1/\Gamma_{nl}$ . The values of  $\tau_{nl}$  calculated in the FMP approach, are in a good agreement with the most reliable data available currently in literature for some low-energy states (see, e.g. the latest version of the database [7]), thus ensuring availability of rather accurate estimates of the lifetimes for arbitrary states. However, with the growth of radial quantum numbers, the computations become more and more complicated. In addition, due to an infinite number of highly excited Rydberg states, detailed tabulations for them become impossible. Instead, a simple analytical equation

with a small number of numerical parameters, based on asymptotic behavior of  $\tau_{nl}$ , may be used for complete presentation of the computed data:

$$\tau_{nl} = \tau_l^0 n^3 C_l(n), \quad (3)$$

where  $\tau_l^0$  is an asymptotic constant; a smooth function  $C_l(n)$ , tending to unity for  $n \gg 1$ , in a wide region of its argument may be presented in terms of a cubic polynomial in powers of  $n^{-1}$ :

$$C_l(n) = 1 + t_1/n + t_2/n^2 + t_3/n^3 \quad (4)$$

Numerical values of coefficients  $t_1, t_2, t_3$  in this polynomial and the factor  $\tau_l^0$  may be determined from the curve fitting polynomial interpolation procedure for specific values of  $n$ . In particular, the results of interpolations are presented in the table for  $nS$ -,  $nP$ -,  $nD$ - and  $nF$ -states ( $l=0,1,2,3$ ) of the  $\text{Be}^+$  ion.

Series	$\tau_l^0$ , ns	$t_1$	$t_2$	$t_3$
$nS$	0.049857	-0.72863	9.8076	-17.151
$nP$	0.071731	-0.03097	14.655	-28.123
$nD$	0.028459	0.046860	4.3348	-18.248
$nF$	0.064014	0.12396	7.0608	-36.641

With so determined constants, the fractional departure of approximation (3)-(4) from the calculated data is below 1% in the region of  $7 < n < 2000$ .

In addition to spontaneous transitions, the BBR of environment with temperature  $T$  induces transitions both downward (decays), with stimulated emission of photons, and upward, with absorption of BBR photons. The rates of BBR-induced decays are determined by the spontaneous rates (separate terms of equation (1)), times the thermal photon occupation number (for each term),  $\bar{n}(\omega, T) = \{\exp[\omega/(kT)] - 1\}^{-1}$ , where  $k = 1/T_a$  is the Boltzmann constant,  $T_a = 315780$  K is the atomic unit of temperature. Summation over upper bound states determines the rate of BBR-induced excitations, and integration over continuum gives the BBR-induced ionization rate. With the use of asymptotic presentations for the photoionization cross sections [8], the integration over continuum is simplified essentially. Simple polynomial presentations are derived from the calculated data for the fractional decay, excitation and ionization rates  $R_{nl}^{d(e,ion)}(T) = \Gamma_{nl}^{d(e,ion)}(T) / \Gamma_{nl}^{sp}$ :

$$R_{nl}^{d(e)}(T) = \frac{a_0^{d(e)} + a_1^{d(e)}x + a_2^{d(e)}x^2}{n^2 [\exp(4T_a/(n^3T)) - 1]}; \quad R_{nl}^{ion}(T) = \frac{a_0^{d(e)} + a_1^{d(e)}x + a_2^{d(e)}x^2}{n^{4/3} [\exp(2T_a/(n^2T)) - 1]}$$

While the width is determined by the imaginary part of the Stark effect on the level energy in the field of the BBR, the real part determines the level shift [8]. Calculations demonstrate significant difference in the  $n$ - and  $T$ -dependencies of the shifts for  $nS$ -,  $nP$ -,  $nD$ - and  $nF$ -series of states in  $\text{Be}^+$ ,  $\text{Mg}^+$  and  $\text{Ca}^+$  ions from those in hydrogen atoms. However, all of them for  $n^2T \gg T_a$  tend to  $n$ -independent values, proportional to  $T^2$  [9]. An important feature of these asymptotic values is their dependencies on the orbital number, which strongly correlates with the oscillator-strengths sum-rule, similar to the case of alkali atoms [9].

- [1] D.J. Larson et al, "Sympathetic cooling of trapped ions: a laser-cooled two-species nonneutral ion plasma", Phys.Rev.Lett. **57**, 70 (1986).
- [2] T. Rosenband et al, "Frequency ratio of  $\text{Al}^+$  and  $\text{Hg}^+$  single-ion optical clocks; Metrology at the 17<sup>th</sup> decimal place", Science **319**, 1808 (2008).
- [3] N.L. Manakov, V.D. Ovsiannikov, L.P. Rapoport, "Atoms in a laser field", Physics Reports **141**, 319 (1986).
- [4] X. L. Zhang, A. T. Gill, L. Isenhower, T. G. Walker and M. Saffman, "Fidelity of a Rydberg-blockade quantum gate from simulated quantum process tomography", Phys. Rev. A. **85** (2012) 042310.
- [5] V. D. Ovsiannikov, A. Derevianko and K. Gibble, "Rydberg spectroscopy in an optical lattice", Phys. Rev. Lett. **107** (2011) 093003.
- [6] Th. Udem, J. Reichert, R. Holzwarth and T.W. Hänsch, "Absolute Optical Frequency Measurement of the Cesium D1 Line with a Mode-Locked Laser", Phys. Rev. Lett. **82**, 3568 (1999).
- [7] Information system "Electronic structure of atoms". Novosibirsk State University. Institute of Automation and Electrometry SB RAS. Available: <http://grotrian.nsu.ru>
- [8] V.D. Ovsiannikov, I.L. Glukhov and E.A. Nekipelov, "Rates of blackbody radiation-induced transitions from Rydberg states of alkali atoms" J. Phys. B **44**, 195010 (2011).
- [9] J.W. Farley and W.H. Wing, "Accurate calculation of dynamic Stark shifts and depopulation rates of Rydberg energy levels induced by blackbody radiation. Hydrogen, helium and alkali-metal atoms", Phys.Rev.A, **23**, 2397 (1981).

# Back action avoiding and mechanical squeezing detection in resolved sideband regime

Alena Demchenko, Sergey P. Vyatchanin

Moscow State University, 119991, Leninskie Gory, Moscow, Russia

alena0703@yandex.ru

## Abstract

We explore the physics of continuous measurement in an optomechanical system based on a Fabry-Perot resonator with one movable mirror and feed-back. It is shown that in resolved sideband limit a) the back action fluctuations may be excluded, b) mechanical squeezing produced by parametric excitation may be detected.

Quantum squeezing of mechanical motion is one of the cases where the quantum behavior of the classical objects is displayed. At the moment this problem is widely discussed applying different schemes and methods [1, 2].

We consider a optical position meter based on a Fabry-Perot resonator with one movable mirror of a resonant frequency  $\omega_R$  and decay rate  $\gamma$  [3]. Homodyne detection of output field provides information on position of movable mirror which is treated as an oscillator of a mass  $m$  with eigen frequency  $\omega_m$ , decay rate  $\gamma_m$  and is in equilibrium with thermal bath. We consider the case when the oscillator's spring constant is parametrically varied with frequency  $2\omega_m$ . As it is known that such system can become unstable so we introduce a feed-back force, that introduces additional decay rate to the system for stability. This scheme is shown on Fig. 1. The read-out laser beam of frequency  $\omega_L$  is detuned from

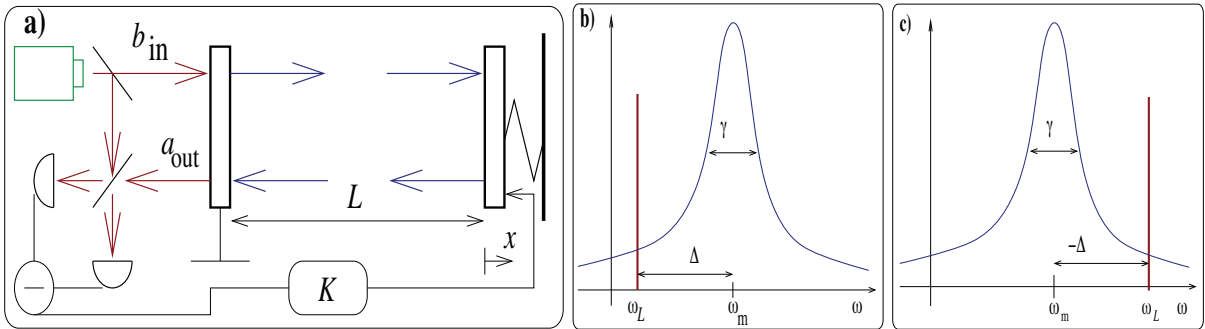


Figure 1: a) Fabry-Perot cavity with one movable mirror. The signal from homodyne detector is used to create feedback force. Laser is detuned from cavity frequency. b) Positive detuning  $\Delta > 0$  (laser frequency  $\omega_L$  is less than cavity frequency  $\omega_R$ ). c) Negative detuning:  $\Delta < 0$ .

the resonant frequency by  $\Delta = \omega_L - \omega_R$  and is considered to have a constant amplitude  $B$  and small quantum fluctuation  $b(t)$ :

$$B_{in}(t) = e^{-i\omega_L t} \left( B + \int_{-\infty}^{\infty} b(\Omega) e^{-i\Omega t} \frac{d\Omega}{2\pi} \right) + h.c. \quad (1)$$

We consider a resolved sideband limit — decay rate  $\gamma_m$  of the oscillator is much smaller than decay rate  $\gamma$  of the cavity and oscillator's eigen frequency  $\omega_m$ . We also assume for simplicity that detuning  $\Delta \equiv \omega_R - \omega_L$  is equal to either  $+\omega_m$  or  $-\omega_m$  [4]:

$$\omega_m \gg \gamma \gg \gamma_m, \quad \Delta \equiv \omega_R - \omega_L = \pm\omega_m \quad (2)$$

In our approximation the oscillator is influenced by a heat bath, a feedback from the measurement and a back-action force. As it was mentioned above we will introduce feedback force that is proportional

to the homodyne current, so that it has a regular part, that adds decay rate to the system, and it also introduces additional fluctuations. So the hamiltonian of the mechanical system is equal to

$$\hat{H} = \hbar\omega_m\hat{a}^+\hat{a} - Fx_0(\hat{a} + \hat{a}^+) + \hat{H}_{bath} - \hbar\left(i\frac{g}{2}e^{2i\omega_mt}\hat{a}^2 - i\frac{g}{2}e^{-2i\omega_mt}\hat{a}^{+2}\right) \quad (3)$$

Here  $\hat{a}$  is annihilation operator of a mechanical mode,  $x_0 = \sqrt{\frac{\hbar}{2m\omega_m}}$  is the amplitude of the zero motion,  $F$  is a sum of forces (including back action and feed back forces) affecting the oscillator,  $\hat{H}_{bath}$  is the hamiltonian of the interaction with the thermal bath and  $g$  is the constant of parametric excitation. In this system we measure the spectral density of the quadrature amplitude  $a_\theta$  in output wave  $a_{out}$ .

$$a_\theta(\Omega) = a_{out}(\Omega)e^{-i\theta} + a_{out}^+(-\Omega)e^{i\theta} \quad (4)$$

Where  $\theta$  is the angle of homodyne detection. In order to register mechanical squeezing we have to get information about mechanical quadrature amplitudes. It means that we should use averaging of  $a_\theta$  over several period of mechanical oscillation  $T = 2\pi/\omega_m$  as following

$$a_c = \langle a_\theta \cos(\omega_mt) \rangle_T, \quad a_s = \langle a_\theta \sin(\omega_mt) \rangle_T \quad (5)$$

## Results

As a result we get that mechanical squeezing may be observed by measurement of two spectral densities (for  $a_c$  and  $a_s$ ) one of which appears to be squeezed and another unsqueezed due to mechanical parametric excitation.

We also show that in resolved sideband limit the back action term in output signal is canceled. (Recall that back action is produced by fluctuation light pressure force proportional to power of optical pump). However, it does not allow to overcome Standard Quantum Limit, the reason of it is introduced *dynamic* back action (introduction of damping into mechanical oscillator).

## References

- [1] Szorkovszky A., Doherty A. Mechanical squeezing via parametric amplification and weak measurement // *arXiv:1107.1294v2 [quant-ph]* 30 Sep 2011. "– 2011.
- [2] Khalili F. Y., Miao H. Quantum back-action in measurements of zero-point mechanical oscillations // *arXiv:1206.0793v1 [quant-ph]*. "– 2012.
- [3] Mari A., Eisert J. Gently modulating opto-mechanical systems // *arXiv:0911.0433v1 [quant-ph]* 2 Nov 2009. "– 2009.
- [4] Marquardt F., Chen J. P. Quantum theory of cavity-assisted sideband cooling of mechanical motion // *Phys. Rev. Lett.* "– 2007. "– Aug. "– Vol. 99. "– P. 093902. <http://link.aps.org/doi/10.1103/PhysRevLett.99.093902>.



tionless flow through thin capillaries, suppression of the classical inertial moment, metastable currents, quantized circulation (vortices), Josephson effect (coherent tunneling), and so on (see, e.g., Refs. [1–6]). There is a close and deep analogy between superfluidity in a neutral system and superconductivity in a charged system [4, 6].

The 3D weakly-interacting Bose gas has all the superfluid properties mentioned above, which can be inferred from the existence of an order parameter represented by the wave function of the Bose–Einstein condensate (BEC). By contrast, there is no BEC in a repulsive 1D Bose gas even at zero temperature in the thermodynamic limit, provided that interactions are independent of particle velocities [7, 8]. This can be easily proved using the Bogoliubov “ $1/q^2$ ” theorem [7]. This predicts a  $1/q^2$  divergence at small momentum in the average occupation number  $n_q$  for nonzero temperature and  $1/q$  divergence for zero temperature. Nevertheless, the existence of BEC is neither a sufficient nor necessary condition for superfluidity [1, 6], and a one-dimensional system of bosons may be superfluid under some conditions. However, whether a system is superfluid or not depends very much on how superfluidity is defined, because one-dimensional systems may exhibit only some but not all of the superfluid phenomena.

Here we study superfluidity in an atomic gas of repulsive spinless bosons in the 1D regime of very narrow ring confinement. The investigations focus mainly on the metastability of the circulating-current states in various regimes. However, we also discuss another important aspect of superfluidity relevant to a 1D system, which is the non-classical moment of inertia or Hess–Fairbank effect [9] and the quantization of circulation. As we argue below, a perfect Hess–Fairbank effect and quantization of circulation occur for the homogeneous gas of repulsive spinless bosons in one dimension, while metastability of currents does not, in general. Note that the Hess–Fairbank effect is much easier to investigate than metastability of current because of its “equilibrium” nature [6, 10]. Indeed, it can be explained with the properties of the low-lying energy excitation spectrum of the system due to the ability of the system to relax to the ground state in the reference frame where the walls (i.e., the trapping potentials) are at rest (see Section 2). The metastability of currents is a much more complicated phenomenon to study, because at sufficiently large gas velocities, the system is obviously not in the ground state but in a metastable state. In order to study such an effect, one needs to understand transitions between states, which presents a more intricate problem.

Ideally, in order to study the decay of ring currents in a controlled manner, the gas should be kept in a ring or a torus-like geometry with defined defects. The defects may cause transitions to the states of lower energies, thus leading to energy dissipation, related to a friction force;

this is called the drag force. The question of metastability then becomes equivalent to the drag force of a small and heavy impurity that is dragged through the resting gas. In the scope of this topical review, we consider mainly infinitesimal impurities and calculate the lowest order terms in linear response of the interacting gas to perturbation by the impurity. The authors of Ref. [11] followed a different approach by calculating the effects of finite impurities on the flow of a weakly-interacting Bose–Einstein condensate.

In spite of rapid progresses in experimental techniques along this line [12–14], so far no conclusive experimental data on the drag force or metastability of ring currents in the 1D Bose gas is available, and thus, this is one of the outstanding fundamental questions remaining about the properties of ultra-cold Bose gases [2]. Not long ago, an experiment along this line was carried out [15], in which the propagation of spin impurity atoms through a strongly interacting one-dimensional Bose gas was observed in a cigar-shaped geometry. The motion of the center-of-mass position of the wave packet is described fairly well by the drag force, calculated with the dynamic structure factor of the Bose gas in the regime of infinite boson interactions. In the recent experiment of Ref. [16], the dynamics of *light* impurities in a bath of bosonic atoms was investigated and the decay of breathing mode oscillations was observed. In another line of experiments, atoms were subjected to a moving optical lattice potential and the momentum transfer was measured [17–19]. This implies that one can experimentally obtain the drag force of a specific external potential acting on the gas. Experiments were also done with ultra-cold atoms in random and pseudo-random potentials. The direct observation of Anderson localization was reported in Refs. [20–22]. In particular, spreading of a 1D Bose gas in artificially created random potentials was experimentally investigated [20]. Below we show that the superfluid–insulator phase diagram of such a system can be obtained by calculating the drag force.

The notion of drag force turns out to be theoretically fundamental, because it generalizes Landau’s famous criterion of superfluidity. According to Landau, an obstacle in a gas, moving with velocity  $v$ , may cause transitions from the ground state of the gas to excited states lying on the line  $\varepsilon = pv$  in the energy–momentum space. If all the spectrum is above this line, the motion cannot excite the system, and it is thus superfluid. However, it is also possible that even when the line intersects the spectrum, the *transition probabilities* to these states are strongly suppressed due to boson interactions or to the specific kind of external perturbing potential. In this case, the drag force gives us a *quantitative* measure of superfluidity.

This paper is organized as follows. The basic model of the 1D Bose gas considered in this paper is introduced

in Section 2. In the subsequent section, we study the Hess–Fairbank effect and its relation to the Landau criterion of superfluidity. In Section 3, we derive an expression for the drag force through the dynamic structure factor within linear response theory and show that the notion of the drag force generalizes the Landau criterion of superfluidity. The values of the drag force in various limiting regimes are calculated in Section 4. In the subsequent section, the Luttinger liquid theory is exploited to describe the drag force at small impurity velocities. An exact method for obtaining the drag force for a finite number of bosons, exploiting the algebraic Bethe ansatz, is briefly discussed in Section 5.3. In Section 5.4 we consider a simple interpolation formula for the DSF, which works for arbitrary strength of the interparticle interactions. In the subsequent section, we show that another approach to the one-dimensional Bose gas, the theory of phase slip transitions [23], reproduces the same power-law behaviour for the drag force as the Luttinger liquid theory does. In Section 5.6, the drag force in the limit of infinite interactions is obtained analytically beyond linear response theory. The decay of ring currents is examined in Section 6. In Section 7.1, the zero-temperature phase diagram is obtained for the superfluid–insulator transition of the one-dimensional Bose gas in moving shallow lattices for arbitrary values of velocity, filling factor, and strength of boson interactions. The motion of the 1D Bose gas in random potentials and the related phase diagram at zero temperature are considered in Section 7.2. Finally, in the conclusion the results and prospects are briefly discussed.

## 2 Landau criterion of superfluidity and Hess–Fairbank effect

*Model* — We model cold bosonic atoms in a waveguide-like micro trap by a simple 1D gas of  $N$  bosons with point interactions of strength  $g_B > 0$  (i.e., the Lieb–Liniger (LL) model [24])

$$H = \sum_{i=1}^N -\frac{\hbar^2}{2m} \frac{\partial^2}{\partial x_i^2} + g_B \sum_{1 \leq i < j \leq N} \delta(x_i - x_j) \quad (1)$$

and impose periodic boundary conditions on the wave functions. The strength of interactions can be measured in terms of the dimensionless parameter  $\gamma \equiv mg_B/(\hbar^2 n)$ , where  $n$  is the linear density and  $m$  is the mass. In the limit of large  $\gamma$ , the model is known as the Tonks–Girardeau (TG) gas [25, 26]. In this limit, it can be mapped onto an ideal *Fermi* gas since infinite contact repulsions emulate the Pauli principle. In the opposite limit of small  $\gamma$ , we recover the Bogoliubov model of weakly interacting bosons. For an overview of theoretical approaches to the one-dimensional Bose gas, see the recent review [27].

*Landau criterion* — In the LL model the total momentum is a good quantum number [28], and periodic boundary conditions quantize it in units of  $2\pi\hbar/L$ , where  $L$  is the ring circumference. Classification of all the excitations can be done [29] in the same manner as for the Tonks–Girardeau gas of non-interacting fermions ( $\gamma \rightarrow +\infty$ ). Thus, in order to create an elementary particle-like excitation, one needs to add a quasimomentum beyond the occupied Fermi segment. By contrast, for a hole-like excitation, one needs to remove a quasimomentum lying inside the Fermi segment. All the excitations can be constructed from the above elementary excitations. Due to the conservation of total number of particles, the number of particle-like excitations coincides with that of hole-like excitations. The low-lying spectrum of  $N = nL$  bosons as shown in Fig. 1 has local minima [30] at the supercurrent states  $I$  ( $I = 0, 1, 2, \dots$ ) with momenta  $p_I = 2\pi n\hbar I$  and excitation energies

$$\varepsilon_I = p_I^2/(2Nm) \quad (2)$$

These correspond to Galilean transformations of the ground state with velocities  $v_I = p_I/(Nm)$ . The minima do not depend on interactions and tend to zero in the limit of large system size at constant density. The first supercurrent state is also called the umklapp excitation [24] by analogy with periodic lattices because it can be reached from the ground state by imparting the momentum  $\hbar K_r$  to each particle, where  $K_r = 2\pi/L$  is the reciprocal wave vector in the ring geometry. As explained above, this changes the total momentum while preserving the internal state of the system.

Suppose that the gas is put into rotation with linear velocity  $v_I$ , and after that, is braked with an artificial macroscopic “obstacle”, e.g., created by a laser beam [31]. In the reference frame where the gas is at rest, the obstacle moves with the velocity  $v_I$ . In a superfluid we expect to see no energy dissipation, and the drag force is zero (the current is persistent). Otherwise one can observe decay of the current. It follows from energy conservation that the transitions from the ground state caused by the moving obstacle with velocity  $v$  lie on the line  $\omega = vk$  in the energy–momentum plane. According to Landau, if the excitation spectrum lies above this line, the motion cannot excite the system, which is then superfluid. As is seen from Fig. 1, the Landau critical velocity (when the line touches the spectrum) equals  $v_c = v_1/2 = \hbar\pi/(mL)$ . This implies that any supercurrent state with  $I \geq 1$  is unstable since  $v_I > v_c$ . However, in 3D we also have similar supercurrent states, which apparently leads to the paradoxical absence of current metastability. The solution to this is that we need to consider not only the spectrum but also *probabilities* of excitations. Below we argue that in the 3D case, the probability to excite supercurrents is vanishingly small, while in the 1D case it depends on the strength of bosonic

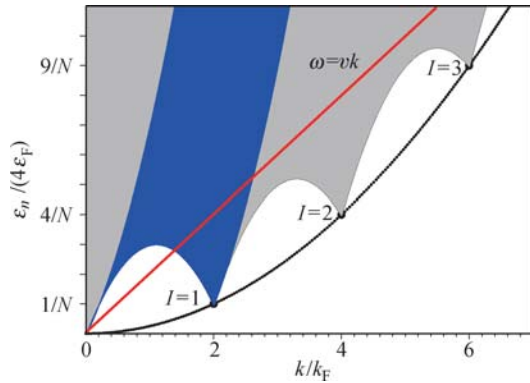


**Fig. 1** Schematic of the excitation spectrum of the 1D Bose gas in a perfectly isotropic ring. The supercurrent states  $I$  lie on the parabola  $\hbar^2 k^2 / (2Nm)$  (dotted line). Excitations occur in the shaded area; the discrete structure of the spectrum is not shown for simplicity. The blue (dark) area represents single particle-hole excitations [29]. Motion of the impurity with respect to the gas causes transitions from the ground state to the states lying on the straight (red) line. Reproduced from Ref. [32], Copyright © 2009 The American Physical Society.

interactions.

*Hess–Fairbank effect* — When the walls of a toroidal container are set into rotation adiabatically with a small tangential velocity  $v_D$ , a superfluid stays at rest while a normal fluid follows the container. This effect leads to a nonclassical rotational inertia of superfluid systems, which can be used to determine the superfluid fraction [6, 10]. For the 1D Bose gas, rotation of the annular trap amounts to shifting the excitation spectrum to  $\varepsilon - v_D p$  as shown in Fig. 2. It is assumed that an unspecified relaxation mechanism allows the system to relax to the ground state in the frame where *the trap is at rest*. The low-lying LL excitation spectrum is a convex function of momentum for  $0 \leq p \leq p_1$  [29], and, hence, the momentum zero state remains the ground state for  $|v_D| < v_c$ . This leads to the Hess–Fairbank effect for the 1D Bose gas for arbitrary repulsive interactions  $\gamma > 0$  [33, 34]. According to this *equilibrium* property which is completely determined by the low-lying energy spectrum [1], the 1D Bose gas has a 100% superfluid fraction and zero rotational inertia at zero temperature. The same results were obtained by using instanton techniques [35] and within Luttinger liquid theory for a finite number of bosons [34, 36].

It is the convexity of the low-lying excitation spectrum between the supercurrent states (see Fig. 2) that allows us to obtain this result without numerical calculations. The minima of energy can be reached only in the supercurrent states [see Fig. 2(b)], whose energy are known analytically with Eq. (2). In the usual way (see, e.g., Ref. [34]), the superfluid component can be defined and obtained numerically through the second derivative of the phase  $\varphi$  in the *twisted* boundary conditions  $\psi(x_1, \dots, x_j + L, \dots, x_N) = \exp(i\varphi)\psi(x_1, \dots, x_j, \dots, x_N)$ ,  $j = 1, \dots, N$ , imposed on

the wave functions. We emphasize that this procedure is equivalent to the method used in this paper, because the Galilean transformation implies a phase gradient of the wave functions observed in the frame of the moving walls, and the gradient leads to twisted boundary conditions. It is also consistent with the definition of the superfluid component in three dimensions through the Fourier-transformed autocorrelation function of the transverse current [6, 10].

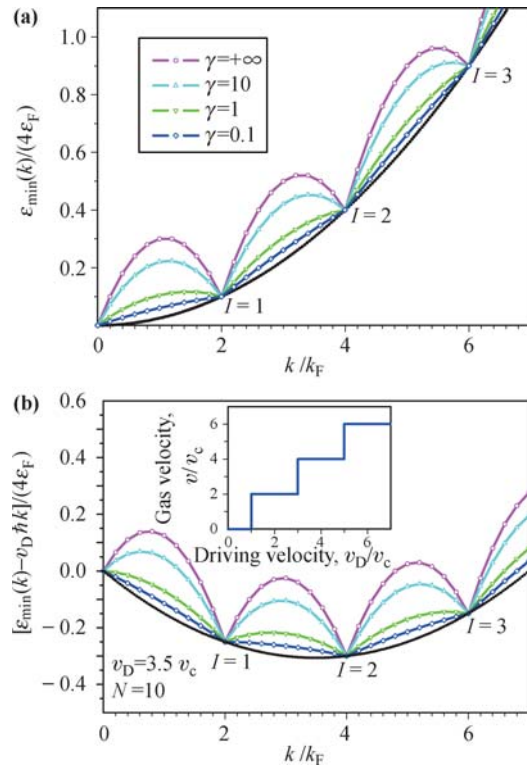


**Fig. 2** (a) Low-lying excitation spectrum  $\varepsilon_{\min}(k)$  for  $N = 10$  particles for 1D repulsive bosons. At  $\gamma \ll 1$ , the low-lying spectrum verges towards that of the ideal Bose gas, which lies on the straight segments between points  $I = 1, 2, 3, \dots$  (b) Quantization of current velocity for 1D repulsive bosons under influence of a moving trap. Shown are the low-energy excitations of the 1D Bose gas in the moving frame  $\varepsilon_{\min}(k) - v_D \hbar k$ , calculated from the Bethe-ansatz equations [24] for different values of the coupling strength (compare with  $\varepsilon_{\min}(k)$  of Fig. 1). Inset: The velocity of the gas at equilibrium changes abruptly at values of driving velocity  $v_D/v_c = 1, 3, 5, \dots$ , since the gas occupies the state with lowest energy. In particular, the system is at rest when the driving velocity is less than  $v_c = v_F/N$  (perfect Hess–Fairbank effect). Here,  $k_F \equiv \pi n$ ,  $v_F \equiv \hbar k_F / m$ , and  $v_F \equiv \hbar^2 k_F^2 / (2m)$ . Reproduced from Ref. [38], Copyright © 2010 Siberian Federal University.

Note that the Bose–Fermi mapping for the TG gas implies that periodic boundary conditions for the Bose gas only translate into periodic boundary conditions for the Fermi gas for odd  $N$  but into antiperiodic ones for even  $N$  [37], in contrast to the true Fermi gas with periodic conditions. One can see that for even  $N$ , there is no Hess–Fairbank effect in the true Fermi gas (although the TG gas always shows the Hess–Fairbank effect). This is due to the instability of fermions at the Fermi point, which results from the degeneracy of the ground state

for an even number of fermions.

### 3 Drag force as a generalization of Landau's criterion of superfluidity

In order to study frictionless motion, let us consider an impurity of mass  $m_i$ , moving with velocity  $\mathbf{v}$  in a medium of particles. For the major part of this topical review, we will treat the interaction between the impurity and Bose gas perturbatively in linear response theory and thus reduce the problem to calculating properties of the integrable 1D Bose gas, although in general the system will lose integrability when adding an impurity. Using Fermi's golden rule, one can easily show (see Appendix A) that the resulting friction leads to an energy loss per unit time given by

$$\dot{E} = - \int \frac{d^D q}{(2\pi)^{D-1}} |\tilde{V}_i(q)|^2 n \frac{(\mathbf{q} \cdot \mathbf{v} - \frac{\hbar q^2}{2m_i}) S(q, \mathbf{q} \cdot \mathbf{v} - \frac{\hbar q^2}{2m_i})}{N} \quad (3)$$

Here  $\tilde{V}_i(q)$  is the Fourier transform of the interaction potential  $V_i(r)$  between the impurity and the particles,  $D$  is the spatial dimension,  $n$  is the density of particles (number of particles per  $D$ -dimensional volume), and  $S(q, \omega)$  is the dynamical structure factor (DSF) of the medium. It is given by the definition [5]

$$S(q, \omega) = \mathcal{Z}^{-1} \sum_{n,m} e^{-\beta E_m} |\langle m | \delta \hat{\rho}_{\mathbf{q}} | n \rangle|^2 \delta(\hbar\omega - E_n + E_m) \quad (4)$$

with  $\mathcal{Z} = \sum_m \exp(-\beta E_m)$  being the partition function and  $\beta$  being the inverse temperature. Here  $\delta \hat{\rho}_{\mathbf{q}} = \sum_j e^{-i\mathbf{q} \cdot \mathbf{r}_j} - N \Delta(\mathbf{q})$  is the Fourier component of the operator of the density fluctuations,  $\Delta(\mathbf{q}) = 1$  at  $\mathbf{q} = 0$  and  $\Delta(\mathbf{q}) = 0$  otherwise. At zero temperature, the structure factor takes a simpler form

$$S(q, \omega) = \sum_n |\langle 0 | \delta \hat{\rho}_{\mathbf{q}} | n \rangle|^2 \delta(\hbar\omega - E_n + E_0) \quad (5)$$

The DSF relates to the time-dependent density correlation through the Fourier transformation

$$S(q, \omega) = N \int \frac{dt d^D r}{(2\pi)^D \hbar} e^{i(\omega t - \mathbf{q} \cdot \mathbf{r})} \langle \delta \hat{\rho}(\mathbf{r}, t) \delta \hat{\rho}(0, 0) \rangle / n \quad (6)$$

where  $\delta \hat{\rho}(\mathbf{r}, t) \equiv \sum_j \delta(\mathbf{r} - \mathbf{r}_j(t)) - n$  is the operator of the density fluctuations. The DSF obeys the  $f$ -sum rule [5]

$$\int_{-\infty}^{+\infty} d\omega \omega S(q, \omega) = N q^2 / (2m) \quad (7)$$

The drag force is defined by the formula  $\dot{E} = -\mathbf{F}_v \cdot \mathbf{v}$ . In this paper, we will use the expression (3) for a heavy

impurity  $v \gg \hbar q / m_i$  in one dimension. It yields for the drag force  $F_v = \int_{-\infty}^{+\infty} dq q |\tilde{V}_i(q)|^2 S(q, qv) / L$ . Using the properties of the DSF  $S(q, \omega) = S(-q, \omega) = e^{\beta \hbar \omega} S(q, -\omega)$ , which follow from its definition (4), we obtain

$$F_v = \int_0^{+\infty} dq q |\tilde{V}_i(q)|^2 S(q, qv) [1 - \exp(-\beta \hbar qv)] / L \quad (8)$$

This is the most general form of the drag force within linear response theory. The form of the impurity interaction potential can be of importance as, e.g., in the cases of shallow lattices and random potentials discussed in Sections 7.1 and 7.2, respectively. When the impurity interaction is of short-range type, we can replace it with good accuracy by a contact interaction  $V_i(r) = g_i \delta(x)$ , which leads to  $\tilde{V}_i(q) = g_i$  and yields at zero temperature [39]

$$F_v \equiv \frac{2g_i^2 nm}{\hbar^2} f_v = g_i^2 \int_0^{+\infty} dq q S(q, qv) / L \quad (9)$$

In the first equality, we introduce the dimensionless drag force  $f_v$  with the help of the "natural" unit  $2g_i^2 nm / \hbar^2$ . Its physical nature will be discussed below in Sections 4.1 and 5.6.

The notion of drag force generalizes the Landau criterion of superfluidity. Indeed, the integral in Eq. (9) is taken along the line  $\omega = qv$  in the  $\omega$ - $q$  plane. If the excitation spectrum lies completely above the line then the integral vanishes, as one can see from the DSF definition (5). On the other hand, the integral can be infinitesimally small or vanish even if the spectrum lies below the line but the excitation probabilities, given by the corresponding matrix elements  $\tilde{V}_i(q) \langle 0 | \delta \hat{\rho}_{\mathbf{q}} | n \rangle$ , are suppressed. The drag force can vanish even if the system is not superfluid in principle, but excitations are not accessed with a given potential. This happens when the matrix elements  $\langle 0 | \delta \hat{\rho}_{\mathbf{q}} | n \rangle$  are not small but the Fourier transform of the impurity potential  $\tilde{V}_i(q)$  takes non-zero values only in a finite region of  $q$ -space. We consider such an interesting case in Sections 7.1 and 7.2 below.

Thus, determining the drag force within linear response theory is reduced to the problem of calculating the dynamic structure factor. Below we consider various approximations for the dynamic structure factor and the associated drag force.

## 4 The drag force in different regimes

### 4.1 Large impurity velocities

Let us consider the case of contact interactions with the impurity,  $V_i(r) = g_i \delta(x)$ . At large impurity velocity  $v \gg \hbar \pi n / m$ , the main contribution to the integral in Eq.

(9) comes from the high momentum region of the DSF, which can be calculated analytically [40]. Indeed, at large velocities, the momentum transfer from the impurity to the particles is big enough to neglect the interparticle interactions. Then one can use the DSF values of the ideal gas [5, 40]

$$S(q, \omega) = \sum_p n_p (1 \pm n_{p+q}) \delta\left(\hbar\omega - \frac{\hbar^2 q^2}{2m} - \frac{\hbar^2 pq}{m}\right) \approx \sum_p n_p \delta\left(\hbar\omega - \frac{\hbar^2 q^2}{2m} - \frac{\hbar^2 pq}{m}\right) \quad (10)$$

Here  $n_p \equiv \langle a_p^\dagger a_p \rangle$  is the average occupation numbers of particles, and the plus is taken for bosons and the minus for fermions. The second equality in Eq. (10) is due to the large momentum  $\hbar q \simeq mv \gg \hbar\pi n$ , which leads to  $n_p n_{p+q} \simeq 0$  for arbitrary values of  $p$ . Substituting Eq. (10) into Eq. (9) yields the value of the drag force  $2g_i^2 mn/\hbar^2$ , which can be used as the force unit.

It is not difficult to see that this result is valid *beyond* linear response theory, given by Eq. (9). Indeed, at sufficiently large particle velocity, the initial particle momentum can be neglected during the scattering. Then in the reference frame where the impurity remains at rest, the relative particle momentum is  $\hbar q \simeq mv$ . Therefore, the reflection coefficient is determined by the squared absolute value of the scattering amplitude in the Born approximation  $m^2 g_i^2 / (\hbar^4 q^2)$ . Each particle, being reflected, transfers momentum  $2\hbar q$ . The total number of scattered particles per unit time is  $nv = n\hbar q/m$ . The product of the last three quantities yields the value of momentum transfer per unit time, that is, the drag force. This quantity, independent of the wave vector, is nothing else but the limiting value of the drag force, obtained above.

#### 4.2 The Tonks–Girardeau regime

Let us first investigate the drag force for the TG gas ( $\gamma \rightarrow +\infty$ ), having the same structure factor as the ideal Fermi gas. The DSF at zero temperature is well-known in the thermodynamic limit [41, 42]

$$S(k, \omega) \frac{\varepsilon_F}{N} = \frac{k_F}{4k} \quad (11)$$

for  $\omega_-(k) \leq \omega \leq \omega_+(k)$ , and zero otherwise. Here  $\omega_\pm(k) = \hbar|2k_F k \pm k^2|/(2m)$  are the limiting dispersions that bound quasiparticle–quasihole excitations (see Fig. 4). By definition,  $k_F \equiv \pi n$  and  $\varepsilon_F \equiv \hbar^2 k_F^2/(2m)$  are the Fermi wave vector and energy of the TG gas, respectively. As follows from Eq. (11) for the DSF, the transition probability from the ground state is inversely proportional to the momentum transfer but does not depend on the excitation energies within the borders  $\omega_\pm(k)$ . Simple integration in Eq. (9) then yields

$$f_v = \begin{cases} v/v_F, & 0 \leq v \leq v_F \\ 1, & v \geq v_F \end{cases} \quad (12)$$

where  $v_F \equiv \hbar\pi n/m$  is the sound velocity in the TG regime. The result is represented in Fig. 3(a). The TG gas is obviously not superfluid.

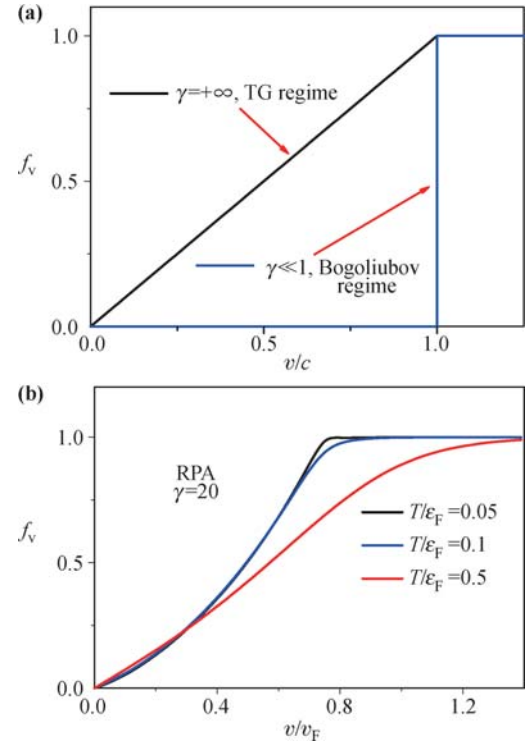


**Fig. 3** The dimensionless drag force (9) versus impurity velocity in various approximations,  $c$  is the speed of sound. **(a)** Tonks–Girardeau and Bogoliubov regimes. **(b)** The random phase approximations (RPA) at non-zero temperatures. The curve becomes smoother when the temperature grows.

#### 4.3 The drag force in the Bogoliubov regime

The opposite regime to the TG gas is the limit of weak interactions  $\gamma \ll 1$  (the Bogoliubov regime). The crucial point in Bogoliubov theory [43] is the developed Bose–Einstein condensate. In spite of the absence of Bose–Einstein condensation in one dimension [8, 44], the upper dispersion curve  $\omega_+(k)$  is well described at small  $\gamma$  [29] by the Bogoliubov relation

$$\hbar\omega_k = \sqrt{T_k^2 + 4T_k\varepsilon_F\gamma/\pi^2} \quad (13)$$

where  $T_k = \hbar^2 k^2/(2m)$  is the free-particle energy spectrum. The Bogoliubov theory also yields the correct values of the ground state energy and chemical potential. This paradox can be explained [45] by a strong singularity of the DSF near  $\omega_+$  in the Bogoliubov regime. As a result, it is localized almost completely within a small vicinity of the upper branch. This tendency can be seen even at  $\gamma = 10$  (Fig. 4). Thus, the behavior of the DSF simulates the  $\delta$ -function spike, which appears due to the Bose–Einstein condensate. One can simply put  $S_{\text{Bog}}(k, \omega) = C\delta(\omega - \omega_k)$  and determine the constant  $C$  from the  $f$ -sum rule (7)

$$S_{\text{Bog}}(k, \omega) = N \frac{T_k}{\hbar \omega_k} \delta(\omega - \omega_k) \quad (14)$$

The drag force is then obtained analytically: it is a step function

$$f_v = \begin{cases} 0, & 0 \leq v \leq c \\ 1, & v \geq c \end{cases} \quad (15)$$

shown in Fig. 3(a). The sound velocity in the Bogoliubov regime is given by  $c = v_F \sqrt{\gamma}/\pi$ . At non-zero temperatures the result does not change. This result was first obtained in Ref. [39] by means of the GP equation. Note that the supersonic impurity motion in three dimensions was earlier studied by the same method in Ref. [46].

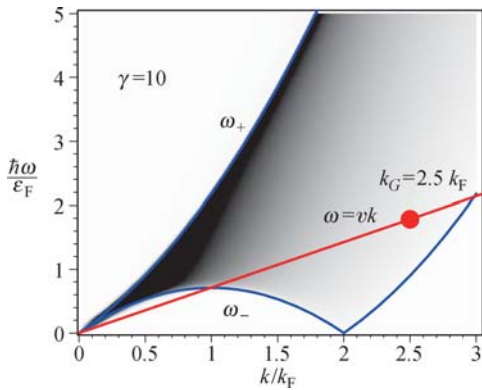


**Fig. 4** Numerical values of the DSE (4) for the coupling parameter  $\gamma = 10$  [60]. The dimensionless value of the rescaled DSE  $S(k, \omega) \varepsilon_F / N$  is shown in shades of gray between zero (white) and 1.0 (black). The upper and lower solid (blue) lines represent the dispersions  $\omega_+(k)$  and  $\omega_-(k)$ , respectively, limiting the single “particle-hole” excitations in the Lieb–Liniger model at  $T = 0$ . The dispersions are obtained numerically by solving the system of integral equations [29]. The gray scale plot of the DSE demonstrates that the main contribution to the DSE comes from the single particle-hole excitations, lying inside the region  $\omega_-(k) \leq \omega \leq \omega_+(k)$  (see also Fig. 1). Only one point at  $k = k_G$ , shown in full (red) circle, contributes to the integral when the perturber is a shallow cosine potential with a reciprocal vector  $k_G$ . Reproduced from Ref. [32], Copyright © 2009 The American Physical Society.

#### 4.4 The linear approximation near the Tonks–Girardeau regime

For finite  $\gamma$ , the model can also be mapped onto a Fermi gas [37] with local interactions, inversely proportional to  $g_B$  [41, 42, 47, 48]. Using the explicit form of the interactions, one can develop the time-dependent Hartree–Fock scheme [41, 42] in the strong-coupling regime with small parameter  $1/\gamma$ . Approximations of the linear response functions on this level are known as Random Phase approximation (RPA) with exchange or generalized RPA [4, 49]. The scheme yields the correct expansion of the DSE up to the first order [41, 42]

$$S(k, \omega) \frac{\varepsilon_F}{N} = \frac{k_F}{4k} \left( 1 + \frac{8}{\gamma} \right) + \frac{1}{2\gamma} \ln \frac{\omega^2 - \omega_-^2}{\omega_+^2 - \omega^2} + O\left(\frac{1}{\gamma^2}\right) \quad (16)$$

for  $\omega_-(k) \leq \omega \leq \omega_+(k)$ , and zero elsewhere. The symbol  $O(x)$  denotes terms of order  $x$  or smaller. The limiting dispersions in the strong-coupling regime take the form

$$\omega_{\pm}(k) = \frac{\hbar |2k_F k \pm k^2|}{2m} \left( 1 - \frac{4}{\gamma} \right) + O\left(\frac{1}{\gamma^2}\right) \quad (17)$$

From the linear part of the dispersion (17) at small momentum  $\omega_{\pm}(k) \simeq ck$ , we obtain the well-known result [29, 34] for the sound velocity at zero temperature  $c = v_F(1 - 4/\gamma) + O(1/\gamma^2)$ .

In the same manner as in Section 4.2, we derive from Eqs. (9) and (16)

$$f_v = \begin{cases} \left[ 1 + 8 \frac{\ln(v/c)}{\gamma} \right] \frac{v}{c}, & 0 \leq v \leq c \\ 1, & v \geq c \end{cases} \quad (18)$$

As expected, the linear approximation (18) works badly for small values of impurity velocity. This is due to the anomalous behaviour of the DSE within the linear approximation in vicinity of the umklapp excitation point at  $\omega = 0$ ,  $k = 2k_F$ . Indeed, Eq. (18) leads to unphysical negative values of the drag force at sufficiently small impurity velocities. For this reason, we need a more careful examination of the drag force in this regime.

## 5 Theoretical approaches

### 5.1 Random phase approximation near the Tonks–Girardeau regime

The DSE in the RPA was calculated and described in details in Section 4.2 of Ref. [42]. The RPA is based on the Hartree–Fock scheme, which is appropriate at sufficiently large interactions between bosons  $\gamma > 8$ . The equation for the drag force within the RPA is derived in Appendix B.

The RPA approximation has some advantages. It always gives positive values of the drag force and is applicable at non-zero temperatures. The results are shown in Fig. 3(b). The RPA scheme can be extended to non-homogeneous systems *beyond the local density approximation* [50]. However, the RPA scheme also works badly in the vicinity of the umklapp excitation. As a consequence, the formula for the drag force (B7), obtained within the RPA, does not reproduce the correct power-law behaviour at small velocities (see discussion in Sections. 5.2 and 5.4 below.). Another disadvantage of the scheme is that the drag force as a function of velocity has an unphysical peak near  $v = c$  at zero temperatures, which becomes quite pronounced for  $\gamma \lesssim 15$ . This is an apparent artifact of RPA. In the next sections we consider much better approximations that work for all values of the interaction strength and impurity velocities.

## 5.2 Luttinger liquid theory

Luttinger liquid theory allows us to correctly describe the low-energy excitations of a 1D system of particles whose interactions are independent of the velocities. It faithfully handles the nonlinear effects of these interactions and yields values of the DSF *at low energies* for arbitrary coupling strength [30, 39] and thus can be used to calculate the drag force at small values of the impurity velocity.

The behaviour of the DSF in the vicinity of the umklapp excitation is related to the long-range asymptotics of the time-dependent density–density correlator. The asymptotics for  $k_F x \gg 1$  and  $t \leq x/c$

$$\frac{\langle \delta \hat{\rho}(x, t) \delta \hat{\rho}(0, 0) \rangle}{n^2} \simeq -\frac{K}{4\pi^2 n^2} \left( \frac{1}{(x-ct)^2} + \frac{1}{(x+ct)^2} \right) + \tilde{A}_1(K) \frac{\cos(2k_F x)}{n^{2K} (x^2 - c^2 t^2)^K} \quad (19)$$

can be justified by generalizing Haldane’s method [30] or using perturbation theory [51, 52] or quantum inverse scattering method [53] or conformal field theory [54, 55]. The first two terms are related to the behaviour of the DSF in vicinity of  $\omega = 0$ ,  $q = 0$ , while the third term is related to the umklapp excitations. Substituting the third term of Eq. (19) into Eq. (6) yields the DSF in the vicinity of the “umklapp” point ( $k = 2k_F = 2\pi n$ ,  $\omega = 0$ ) [39]

$$\frac{S(k, \omega)}{N} = \frac{nc}{\hbar\omega^2} \left( \frac{\hbar\omega}{mc^2} \right)^{2K} A_1(K) \left( 1 - \frac{\omega_-^2(k)}{\omega^2} \right)^{K-1} \quad (20)$$

for  $\omega \geq \omega_-(k)$ , and zero otherwise. Within Luttinger-liquid theory, the dispersion is *linear* near the umklapp point:  $\omega_-(k) \simeq c|k - 2\pi n|$ . By definition,  $K \equiv \hbar\pi n/(mc)$  is the Luttinger parameter. For repulsive bosons, the value of parameter  $K$  lies between 1 (TG gas) and  $+\infty$  (ideal Bose gas). The value of the Luttinger parameter in the strong-coupling regime

$$K = 1 + 4/\gamma + O(1/\gamma^2) \quad (21)$$

is derived with the expression for the sound velocity obtained in Section 4.4. The coefficients in Eqs. (19) and (20) are related by [56]

$$\tilde{A}_1(K) = \frac{\Gamma^2(K)}{2\pi} \left( \frac{2K}{\pi} \right)^{2K} A_1(K) \quad (22)$$

with  $\Gamma(K)$  being the gamma function. The coefficient  $A_1(K)$  is non-universal, and is explicitly known for the Lieb–Liniger model [57, 58]. We will make use of its value in two limiting cases:  $A_1(K) = \pi/4$  at  $K = 1$  and  $A_1(K) \simeq 4^{1-3K} \exp(-2\gamma_c K) \pi / \Gamma^2(K)$  for  $K \gg 1$  [39, 56], where  $\gamma_c = 0.5772\dots$  is the Euler constant.

By comparing the first-order expansion (16) in the vicinity of the umklapp point with Eq. (20) and using the expansion (21), one can easily obtain [45] the model-dependent coefficient at large but *finite* interactions when  $K - 1 \ll 1$

$$A_1(K) = \frac{\pi}{4} \left[ 1 - (1 + 4 \ln 2)(K - 1) \right] + O((K - 1)^2) \quad (23)$$

Using the DSF (20) predicted by Luttinger theory and equation (9) for the drag force, we arrive at the expression for the drag force at small velocities  $v \ll c$  [39]

$$F_v = \sqrt{\pi} \frac{\Gamma(K)}{\Gamma(K + 1/2)} A_1(K) \frac{g_1^2 n^2}{\hbar v} \left( 2K \frac{v}{c} \right)^{2K} \quad (24)$$

In the TG regime, this formula yields the same values of the drag force as Eq. (12). Equation (24) gives us the universal exponent of the power-law behaviour of the drag force at small velocities:  $F_v \sim v^{2K-1}$ . The same result was obtained in Ref. [36]. While the non-universal coefficient  $A_1(K)$  is now known for arbitrary strength of interactions [57–59], its actual expression is too unwieldy to be considered here. In Section 5.4 we prefer to consider another approach, which allows us to determine it approximately.

## 5.3 The algebraic Bethe ansatz and ABACUS

The exact integrability of the Lieb–Liniger model now permits the direct numerical calculation of dynamical correlation functions such as the DSF [60] for systems with finite numbers of particles using the ABACUS algorithm [61]. The strategy consists in using the Lehmann representation (5). The eigenstates themselves are constructed by the Bethe Ansatz. The state norms [62, 63] and matrix element of the density operator [64, 65] being exactly known, the sum over intermediate states can be taken starting from the dominant few-particle states and let run until a satisfactory saturation of sum rules is achieved. The results for the DSF take the form illustrated in Fig. 4. For generic values of  $\gamma$ , most of the signal is concentrated between the dispersions  $\omega_+(k)$  and  $\omega_-(k)$  of single particle/hole (Type 1/2 in Lieb’s notation) excitations. The signal is by construction identically zero below  $\omega_-(k)$  (since no eigenstates are found there); above  $\omega_+(k)$ , the signal is carried by multiple particle–hole excitations and is very weak in view of the small matrix elements of the density operator between these states and the ground state.

We use data for  $N = 150$  particles ( $\gamma = 5$  and 20),  $N = 200$  ( $\gamma = 1$ ) and  $N = 300$  ( $\gamma = 0.25$ ). The  $f$ -sum rule saturations at  $k = 2k_F$  were 99.64% ( $\gamma = 20$ ), 97.81% ( $\gamma = 5$ ), 99.06% ( $\gamma = 1$ ) and 99.08% ( $\gamma = 0.25$ ), the saturation getting better at smaller momenta. The drag force is computed from the numerical DSF data in

the following way. Since the DSF in finite size is given by discrete but densely distributed  $\delta$ -function peaks, we consider the integral

$$\begin{aligned} F^I(v) &\equiv \frac{g_1^2}{L} \int_0^\infty dq \int_0^{qv} d\omega S(q, \omega) \\ &= \frac{g_1^2}{\hbar L} \int_0^\infty dq \sum_n |\langle 0 | \delta \hat{\rho}_q | n \rangle|^2 \Theta(\hbar qv - E_n + E_0) \end{aligned} \quad (25)$$

whose derivative with respect to  $v$  simply gives the drag force (9). Here  $\Theta$  is the Heaviside step function. The integral in  $\omega$  conveniently gets rid of all energy  $\delta$ -functions in the expression for the DSF, and this integrated quantity is readily computed without need for smoothing using the raw ABACUS data for the DSF. The derivative with respect to  $v$  can then be taken numerically by fitting an interpolating polynomial to the data points for  $F^I(v)$  in the vicinity of the velocity for which the drag force needs to be calculated. The resulting data for the drag force are illustrated in Fig. 5(a).

The advantage of this method is that the reliability of the results is more or less independent of the value of the interaction parameter, in the sense that states and matrix elements can be individually constructed irrespective of what  $\gamma$  is. The remaining issues are the distribution of correlation weight among the excitations, and how this affects the speed of convergence. The limit of very small  $\gamma$  is the easiest to treat, since only very few states in the vicinity of the Type 1 mode are of importance. The DSF then becomes almost a  $\delta$ -function in the Type 1 dispersion relation, and the drag force tends to the step function as expected in this limit. The opposite case of infinite  $\gamma$  is also straightforward since then only single particle-hole excitations have non-negligible matrix elements, the drag force becomes a constant between Type 1 and 2 dispersions, and the drag force acquires a constant slope. For interaction values between these two extremes, many eigenstates must be summed over for good convergence, and the DSF takes on a nontrivial lineshape making the drag force take the positive-curvature shapes in Fig. 5(a).

#### 5.4 An effective approximation for the dynamic structure factor and drag force

In Refs. [45, 66], an interpolating expression was suggested for the DSF:

$$S(k, \omega) = C \frac{(\omega^\alpha - \omega_-^\alpha)^{\mu_-}}{(\omega_+^\alpha - \omega^\alpha)^{\mu_+}} \quad (26)$$

for  $\omega_-(k) \leq \omega \leq \omega_+(k)$ , and  $S(k, \omega) = 0$  otherwise. Here,  $\mu_+(k)$  and  $\mu_-(k)$  are the exact exponents [67, 68]

$$S(k, \omega) \sim |\omega - \omega_\pm(k)|^{\mp \mu_\pm(k)} \quad (27)$$

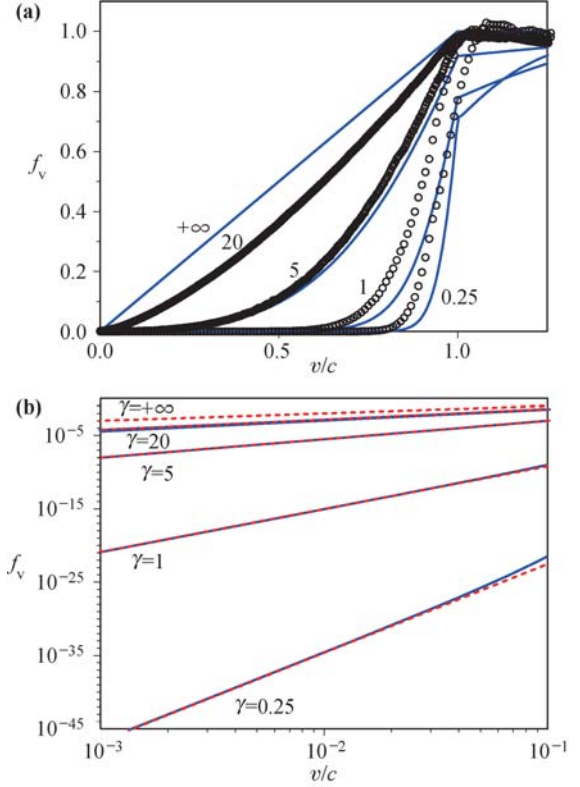


**Fig. 5** The dimensionless drag force versus the velocity (relative to the sound velocity) of the impurity at various values of the coupling parameter  $\gamma$ . (a) The solid (blue) lines represent the force obtained with Eqs. (9) and (26), open circles are the numerical data obtained using ABACUS [60]. (b) The values of the dimensional drag force obtained from the interpolation formula (26) [solid (blue) lines] are compared with that of the analytical formula (29) for small velocities [dashed (red) lines].

at the borders of the spectrum  $\omega_\pm(k)$  and  $\omega_-(k)$ . We also put by definition  $\alpha \equiv 1 + 1/\sqrt{K}$ . The most general way of obtaining  $\omega_\pm(k)$ ,  $\mu_\pm(k)$ , and  $K$  is to solve numerically the corresponding integral equations of Refs. [29] and [67], respectively.

It follows from energy and momentum conservation that  $S(k, \omega)$  is exactly equal to zero below  $\omega_-(k)$  for  $0 \leq k \leq 2\pi n$ . In the other regions of  $\omega > \omega_+$  and  $\omega < \omega_-$  (for  $k > 2\pi n$ ), possible contributions can arise due to coupling to multi-particle excitations [29]. However, these contributions are known to vanish in the Tonks-Girardeau ( $\gamma \rightarrow \infty$ ) and Bogoliubov ( $\gamma \rightarrow 0$ ) limits and are found to be very small numerically for finite interactions [60].

The exponents  $\mu_\pm$  are non-negative [69]. As a consequence, the DSF diverges at the upper branch  $\omega_+$ . At the lower branch  $\omega_-$ , the DSF shows a continuous transition to zero for any finite value of  $\gamma$  except for the specific point  $\gamma = +\infty$  (or  $K = 1$ ) of the Tonks-Girardeau gas, where the DSF remains finite but has a discontinuous transition to zero at both boundaries  $\omega_-$  and  $\omega_+$ .

The normalization constant  $C$  depends on momentum but not on frequency and is determined from the  $f$ -sum rule (7). The expression (26) is applicable for all ranges

of the parameters  $k$ ,  $\omega$ , and  $\gamma$  with increasing accuracy at large  $\gamma$  [45].

The parameter  $\alpha$  is needed to reconcile the limiting value of the exponent  $\mu_-(2\pi n) = 2\sqrt{K}(\sqrt{K} - 1)$  in the vicinity of the umklapp point [67] and the Luttinger theory predictions, given by Eq. (20). Now one can see from (26) that

$$S(k, \omega) \sim \begin{cases} \omega^{2(K-1)}, & k = 2\pi n \\ (\omega - \omega_-)^{\mu_-(k)}, & k \neq 2\pi n \end{cases} \quad (28)$$

Thus, the suggested formula (26) is consistent with both the Luttinger liquid behavior at the umklapp point and Imambekov's and Glazman's power-law behavior in its vicinity, as it should be. A more detailed discussion can be found in Ref. [45]. Similar approximations for the DSF of 1D Bose gas, confined in a harmonic trap, are considered in Ref. [70].

The drag force can now be calculated by means of Eqs. (9) and (26) for arbitrary strength of interactions and arbitrary velocities. The results are shown in Fig. 5(a).

For the important question whether persistent currents may exist at all, the small velocity regime is most relevant, which is dominated by transitions near the first supercurrent state (umklapp point at  $\omega = 0$  and  $k = 2k_F$ ). The drag force in this regime has a power-law dependence on the velocity  $F_v \sim v^{2K-1}$  for  $v \ll c$ , as first found by Astrakharchik and Pitaevskii [39]. From Eqs. (9) and (26) we obtain

$$f_v \equiv \frac{F_v \pi \varepsilon_F}{g_1^2 k_F^3} \simeq 2K \left( \frac{v}{v_F} \right)^{2K-1} \left[ \frac{4\varepsilon_F}{\hbar \omega_+(2k_F)} \right]^{2K} \times \frac{\Gamma(1 + \frac{2K}{\alpha} - \mu_+(2k_F))}{\Gamma(\frac{2K}{\alpha}) \Gamma(1 - \mu_+(2k_F))} \times \frac{\Gamma(1 + \mu_-(2k_F)) \Gamma(1 + \frac{1}{\alpha})}{\Gamma(1 + \mu_-(2k_F) + \frac{1}{\alpha})} \quad (29)$$

where  $\Gamma(x)$  is Euler's Gamma-function, and  $\mu_-(2k_F) = 2\sqrt{K}(\sqrt{K} - 1)$  [67]. This formula is valid for *arbitrary* coupling constant and works even in the Bogoliubov regime at  $\gamma \ll 1$ . In practice, Eq. (29) works well up to  $v \lesssim 0.1c$  [see Fig. 5(b)]. The strong suppression of the drag force in the Bogoliubov regime appears because of the large exponent value  $2K - 1 \gg 1$  and the large argument  $2K/\alpha \gg 1$  of the gamma function in the denominator. Certainly, drag force values of order  $10^{-40}$  lie beyond realizable experiments and as a matter of fact, tell us about superfluidity in this regime.

## 5.5 Drag force from the phase slip transitions

The quantum number  $I$ , describing the supercurrent with energy (2), is nothing else but the phase winding number of the original Bose field  $\Psi = \sqrt{n}e^{i\Phi}$  [30]. The transitions between the supercurrent states are the

phase slip transitions, changing the phase winding number. One can write down explicitly the low-energy Hamiltonian [23] that consists of the supercurrent states and phonon excitations, interacting due to a static impurity. The interaction  $V_i(x)$  between the impurity and bosons can be rewritten in terms of the supercurrent states and the phonons. One can then directly derive the transition probability per unit time between the supercurrent states  $I$  and  $I'$  from Fermi's golden rule [71]. The result reads at zero temperature [see Eq. (8) of Ref. [71]]

$$W_{II'} = \frac{|gg_in|^2}{\hbar \Gamma[1 + \alpha] \Gamma[\frac{1}{2} + \alpha]} \frac{4\pi^{3/2} \alpha}{\xi_{II'}} \left( \frac{\xi_{II'}}{\tilde{\gamma} \epsilon_0} \right)^{2\alpha} \quad (30)$$

where  $\alpha \equiv (I - I')^2 K$  and  $\xi_{II'} \equiv \varepsilon_I - \varepsilon_{I'}$ . The transition probability (30) is determined up to an overall factor, because the dimensionless parameters  $g$  and  $\tilde{\gamma}$ , which are of the order of 1, cannot be defined exactly from the long-range effective Hamiltonian. The energy  $\epsilon_0$  is a characteristic high-energy cutoff for the phonon spectrum.

For the  $I$ th supercurrent decay at zero temperature due to the static impurity, the dominant contribution comes from the transition to the  $(I - 1)$ th state, and one can write for the energy loss per unit time

$$\dot{E} = W_{I, I-1} \xi_{I, I-1} = \frac{|gg_in|^2 4\pi^{3/2} K}{\hbar \Gamma(1 + K) \Gamma(\frac{1}{2} + K)} \left( \frac{\xi_{I, I-1}}{\tilde{\gamma} \epsilon_0} \right)^{2K} \quad (31)$$

For large winding number  $I$ , we have the relation  $\xi_{I, I-1} \simeq 2\pi n \hbar v_I$ , resulted from Eq. (2). By putting the energy cutoff  $\epsilon_0$  to be equal to  $2\pi n \hbar c$  and remembering the definition of the drag force  $|\dot{E}| = F_v v$ , we obtain from Eq. (31)

$$F_v = |gg_in|^2 \frac{4\pi^{3/2}}{\hbar \Gamma(K) \Gamma(\frac{1}{2} + K)} \frac{1}{v} \left( \frac{v}{\tilde{\gamma} c} \right)^{2K} \quad (32)$$

Thus, we come to the dependence  $F_v \sim v^{2K-1}$  at small velocities, in agreement with the previous results (24) and (29).

## 5.6 Direct calculation for the Tonks–Girardeau gas beyond linear response theory

In this section we consider the TG gas, or the ideal gas of spin-polarized fermions. In order to find the drag force, we choose a frame of reference, in which the massive impurity is at rest. Moving particles are then scattered by the impurity potential  $V_i(x) = g_i \delta(x)$ . For an *ideal* Fermi gas the scattering process for each particle is *independent* of the scattering of the other particles. The reflection coefficient for a particle with wave vector  $k$  is easily determined from the one-body Schrödinger equation:  $r(k) = m^2 g_i^2 / (m^2 g_i^2 + \hbar^4 k^2)$ . If  $dN_k$  is the number of particles with wave vectors lying between  $k$  and  $k + dk$ , then these particles transfer momentum to the impurity

per unit time  $dF = 2\hbar^2 nr(k)k^2 dN_k/m$ . Since in the chosen frame of reference, the momentum distribution is the Fermi distribution shifted by  $mv$ , we can write down the explicit expression of the drag force

$$F_v = \frac{2mng_i^2}{\hbar^2} \begin{cases} \xi + \frac{\gamma_i}{2\pi} \left( \arctan \frac{\pi(1-\xi)}{\gamma_i} - \arctan \frac{\pi(1+\xi)}{\gamma_i} \right), & 0 \leq \xi \leq 1 \\ 1 + \frac{\gamma_i}{2\pi} \left( \arctan \frac{\pi(\xi-1)}{\gamma_i} - \arctan \frac{\pi(1+\xi)}{\gamma_i} \right), & \xi \geq 1 \end{cases} \quad (34)$$

Here we denote  $\gamma_i \equiv g_i m / (\hbar^2 n)$ , and  $\xi \equiv v/v_F$ . The results are shown in Fig. 6. As discussed in Section 4.1, the limiting value of the drag force at large velocities coincides with that obtained within linear response theory. At small impurity coupling  $\gamma_i \ll 1$ , Eq. (34) reproduces the linear response formula (12) [see Fig. 3(a)].

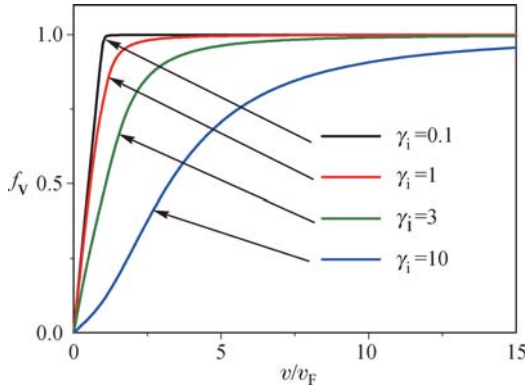


**Fig. 6** The diagram shows the dimensionless drag force (9) for the TG gas at various values of the *impurity* coupling parameter  $\gamma_i \equiv g_i m / (\hbar^2 n)$ . The results are obtained *beyond* the linear response approximation. Note that the absolute value of the drag force  $F_v$  is proportional to  $\gamma_i^2$ .

## 6 Consequence of drag force: Velocity damping

In the presence of an obstacle as, e.g., shown in Fig. 7, a ring current can decay due to successive transitions to supercurrent states with smaller momentum. Starting in one of the local minima of the excitation spectrum as seen in Fig. 1, the kinetic energy of the center-of-mass translation will be transformed into elementary

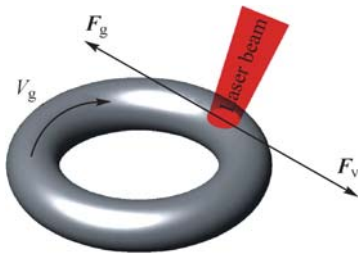


**Fig. 7** An experimental scheme to observe current decays. An artificial “impurity” is created by optical methods. It can be switched on adiabatically or abruptly.

$$F_v = \frac{2\hbar^2}{m} \int \frac{dk}{2\pi} n(k - mv/\hbar) \text{sign}(k) r(k) k^2 \quad (33)$$

where  $n(k) = 1$  for  $-\pi n \leq k \leq \pi n$ , and zero otherwise. The integral is readily taken

excitations above a lower supercurrent state while still conserving the total energy. The elementary excitations are quasiparticle–quasihole excitations in the Bethe–Ansatz wave function [29]. Both in energy and character most of these excitations lie between the phonon-like  $\omega_+$  branch and the  $\omega_-$  branch, which is related to dark solitons (see Fig. 4). Assuming that these excitations have little effect on successive transitions, we estimate [32] the decay of the center-of-mass velocity  $v$  by the classical equation  $Nm\dot{v} = -F_v(v)$ , where  $F_v$  is given by Eqs. (9) and (26). This equation was integrated numerically and the result is shown in Fig. 8. At the initial supersonic velocity, where the drag force is saturated [see Fig. 5(a)] the supercurrent experiences constant deceleration. For  $v \lesssim c$  the drag force decreases and consequently the deceleration slows down. For the TG gas we find an analytical solution for exponential decay  $v(t) = v_0 \exp(-t/\tau)$  for  $v_0 \leq v_F$ . In the weakly-interacting regime, the decay may be slow compared to experimental time scales.

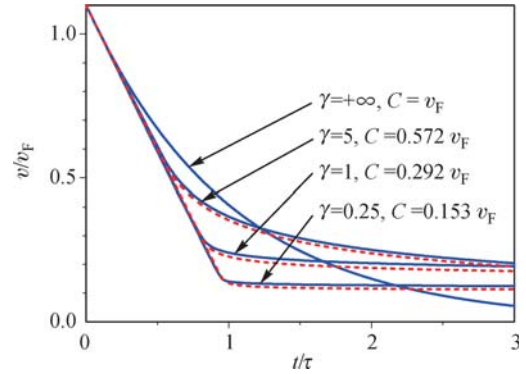


**Fig. 8** Decay of the ring current velocity of 1D bosons from the initial velocity of  $1.1v_F$  at  $t = 0$ . The solid (blue) and dashed (red) lines represent the results obtained with the approximate formula and ABACUS, respectively. The time scale is  $\tau = N\pi\hbar^3 / (2mg_i^2)$ . Reproduced from Ref. [32], Copyright © 2009 The American Physical Society.

## 7 Drag force in extended potentials

### 7.1 1D bosons in a moving shallow lattice

Equation (8) can be verified experimentally for different types of obstacles: for  $V_i(x) = g_i\delta(x)$  all the points

at the transition line contribute to the drag force, while for the periodic potential with the spatial period  $a$  only a set of discrete points in the  $\omega$ - $k$  plane do [32, 38]. This is simply due to the fact that a periodic potential has only a discrete set of Fourier components with momenta  $jk_G$  with  $j$  being integer and  $k_G \equiv 2\pi/a$  being the reciprocal lattice vector. For instance, we have two nonzero components  $k_G$  and  $-k_G$  for optical lattice potential  $V_i(x) = g_L \cos(2\pi x/a)$

$$|\tilde{V}_i(q)|^2/L = \pi g_L^2 [\delta(q - k_G) + \delta(q + k_G)]/2 \quad (35)$$

in the thermodynamic limit ( $n = \text{const}$ ,  $L \rightarrow \infty$ ). The filling factor of the lattice, that is, the number of particles per site, is given by  $\alpha = 2\pi n/k_G$ , because the total number of lattice periods equals  $Lk_G/(2\pi)$ . Substituting Eq. (35) into the general expression for the drag force (8), we obtain at zero temperature

$$F_v = \pi g_L^2 k_G S(k_G, k_G v)/2 \quad (36)$$

The values of the obtained drag force can easily be estimated with the  $\omega$ - $k$  diagram for the DSF (see Fig. 4). Note that the drag force is now proportional to the total number of particles, by contrast to the point-like impurity case, described by Eq. (9). This is because the lattice potential is non-local.

Let us recall that the model considered in this paper assumes periodic boundary conditions. However, according to the general principles of statistical mechanics, the boundary conditions do not play a role in the thermodynamic limit. Hence, the obtained formula (36) can be exploited at sufficiently large number of particles even in the case of a cigar-shaped quasi-1D gas of bosons. This equation gives us the momentum transfer per unit time from a moving shallow lattice, which can be measured experimentally [17–19].

In the case of Bogoliubov and TG regimes, the drag force admits analytic solutions. As discussed in Section 4.3, at small  $\gamma$  the upper dispersion curve  $\omega_+(k)$  is described well by the Bogoliubov relation (13), and the behavior of the DSF simulates the  $\delta$ -function spike in accordance with Eq. (14). We derive from Eqs. (14) and (36)

$$F_v = \frac{g_L^2 mL}{\hbar^2} \frac{1}{2\alpha\xi} \delta\left(\xi - \sqrt{\frac{1}{\alpha^2} + \frac{\gamma}{\pi^2}}\right) \quad (37)$$

where by definition  $\xi \equiv v/v_F$ .

In the TG regime, discussed in Section 4.2, the DSF is given by Eq. (11) with the limiting dispersions  $\omega_{\pm}$  being known analytically. Then Eqs. (11) and (36) yield

$$F_v = g_L^2 mL/(4\hbar^2) [\Theta(\xi - \xi_+) - \Theta(\xi - \xi_-)] \quad (38)$$

where we put by definition  $\xi_{\pm} \equiv |1 \pm 1/\alpha|$ .

The values of the drag force (36) obtained from the interpolating expression for DSF (26) is shown in Figs.

9 and 10. The filling factor  $\alpha = 1$  ( $k_G = 2k_F$ ) corresponds to the Mott insulator state in a deep lattice. As can be seen from Fig. 4, at this value of the reciprocal vector the DSF is almost independent of  $\omega$  when  $\gamma \gg 1$ , and the drag force takes non-zero values for arbitrary  $v \leq \omega_+(k_G)/k_G$  (see Fig. 9).

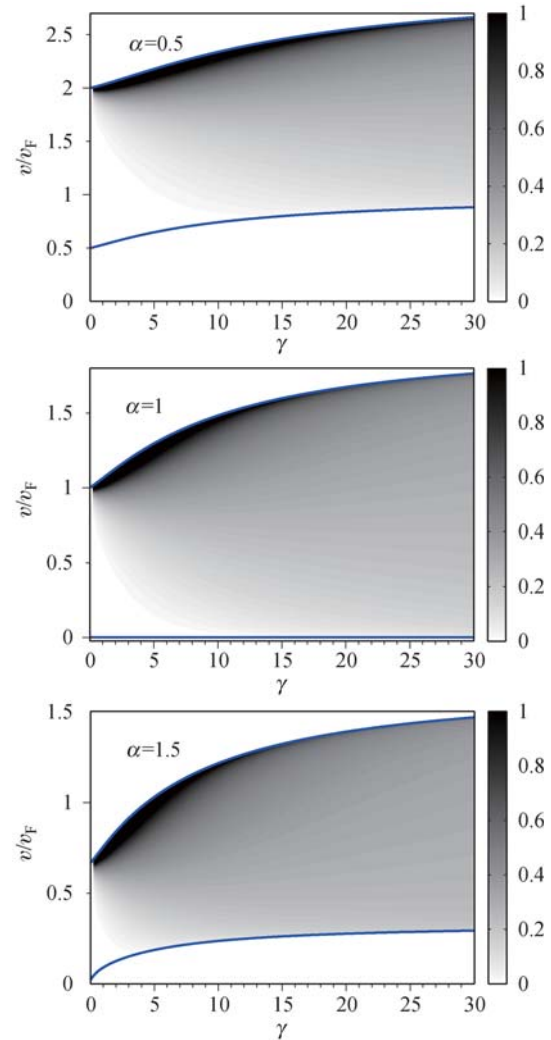


**Fig. 9** Zero temperature phase diagram for superfluid–insulator transition of the Bose gas in a moving shallow lattice: dimensionless drag force  $F_v \hbar^2 / (g_L^2 mL)$  versus the lattice velocity (in units  $v_F$ ) and the interaction strength  $\gamma$  at various values of the filling factor  $\alpha$ . The dimensionless values are represented in shades of gray between zero (white) and 1.0 (black). The solid (blue) lines correspond to the DSF borders  $\omega_+(k)$  and  $\omega_-(k)$ , respectively.

By contrast, at small  $\gamma$  its non-zero values practically localize in the vicinity of  $v = \omega_+(k_G)/k_G$ , as shown in Fig. 10. Then superfluidity breaks down when the point  $\omega = vk_G$  and  $k = k_G$  lies exactly on the Bogoliubov dispersion curve (see Fig. 4). Taking into account that the Bogoliubov dispersion is very close to the free particle one, we obtain for the break point  $k_G v = \hbar k_G^2 / (2m)$ . One can see that this point coincides with the point of dynamical instability for bosons in the cosine shallow lattice. Indeed, the dynamical instability appears at a value of lattice velocity  $v$  corresponding to a negative

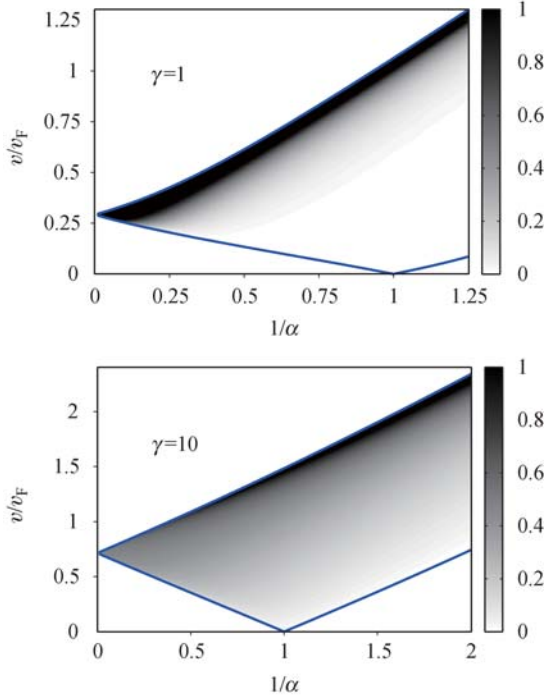


**Fig. 10** The same diagram as shown in Fig. 9, but here the drag force is represented as a function of velocity and inverse filling factor.

curvature of the Bloch dispersion curve at the momentum  $mv/\hbar$ . This is because in the reference frame where the lattice is at rest, particles' momenta are shifted by the value  $mv/\hbar$ , and the effective mass, given by the second derivative of the curve in this point, becomes negative. This implies that the effective kinetic energy of particles and the interaction energy have different signs, which immediately leads to the instability of the repulsive Bose gas at sufficiently large numbers of particles. For a shallow lattice, the Bloch dispersion curve is very close to that of free particles, except for momenta near the edge of the Brillouin zone  $k = \pm k_G/2$ , where the dispersion has a negative curvature (see, e.g., Ref. [72]). Hence, the condition for the dynamical instability takes the form  $k_G/2 = mv/\hbar$ . This coincides with the above condition for the break point, obtained within the generalized Landau criterion of superfluidity, suggested in Section 3. A similar analysis can also be carried out for the TG gas.

The frictionless motion at some values of the parameters  $v$ ,  $\gamma$ ,  $\alpha$  is consistent with the presence of persistent currents in the 1D Bose–Hubbard model [73–78]. As discussed in Section 3, the drag force can be considered as a measure for superfluidity in the absence of the order parameter. Then Fig. 9 represents the phase diagrams in the  $v - \gamma$  and  $v - 1/\alpha$  planes. They are similar to that of Ref. [75]. One can see from the diagrams that there is no sharp transition from superfluid to isolated phase in 1D, which is consistent with the experimental findings of Ref. [19]. Note that in paper [78], superfluidity

was examined in terms of quantum phase slips, discussed in Section 5.5. So, both the quasiparticle and quantum phase slip descriptions lead to the same results.

## 7.2 1D Bose gas in a moving random potential

Recently, direct observation of Anderson localization with a controlled disorder was reported in a one-dimensional waveguide [20]. An initially trapped Bose gas is released into a one-dimensional waveguide, where it is exposed to an artificially created speckled potential. The wave function of the spreading atoms can be directly measured by optical methods.

Anderson localization was initially predicted for a system of non-interacting particles [79]. Modern experimental technique in cold atoms allows to control the strength of interparticle interactions and the parameters of speckled potentials as well (see, e.g., reviews [80, 81]). Delocalization of a disordered bosonic system by repulsive interactions was observed [22]. Thus, the interplay between interactions and disorder remains a fundamental problem in this field. Considerable attention has recently been given to this problem in many papers [82–91]. Most of the papers consider weakly-interacting bosons or the regime of infinite interactions (TG gas). By using the generalized Landau criterion of superfluidity, introduced in Section 3), one can study the behaviour of a 1D Bose gas in weak random potentials and obtain the superfluid-insulator phase diagram for *arbitrary* strength of boson interactions.

It is convenient to consider random potentials by introducing an ensemble of various potentials. Then the random potential features can be obtained by averaging over the ensemble. One of the most important characteristics of random potentials, created with speckled laser beams, is their correlation function  $\langle V_i(x)V_i(x') \rangle = g(x - x')$ , where  $\langle \dots \rangle$  stands for the average over the random potential ensemble. For an arbitrary potential profile, the drag force is calculated with Eq. (8). Taking the average of this equation with respect to the ensemble, we obtain the drag force acting from the moving random potentials. At zero temperature, we derive

$$\langle F_v \rangle = \int_0^{2k_C} dk k \tilde{g}(k) S(k, kv) \quad (39)$$

Here  $\tilde{g}(k) \equiv \langle |\tilde{V}_i(k)|^2 \rangle / L$  is the Fourier transform of the correlation function  $g(x)$ . The integration in (39) is limited, because for speckled laser beams, the function  $\tilde{g}(k)$  always has a finite support due to the limited aperture of the diffusion plate generating the random phase [92, 93]. So,  $\tilde{g}(k) = 0$  for  $|k| > 2k_C$ . For estimations, we take a realistic correlation function [92, 93]  $\tilde{g}(k) = \pi V_R^2 \sigma_r \Theta\left(1 - \frac{|k|\sigma_r}{2}\right) \left(1 - \frac{|k|\sigma_r}{2}\right)$ . Here  $\sigma_r \equiv 1/k_C$

is the random potential correlation length, depending on the parameters of the experimental device. It is usually of the order of  $1 \mu\text{m}$  [81]. Thus, we have three parameters governing the phase diagram: the potential velocity, the interaction strength, and the correlation length.

Like the lattice potential, the random potential is non-local, and, as a consequence, the drag force (39) is proportional to the total number of particles. The results obtained with the interpolating formula (26) are shown in Fig. 11. As for the shallow lattice potentials, the figure can be treated as the zero-temperature phase diagram for the superfluid–insulator transition: superfluidity assumes zero or strongly suppressed values of the drag force.

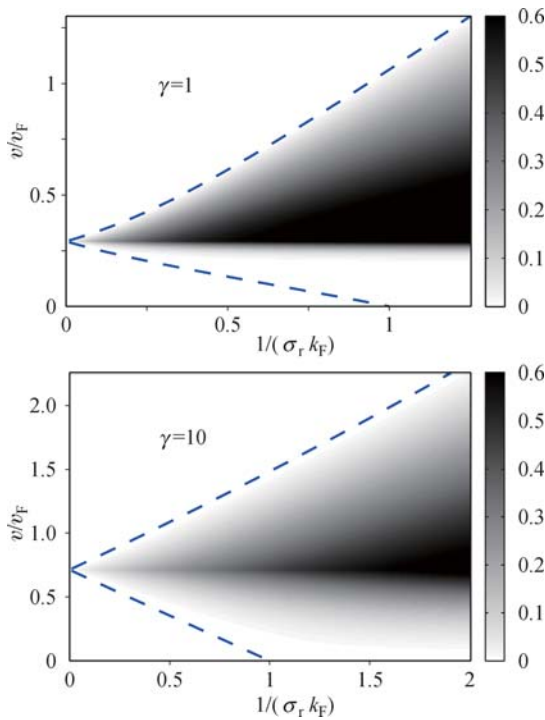


**Fig. 11** Zero temperature phase diagram for superfluid–insulator transition of the Bose gas in a moving random potential: drag force (in units of  $2\pi m V_R^2 \sigma_r N / \hbar^2$ ) versus the potential velocity (in units  $v_F$ ) and the inverse correlation length (in units  $k_F$ ). The dashed (blue) lines correspond to the intersection of the limiting dispersions  $\omega_{\pm}$  and the transition line:  $v = \sigma_r \omega_{\pm}(2/\sigma_r)/2$ . On the left to the lines, the drag force is zero, because within the integration limits of Eq. (39), the values of the DSF is zero (see Fig. 4).

In the Bogoliubov and TG regimes, one can find the drag force analytically. For  $\gamma \ll 1$ , we obtain from Eqs. (14) and (39)

$$\langle F_v \rangle = F_0 \Theta(\xi - \xi_c) \Theta(1 - t) (1 - t) \quad (40)$$

Here  $F_0 \equiv 2\pi m V_R^2 \sigma_r N / \hbar^2$  is a unit of force,  $t \equiv \pi n \sigma_r \sqrt{\xi^2 - \xi_c^2}$ , and  $\xi_c = \sqrt{\gamma}/\pi$  is the sound velocity (in units of  $v_F$ ) in the Bogoliubov regime. In the TG regime, Eqs. (11) and (39) yield

$$\langle F_v \rangle = F_0 [f_1 + (f_2 - f_1) \Theta(\lambda_+ - \lambda_0) - f_2 \Theta(\lambda_- - \lambda_0)] \quad (41)$$

where we introduce the notations  $\lambda_0 \equiv 2/(\pi n \sigma_r)$ ,  $\lambda_{\pm} \equiv 2|\xi \pm 1|$ ,  $f_1 \equiv \frac{1}{4}(\lambda_+ - \lambda_-)(1 - \frac{\lambda_+ + \lambda_-}{2\lambda_0})$ ,  $f_2 \equiv \frac{(\lambda_0 - \lambda_-)^2}{8\lambda_0}$ .

The obtained results are in accordance with the existence of a mobility edge for a particle moving in a random potential with a finite correlation length  $\sigma_r$ . In this case, the mobility edge is given by [83, 85]  $k_{\text{mob}} = k_C \equiv 1/\sigma_r$ . If  $|k| > k_C$ , then the  $k$ -wave propagation is not suppressed, while in the opposite case, the particle wave function is localized (Anderson localization), which leads to the particle immobility. In the TG regime, the gas is equivalent to the ideal Fermi gas, where the mobile particles lie in the vicinity of the Fermi points. In the reference frame where the random potential is at rest, the absolute value of momentum of the lowest Fermi level is given by  $\hbar k'_F = |\hbar k_F - mv|$ . When  $k'_F > k_C$ , the system should be superfluid. This is consistent with Eq. (39), which yields zero value of the drag force for  $k'_F > k_C$ . Indeed, the value  $2k'_F$  corresponds to the cross point of the dispersion curves for the TG gas and the transition line:  $\omega_{\pm}(2k'_F) = 2k'_F v$ , where  $\omega_{\pm}$  is given by Eq. (17) with infinite  $\gamma$ . Once  $2k'_F > 2k_C$  then the value of drag force is zero, because the DSF is zero within the limits of integration in Eq. (39) (see Fig. 4).

## 8 Conclusions

The absence of a well-defined order parameter makes the behavior of the 1D Bose gas rather unusual in comparison to the 3D case. As shown in Section 2, the 1D Bose gas exhibits superfluid phenomena of equilibrium type (Hess–Fairbank effect, analogous to the Meissner effect in superconductivity) but in general does not show dynamic superfluid phenomena, such as persistent currents in a ring. Instead of a phase transition to full superfluidity as is known in 3D, the 1D Bose gas shows a smooth crossover and reaches the metastability of currents only in a weakly-interacting limit. In this case, the drag force, being a simple integral parameter, can be chosen as *a quantitative measure of superfluidity*. Superfluidity assumes zero or strongly suppressed values of the drag force for the Bose gas moving in different small external potentials. Which value of the drag force should be taken as the transition threshold becomes a question of convention in 1D.

The drag force turns out to be fundamental, because it generalizes the Landau criterion of superfluidity. The generalized Landau criterion, based only on energy and momentum conservation, does work when the usual Landau criterion fails. This is because the drag force effectively involves not only the spectrum but *the probability of transitions* to excited states. A good example is the dynamical instability of weakly-interacting 1D bosons, moving in a shallow lattice. As shown in Section 7.1, the generalized Landau criterion not only successfully pre-

dicts the dynamical instability of the system but gives the quantitative characteristics of the phase transition.

It should be noted that the suggested approach has an apparent disadvantage. Being based on the first order time-dependent perturbation theory, the scheme cannot describe changes of the ground state caused by the perturbing potential. Despite of this fact, it can describe well the superfluid–insulator phase diagram, when the system propagates through shallow lattices or random potentials.

**Acknowledgements** The authors are grateful to Antony Leggett, Lev Pitaevskii, Hans–Peter Büchler, Andrey Kolovsky, Anatoly Polkovnikov, and Andrew Sykes for fruitful discussions. J.-S. Caux acknowledges the support from the FOM foundation of the Netherlands. AYC acknowledges a visiting grant from the INSTANS activity of the European Science Foundation and the support from the JINR-IFIN-HH projects and thanks Massey University for their hospitality. J. Brand was supported by the Marsden Fund Council (contract MAU0706) from Government funding, administered by the Royal Society of New Zealand.

## Appendix A: General formula for the drag force from Fermi’s golden rule

Once an impurity moves into a homogeneous medium with velocity  $\mathbf{v}$ , it is scattered by the medium particles. In general, the scattering leads to transitions with momentum and energy transfer and, consequently, to a finite value of energy loss per unit time. It can be calculated within linear response theory [5, 39, 94] or from Fermi’s golden rule [94, 95].

During the scattering, the initial state of the composite system is assumed to be  $|\mathbf{k}_{\text{in}}, m\rangle = |\mathbf{k}_{\text{in}}\rangle|m\rangle$ , where  $|m\rangle$  is initial state of the medium, the incident particle state is the plane wave  $|\mathbf{k}\rangle = \exp(i\mathbf{k}\cdot\mathbf{y})/\sqrt{V}$  with wave vector  $\mathbf{k}_{\text{in}}$ , and  $V = L^D$  is the  $D$ -dimensional volume. The wave vector is connected to the initial velocity by the relation  $\mathbf{v} = \hbar\mathbf{k}_{\text{in}}/m_i$ . The same notations are adopted for the final state  $|\mathbf{k}_{\text{f}}, n\rangle = |\mathbf{k}_{\text{f}}\rangle|n\rangle$ . The rate for the scattering process (that is, the transition probability per unit time) is given in the lowest order in the impurity interaction by Fermi’s golden rule

$$w(\mathbf{k}_{\text{in}}, \mathbf{k}_{\text{f}}) = \frac{2\pi}{\hbar} \sum_n |\langle \mathbf{k}_{\text{f}}, n | H' | \mathbf{k}_{\text{in}}, m \rangle|^2 \times \delta(E_n + T_{\mathbf{k}_{\text{f}}} - E_m - T_{\mathbf{k}_{\text{in}}}) \quad (\text{A1})$$

where  $T_{\mathbf{k}} = \hbar^2 k^2/(2m)$  is the energy dispersion for the impurity. The momentum and energy transfer are given by

$$\hbar\mathbf{q} = \hbar\mathbf{k}_{\text{in}} - \hbar\mathbf{k}_{\text{f}} \quad (\text{A2})$$

$$\hbar\omega = T_{\mathbf{k}_{\text{in}}} - T_{\mathbf{k}_{\text{f}}} = \hbar\mathbf{q} \cdot \mathbf{v} - \hbar^2 q^2/(2m_i) \quad (\text{A3})$$

respectively.

Performing the integration over  $\mathbf{y}$  in the matrix element of the interaction Hamiltonian  $H' = \sum_j V_i(|\mathbf{y} - \mathbf{x}_j|)$

yields for  $\mathbf{q} \neq 0$

$$|\langle \mathbf{k}_{\text{f}}, n | H' | \mathbf{k}_{\text{in}}, m \rangle|^2 = |\tilde{V}_i(q)|^2 |\langle n | \delta\hat{\rho}_{\mathbf{q}} | m \rangle|^2 / V^2 \quad (\text{A4})$$

At nonzero temperature, the medium can be in an arbitrary initial state  $|m\rangle$  with the statistical probability  $\exp(-\beta E_m)/\mathcal{Z}$ . In this case, the transition rate (A1) should be averaged over the statistical ensemble, and we arrive at

$$w(\mathbf{q}) = \frac{2\pi}{\hbar} \frac{|\tilde{V}_i(q)|^2}{V^2} S\left(q, \hbar\mathbf{q} \cdot \mathbf{v} - \frac{\hbar^2 q^2}{2m_i}\right) \quad (\text{A5})$$

Here we use Eq. (A4) and the definition of the DSF (4).

In order to obtain the energy loss per unit time, we need to sum up the energy transfer (A3) weighted with the rate (A5) over all the final states

$$\dot{E} = - \sum_{\mathbf{q}} w(\mathbf{q}) \left( \hbar\mathbf{q} \cdot \mathbf{v} - \frac{\hbar^2 q^2}{2m_i} \right) \quad (\text{A6})$$

Replacing the sum by the integral in the thermodynamic limit  $\sum_{\mathbf{q}} \rightarrow V/(2\pi)^D \int d^D q$  and substituting Eq. (A5) yield Eq. (3).

## Appendix B: The drag force in the RPA approximation

### B.1 The general expression

In this appendix, we will use the dimensionless variables  $\lambda \equiv q/k_{\text{F}}$ ,  $\nu \equiv \hbar\omega/\varepsilon_{\text{F}}$ ,  $\xi \equiv v/v_{\text{F}}$ , where  $k_{\text{F}} \equiv \pi n$ ,  $\varepsilon_{\text{F}} \equiv \hbar^2 k_{\text{F}}^2/(2m)$ , and  $v_{\text{F}} \equiv \hbar k_{\text{F}}/m$  are the Fermi wave vector, energy, and velocity, respectively. Besides, it is convenient to introduce the small parameter  $\alpha \equiv 2/\gamma$ , which can take the values  $0 \leq \alpha \leq 1/4$  within the RPA scheme [42]. In terms of the new variables, Eq. (9) reads

$$f_{\nu} \equiv \frac{F_{\nu} \pi \varepsilon_{\text{F}}}{g_i^2 k_{\text{F}}^3} = \int_0^{+\infty} d\lambda \lambda s(\lambda, 2\xi\lambda) \quad (\text{B1})$$

where we put  $s(\lambda, \nu) \equiv \varepsilon_{\text{F}} S(k_{\text{F}}\lambda, \varepsilon_{\text{F}}\nu/\hbar)/N$ .

The DSF in the RPA approximation was calculated and described in details in Section 4.2 of paper [42]. The result at zero temperature can be written in the form

$$s(\lambda, \nu) = s_{\text{reg}}(\lambda, \nu) + \tilde{A}(\lambda)\delta(\nu - \nu_0(\lambda)) \quad (\text{B2})$$

with the regular part of the dimensionless DSF

$$s_{\text{reg}}(\lambda, \nu) \equiv \frac{\lambda}{4} \frac{(1 - 3\alpha)^2(1 - 2\alpha)}{[(1 - 3\alpha)^2\lambda - \alpha h \ln f]^2 + [\alpha\pi h]^2} \quad (\text{B3})$$

This part is localized in the same region  $|\lambda^2 - 2\lambda|(1 - 2\alpha) \leq \nu \leq (\lambda^2 + 2\lambda)(1 - 2\alpha)$ , as the DSF in the linear approximation, given by Eqs. (16) and (17). Here we put by definition

$$f(\lambda, \nu) \equiv \left| \frac{\nu^2 - (\lambda^2 - 2\lambda)^2(1 - 2\alpha)^2}{\nu^2 - (\lambda^2 + 2\lambda)^2(1 - 2\alpha)^2} \right| \quad (\text{B4})$$

and

$$h(\lambda, \nu) \equiv (1 - 9\alpha/4) \frac{\lambda^2}{2} - \frac{\alpha}{2} - \frac{\nu^2}{8\lambda^2} \frac{3\alpha(1 - 8\alpha/3)}{(1 - 2\alpha)^2} \quad (\text{B5})$$

The quantities in Eq. (B2) are given by  $\tilde{A}(\lambda) \equiv A(k_F \lambda)/N$ ,  $\nu_0(\lambda) \equiv \hbar\omega_0(k_F \lambda)/\varepsilon_F$  with  $A(q)$  and  $\omega_0(q)$  being defined exactly in Section 4.2 of Ref. [42]. By employing the general formula (B1) and the RPA expression (B2), we can evaluate the drag force by numerical integration. The  $\delta$ -function contribution appears as a result of intersection of the curve  $\nu_0(\lambda)$  and the line  $2\xi\lambda$  in the  $\nu$ - $\lambda$  plane and does not play a role at small values of the impurity velocity, see Fig. 12. One can easily show that the  $\delta$ -contribution appears for  $\alpha \leq 2/9$  when  $\xi_-(\alpha) \leq \xi \leq \xi^*(\alpha)$  or  $\xi \geq \xi_+(\alpha)$ , where

$$\xi^*(\alpha) = (1 - 2\alpha) \sqrt{\frac{(1 - 3\alpha)^2/\alpha^2 - 1}{3(1 - 8\alpha/3) + (1 - 3\alpha)^2/\alpha^2}}$$

$$\xi_{\pm}(\alpha) = (1 - 2\alpha) \frac{4 - 9\alpha \pm \sqrt{\alpha}\sqrt{16 - 71\alpha + 80\alpha^2}}{4(1 - 3\alpha + 2\alpha^2)}$$

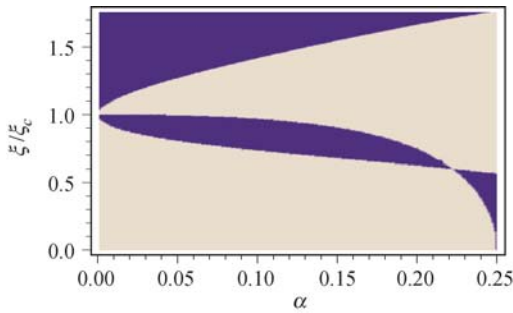


**Fig. 12** The dark (blue) region shows where the  $\delta$ -function contribution exists. Such a contribution results from the intersection of the curve  $\nu_0(\lambda)$  and the line  $2\xi\lambda$  in the  $\nu$ - $\lambda$  plane. One can see that there is no  $\delta$ -function contribution at sufficiently small velocity of the impurity. Here  $\xi_c \equiv c/v_F$ , and  $\xi_c \simeq 1 - 2\alpha$  in the strong-coupling regime.

## B.2 The drag force for small velocities at zero temperature

Since at the small velocities the linear approximation (18) fails, we need to apply here the full RPA expression for the drag force. At small values of  $\xi = v/v_F$ , the limits of the integral in Eq. (B1) becomes very close to each other, and we can put  $f_v = \int_{2(1-\xi/\xi_c)}^{2(1+\xi/\xi_c)} d\lambda \lambda s(\lambda, \nu = 2\xi\lambda) \simeq s_{\text{reg}}(2, 4\xi)8\xi/\xi_c$  and obtain from Eq. (B3)

$$f_v \simeq \frac{4\xi(1 - 3\alpha)^2}{D^2 + \alpha^2\pi^2 \left[ 2 - 5\alpha - \frac{\xi^2}{\xi_c^2} \frac{3\alpha}{2} \left( 1 - \frac{8\alpha}{3} \right) \right]^2} \quad (\text{B6})$$

where

$$D \equiv 2(1 - 3\alpha)^2 + \alpha \left[ 2 - 5\alpha - \frac{\xi^2}{\xi_c^2} \frac{3\alpha}{2} \left( 1 - \frac{8\alpha}{3} \right) \right] \ln \left( 4 \frac{\xi_c^2}{\xi^2} - 1 \right)$$

In principle, the logarithmic term should dominate in the denominator when  $\xi \rightarrow 0$  and one can neglect all the

other terms; however, this approximation works only at very small values of  $\xi$ . A much better approximation can be obtained by keeping the logarithmic term together with the zero-order terms in  $\xi$ :

$$f_v \simeq \frac{(1 - 3\alpha)^2}{(1 - 5\alpha/2)^2} \frac{\xi}{\left[ \frac{(1 - 3\alpha)^2}{1 - 5\alpha/2} - 2\alpha \ln \frac{\xi}{2\xi_c} \right]^2 + \alpha^2\pi^2} \quad (\text{B7})$$

## References and notes

1. A. J. Leggett, *Rev. Mod. Phys.*, 1999, 71(2): S318
2. A. J. Leggett, *Rev. Mod. Phys.*, 2001, 73(2): 307
3. É. B. Sonin, *Sov. Phys. Usp.*, 1982, 25: 409
4. P. Nozières and D. Pines, *The Theory of Quantum Liquids: Superfluid Bose Liquids*, Redwood City: Addison-Wesley, 1990
5. L. Pitaevskii and S. Stringari, *Bose-Einstein Condensation*, Oxford: Clarendon, 2003
6. A. J. Leggett, *Quantum Liquids: Bose Condensation and Cooper Pairing in Condensed-Matter Systems*, Oxford: Oxford University Press, 2006
7. N. N. Bogoliubov, *Quasi-Expectation Values in Problems of Statistical Mechanics*, New York: Gordon and Breach, 1961
8. P. C. Hohenberg, *Phys. Rev.*, 1967, 158(2): 383
9. G. B. Hess and W. M. Fairbank, *Phys. Rev. Lett.*, 1967, 19: 216
10. A. J. Leggett, *Phys. Fenn.*, 1973, 8: 125
11. A. G. Sykes, M. J. Davis, and D. C. Roberts, *Phys. Rev. Lett.*, 2009, 103(8): 085302
12. S. Gupta, K. W. Murch, K. L. Moore, T. P. Purdy, and D. M. Stamper-Kurn, *Phys. Rev. Lett.*, 2005, 95(14): 143201
13. C. Ryu, M. F. Andersen, P. Cladé, V. Natarajan, K. Helmerston, and W. D. Phillips, *Phys. Rev. Lett.*, 2007, 99(26): 260401
14. S. E. Olson, M. L. Terraciano, M. Bashkansky, and F. K. Fatemi, *Phys. Rev. A*, 2007, 76(6): 061404
15. S. Palzer, C. Zipkes, C. Sias, and M. Köhl, *Phys. Rev. Lett.*, 2009, 103(15): 150601
16. J. Catani, G. Lamporesi, D. Naik, M. Gring, M. Inguscio, F. Minardi, A. Kantian, and T. Giamarchi, arXiv:1106.0828, 2011
17. L. Fallani, L. De Sarlo, J. E. Lye, M. Modugno, R. Saers, C. Fort, and M. Inguscio, *Phys. Rev. Lett.*, 2004, 93(14): 140406
18. C. D. Fertig, K. M. O'Hara, J. H. Huckans, S. L. Rolston, W. D. Phillips, and J. V. Porto, *Phys. Rev. Lett.*, 2005, 94(12): 120403
19. J. Mun, P. Medley, G. K. Campbell, L. G. Marcassa, D. E. Pritchard, and W. Ketterle, *Phys. Rev. Lett.*, 2007, 99(15): 150604
20. J. Billy, V. Josse, Z. Zuo, A. Bernard, B. Hambrecht, P. Lugan, D. Clément, L. Sanchez-Palencia, P. Bouyer, and A. Aspect, *Nature*, 2008, 453(7197): 891
21. G. Roati, C. D'Errico, L. Fallani, M. Fattori, C. Fort, M. Zaccanti, G. Modugno, M. Modugno, and M. Inguscio, *Nature*, 2008, 453(7197): 895
22. B. Deissler, M. Zaccanti, G. Roati, C. D'Errico, M. Fattori, M. Modugno, G. Modugno, and M. Inguscio, *Nat. Phys.*, 2010, 6(5): 354

23. V. A. Kashurnikov, A. I. Podlivaev, N. V. Prokof'ev, and B. V. Svistunov, *Phys. Rev. B*, 1996, 53(19): 13091
24. E. H. Lieb and W. Liniger, *Phys. Rev.*, 1963, 130(4): 1605
25. L. Tonks, *Phys. Rev.*, 1936, 50(10): 955
26. M. Girardeau, *J. Math. Phys.*, 1960, 1(6): 516
27. M. A. Cazalilla, R. Citro, T. Giamarchi, E. Orignac, and M. Rigol, arXiv:1101.5337, 2011, to appear in *Rev. Mod. Phys.*
28. In this paper we use the linear momentum and coordinates and velocities. The angular momentum and angle and angular velocity can easily be written as  $L_z = pL/(2\pi)$ ,  $\varphi = 2\pi x/L$ ,  $\omega_z = 2\pi v/L$ , respectively.
29. E. H. Lieb, *Phys. Rev.*, 1963, 130(4): 1616
30. F. D. M. Haldane, *Phys. Rev. Lett.*, 1981, 47: 1840, note a misprint in Eq. (7) for the density-density correlator: the sign before the second term should be minus.
31. C. Raman, M. Köhl, R. Onofrio, D. S. Durfee, C. E. Kulewicz, Z. Hadzibabic, and W. Ketterle, *Phys. Rev. Lett.*, 1999, 83(13): 2502
32. A. Y. Cherny, J. S. Caux, and J. Brand, *Phys. Rev. A*, 2009, 80(4): 043604
33. M. Ueda and A. J. Leggett, *Phys. Rev. Lett.*, 1999, 83(8): 1489
34. M. A. Cazalilla, *J. Phys. B*, 2004, 37(7): S1
35. H. P. Büchler, V. B. Geshkenbein, and G. Blatter, *Phys. Rev. Lett.*, 2001, 87(10): 100403
36. R. Citro, A. Minguzzi, and F. W. J. Hekking, *Phys. Rev. B*, 2009, 79(17): 172505
37. T. Cheon and T. Shigehara, *Phys. Rev. Lett.*, 1999, 82(12): 2536
38. A. Y. Cherny, J. S. Caux, J. Brand, and J. Sib, *Fed. Univ. Math. Phys.*, 2010, 3: 289
39. G. E. Astrakharchik and L. P. Pitaevskii, *Phys. Rev. A*, 2004, 70: 013608, note misprints in Eq. (20) for the drag force in this paper.
40. P. C. Hohenberg and P. M. Platzman, *Phys. Rev.*, 1966, 152(1): 198
41. J. Brand and A. Y. Cherny, *Phys. Rev. A*, 2005, 72(3): 033619
42. A. Y. Cherny and J. Brand, *Phys. Rev. A*, 2006, 73(2): 023612
43. N. N. Bogoliubov, *J. Phys. USSR*, 1947, 11: 23, reprinted in Ref. [49]
44. N. N. Bogoliubov, *Lectures on Quantum Statistics*, Vol. 2, New York: Gordon and Breach, 1970
45. A. Y. Cherny and J. Brand, *Phys. Rev. A*, 2009, 79(4): 043607
46. D. L. Kovrizhin and L. A. Maksimov, *Phys. Lett. A*, 2001, 282(6): 421
47. M. D. Girardeau and M. Olshanii, *Phys. Rev. A*, 2004, 70(2): 023608
48. B. E. Granger and D. Blume, *Phys. Rev. Lett.*, 2004, 92(13): 133202
49. D. Pines (Ed.), *The Many-Body Problem*, New York: W. A. Benjamin, 1990
50. M. Gattobigio, *J. Phys. B*, 2006, 39(10): S191
51. V. N. Popov, *Theor. Math. Phys.*, 1972, 11: 565
52. V. N. Popov, *Functional Integrals in Quantum Field Theory and Statistical Physics*, Dordrecht: Reidel, 1983
53. V. E. Korepin, N. M. Bogoliubov, and A. G. Izergin, *Quantum Inverse Scattering Method and Correlation Functions*, Cambridge: Cambridge University Press, 1993, see Section XVIII.2
54. A. D. Mironov and A. V. Zabrodin, *Phys. Rev. Lett.*, 1991, 66(5): 534
55. A. O. Gogolin, A. A. Nersisyan, and A. M. Tsvelik, *Bozonization and Strongly Correlated Systems*, Cambridge: Cambridge University Press, 1998
56. G. E. Astrakharchik, *Quantum Monte Carlo Study of Ultracold Gases*, Ph.D. thesis, Università degli Studi di Trento, 2004, Section 1.7.4
57. N. Kitanine, K. K. Kozłowski, J. M. Maillet, N. A. Slavnov, and V. Terras, *J. Stat. Mech.: Th. Exp.*, 2009, 2009: P04003
58. A. Shashi, L. I. Glazman, J. S. Caux, and A. Imambekov, arXiv:1010.2268, 2010
59. A. Shashi, L. I. Glazman, J. S. Caux, and A. Imambekov, *Phys. Rev. B*, 2011, 84(4): 045408
60. J. S. Caux and P. Calabrese, *Phys. Rev. A*, 2006, 74(3): 031605
61. J. S. Caux, *J. Math. Phys.*, 2009, 50(9): 095214
62. M. Gaudin, *La fonction d'onde de Bethe.*, Collection du Commissariat à l'Energie Atomique. Serie Scientifique. Paris etc.: Masson. XVI, p330, 1983
63. V. E. Korepin, *Commun. Math. Phys.*, 1982, 86(3): 391
64. N. A. Slavnov, *Teor. Mat. Fiz.*, 1989, 79: 232
65. N. A. Slavnov, *Teor. Mat. Fiz.*, 1990, 82: 273
66. A. Y. Cherny and J. Brand, *J. Phys.: Conf. Ser.*, 2008, 129: 012051
67. A. Imambekov and L. I. Glazman, *Phys. Rev. Lett.*, 2008, 100(20): 206805
68. Note that the field theory predictions of [67] actually include a singularity also for  $\omega > \omega_+(k)$ , with a universal shoulder ratio. We neglect this here since it gives only a small correction to the results.
69. We slightly change the notations: our  $\omega_{\pm}$  and  $\pm\mu_{\pm}$  correspond to  $\omega_{1,2}$  and  $\mu_{1,2}$  in Ref. [67], respectively. We also denote the density of particles  $n$  and the Fermi wavevector for quasiparticles  $q_0$  instead of  $D$  and  $q$  used in Refs. [53, 67], respectively.
70. V. N. Golovach, A. Minguzzi, and L. I. Glazman, *Phys. Rev. A*, 2009, 80(4): 043611
71. Y. Kagan, N. V. Prokof'ev, and B. V. Svistunov, *Phys. Rev. A*, 2000, 61(4): 045601
72. J. M. Ziman, *Principles of the Theory of Solids*, Cambridge: Cambridge University Press, 1972
73. A. Trombettoni and A. Smerzi, *Phys. Rev. Lett.*, 2001, 86(11): 2353
74. E. Altman, A. Polkovnikov, E. Demler, B. I. Halperin, and M. D. Lukin, *Phys. Rev. Lett.*, 2005, 95(2): 020402
75. A. Polkovnikov, E. Altman, E. Demler, B. Halperin, and M. D. Lukin, *Phys. Rev. A*, 2005, 71(6): 063613
76. J. Ruostekoski and L. Isella, *Phys. Rev. Lett.*, 2005, 95(11): 110403
77. A. R. Kolovsky, *New J. Phys.*, 2006, 8(9): 197
78. I. Danshita and C. W. Clark, *Phys. Rev. Lett.*, 2009, 102(3): 030407
79. P. W. Anderson, *Phys. Rev.*, 1958, 109(5): 1492
80. L. Sanchez-Palencia and M. Lewenstein, *Nat. Phys.*, 2010, 6(2): 87
81. G. Modugno, *Rep. Prog. Phys.*, 2010, 73(10): 102401

82. L. Sanchez-Palencia, *Phys. Rev. A*, 2006, 74(5): 053625
83. L. Sanchez-Palencia, D. Clément, P. Lugan, P. Bouyer, G. V. Shlyapnikov, and A. Aspect, *Phys. Rev. Lett.*, 2007, 98(21): 210401
84. P. Lugan, D. Clément, P. Bouyer, A. Aspect, M. Lewenstein, and L. Sanchez-Palencia, *Phys. Rev. Lett.*, 2007, 98(17): 170403
85. P. Lugan, D. Clément, P. Bouyer, A. Aspect, and L. Sanchez-Palencia, *Phys. Rev. Lett.*, 2007, 99(18): 180402
86. T. Paul, P. Schlagheck, P. Leboeuf, and N. Pavloff, *Phys. Rev. Lett.*, 2007, 98(21): 210602
87. A. S. Pikovsky and D. L. Shepelyansky, *Phys. Rev. Lett.*, 2008, 100(9): 094101
88. G. Kopidakis, S. Komineas, S. Flach, and S. Aubry, *Phys. Rev. Lett.*, 2008, 100(8): 084103
89. G. M. Falco, T. Nattermann, and V. L. Pokrovsky, *Phys. Rev. B*, 2009, 80(10): 104515
90. I. L. Aleiner, B. L. Altshuler, and G. V. Shlyapnikov, *Nat. Phys.*, 2010, 6(11): 900
91. J. Radić, V. Bačić, D. Jukić, M. Segev, and H. Buljan, *Phys. Rev. A*, 2010, 81(6): 063639
92. J. W. Goodman, *Statistical Properties of Laser Speckle Patterns*, in: *Laser Speckle and Related Phenomena*, edited by J.-C. Dainty, Berlin: Springer-Verlag, 1975, pp 9–75
93. D. Clément, A. F. Varón, J. A. Retter, L. Sanchez-Palencia, A. Aspect, and P. Bouyer, *New J. Phys.*, 2006, 8(8): 165
94. D. Pines and P. Nozières, *The Theory of Quantum Liquids: Normal Fermi Liquids*, New York: W. A. Benjamin, 1966, see Eq. (2.69)
95. E. Timmermans and R. Côté, *Phys. Rev. Lett.*, 1998, 80(16): 3419

# Squeezing of optomechanical modes in detuned Fabry-Perot interferometer

Andrey A. Rakhubovsky

Physics Department, Moscow State University, Moscow 119992 Russia

\* Electronic address: [rkh@hbar.phys.msu.ru](mailto:rkh@hbar.phys.msu.ru)

Sergey P. Vyatchanin

Physics Department, Moscow State University, Moscow 119992 Russia

**Abstract:** Analysis of optomechanical system formed by movable mirror of Fabry-Perot cavity pumped by detuned laser is carried out. Possibility of squeezing of optomechanical modes created by optical spring via modulation of pumping power is shown.

## 1. Introduction

There is currently very big and constantly growing interest to the field of optomechanics, including studies of micro- and nanomechanical devices (e.g. membranes, toroids, cantilevers, cavities) coupled to a mode of pumping light [1-4]. The studies in this field are aimed to optical cooling of mechanical mode motion towards the ground state and preparation of mechanical object in non-classical state (e.g. squeezed or Fock one).

At the same time needs of precision displacement measurement in gravitational-wave astronomy led to construction of interferometric antennae with noises of mechanical coordinate close to the quantum level [5]. Initially free test masses (mirrors) of such antenna could be effectively turned to oscillators by means of optical spring which is a restoring force acting on the mirrors of interferometer pumped by a detuned laser. It is worth noting that spring provided by means of optical rigidity is accompanied by very small level of own noises. Consideration of this system could be done in terms of optomechanical modes arising from interaction of pump with mirrors. Estimations show that each of this modes could be treated as a high-Q oscillator and for gravitational antenna like Advanced LIGO there is only a few quanta of mechanical motion in each mode [6]. This means that one could expect non-classical behavior of this modes despite the masses of antenna mirrors being equal to 40 kg.

As an idea for initial experiment we propose a scheme which allows squeezing of quantum fluctuations in quadrature amplitudes of optomechanical modes. The spring constant in this modes is proportional to pump laser power and could be easily accessed via modulation of latter. Hence modulation of laser power at frequency twice bigger than one of one of the modes could provide desired parametric squeezing. We also show that the evidence of this squeezing could be found in light emerging the interferometer.

## 2. Description of model



Fig. 1. Scheme of Fabry-Perot cavity with movable mirror (rightmost one).

It is well known [7] that the differential mode of a Michelson/Fabry-Perot interferometer working in dark-port regime typical for gravitational antenna is equivalent to a single Fabry-Perot cavity. We use a model of Fabry-Perot cavity pumped by a detuned laser that creates an optical spring. To compensate the instability introduced by it we measure the phase quadrature of light leaving the cavity and apply to the movable mirror feedback force proportional to time derivative of measurement result (in principle the instability could be fought by additional pump [8] so the feedback is noway crucial for any results as it is used only for stabilization of mechanical motion).

The system is described by two variables: the displacement  $y$  of movable mirror and by amplitude quadrature  $b$  of light inside the cavity. Equations of motion for this system take the form:

$$\dot{b} + g\dot{b} + 2b + Ay = N_1 \quad (1a)$$

$$\ddot{y} - Ab + \alpha\dot{b} = N_2 \quad (1b)$$

with  $g$  being optical relaxation rate,  $\alpha$  being feedback coefficient and  $N_{1,2}$  being noise forces provided by input light fluctuations. Note that we do not take into account any thermal or seismic noises of mechanical degree of freedom. This seems to be reasonable for gravitational antenna like Advanced LIGO [2] because quantum noise of light is dominant in its scheme. Quantity  $A$  stands for coupling constant proportional to the

optical spring coefficient. If we modulate the pump power at frequency  $2p$ , the coupling coefficient will depend on time like  $A(1 + 2m \cos(2pt + \varphi))$ .

### 3. Eigen modes decomposition

As in the case of conventional coupled oscillators one can treat the system in terms of eigen modes. The evolution of oscillator system could be written as a sum of eigen oscillations:

$$\begin{pmatrix} b \\ y \end{pmatrix} = \sum_{i=1}^{i=2} \vec{v}_i g_i e^{-i\omega_i t} + h.c. \quad (2)$$

Here  $\vec{v}_i$  are vectors of amplitude distribution in modes and  $\omega_i$  are eigen frequencies of those modes. Quantities  $g_i$  are eigen modes amplitudes. The term «h.c.» stands for hermitian conjugate.

We then plug expressions (2) into the system (1) which results in system of equations for eigen modes amplitudes. Assuming these quantities to be *slow* i.e. not to significantly change on time scales compared to oscillation periods  $2\pi/\omega_i$  one can get rid of rapidly oscillating terms and to write shortened equations for amplitudes. This results in linear system over these quantities which is solved using Kramer's rule.

Defining the quadratures of eigen modes amplitudes as  $G^\pm(x) = (g(x) \pm g^*(-x))/\sqrt{2}$  (where  $x$  stands for spectral frequency) one can estimate spectral densities of these quadratures. These estimations show that if there is modulation of pump power on twice the frequency of one of the modes then one of quadratures of this mode is squeezed and another one is anti-squeezed. Spectral densities of other mode quadratures are not affected by this modulation.

### 4. Readout

The evidence of the squeezing could be found in phase quadrature  $a_2^o$  of light emerging cavity namely in the following quantity for eigen mode with number  $j$ :

$$A^\pm(x) = \frac{a_2^o(x + \omega_j) \pm a_2^o(x - \omega_j)}{\sqrt{2}} \quad (3)$$

The spectral densities of these quantities are plotted in fig. 2. (normalized to the shot noise level) for different values of modulation coefficient. As is expected one of the quadratures appears to be squeezed and another one anti-squeezed with value of squeezing proportional to coefficient of modulation.

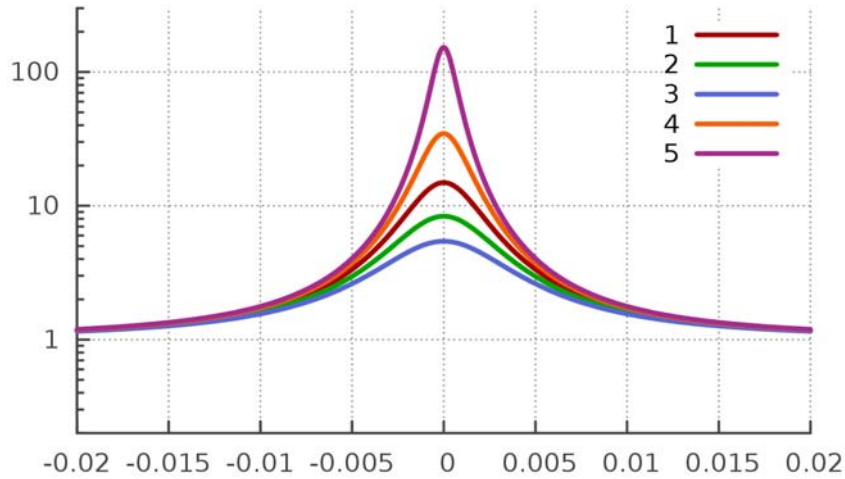


Fig. 2. Spectral densities of output field quadratures defined in eqn. (3) normalized to shot noise level versus dimensionless frequency. Trace 1: both quadratures in case of absent modulation; traces 2 and 3: squeezed quadrature for two values of modulation coefficient; traces 4 and 5: anti-squeezed quadrature for the same values of modulation coefficient.

- [1] J. D. Thompson, B. M. Zwickl, A. M. Jayich, F. Marquardt, S. M. Girvin, and J. G. E. Harris, Nature 452, 72 (2008)
- [2] M. Eichenfield, J. Chan, R. M. Camacho, K. J. Vahala and O. Painter, Nature 462, 78 (2009)
- [3] M. R. Vanner, I. Pikovski, G. D. Cole, M. S. Kim, C. Brukner, K. Hammerer, G. J. Milburn, and M. Aspelmeyer, Proceedings of the National Academy of Sciences of the United States of America 108, 16182 (2011)
- [4] E. Verhagen, S. Weis, A. Schliesser, and T. J. Kippenberg, Nature 482, 63 (2012)
- [5] G. M. Harry and the LIGO Scientific Collaboration, Classical and Quantum Gravity 27, 084006 (2010)
- [6] A. A. Rakhubovsky and S. P. Vyatchanin, Physics Letters A 376, 1405 (2012)
- [7] A. Buonanno and Y. Chen, Phys. Rev. D 65, 042001 (2002)
- [8] H. Rehbein, H. Muller-Ebhardt, K. Somiya, S.L. Danilishin, C. Li, R. Schnabel, K. Danzmann, and Y. Chen, Phys. Rev. D 78, 062003 (2008)

# Steady State of Atoms in a Standing Wave: Quantum Description and Localization Effects

**R.Y. Ilenkov<sup>1</sup>, D.V. Brazhnikov<sup>1</sup>, A.V. Taichenachev<sup>1,2</sup>, V.I. Yudin<sup>1-3</sup>,**

<sup>1</sup>*Institute of Laser Physics SB RAS Ac. Lavrentyev's prosp., 13/3, Novosibirsk, 630090 Russia*

<sup>2</sup>*Novosibirsk State University, ul. Pirogova 2, Novosibirsk, 630090 Russia*

<sup>3</sup>*Novosibirsk State Technical University, pr. Karla Marksa 20, Novosibirsk, 630073 Russia*

*e-mail address: ilenkov.roman@gmail.com, phd7@rambler.ru, taichenachev@hotmail.ru, viyudin@mail.ru*

**Abstract:** Scientific task is investigation of two-level atoms laser cooling. For this purpose we developed an exact quantum calculation method with taking into full account recoil effects. A new effect of anomalous localization of atoms in a strong laser field was discovered.

Invention and application such precise and powerful tool as a laser have opened for scientists a wide range of opportunities for atom manipulation: acceleration, deceleration, localization, deflection, and focusing. Laser cooling has become the integral part of both fundamental science and many practical applications (high-precision frequency and time standards, nanolithography, quantum information and many others). In addition, the strong evidence of importance and interest to this area is the Nobel Prize in 1997, which have been awarded some of the pioneers in the field of laser cooling (e.g., [1]).

Theoretical description of kinetics of neutral atoms in the polarized light fields with taking into account a real atomic level structure, coherent effect, the recoil effect and others is both important and challenging problem. The first step toward understanding the mechanisms of interaction between atoms and light was called semiclassical approach [2]. It lies in the fact that the equations for the density matrix can be reduced to the Fokker-Planck equation for the Wigner function in the phase space. Simplicity of this approach has allowed scientists to understand many of cooling mechanisms in usual and ordinary terms of force and diffusion. However, this approach can only be applied in certain limited cases. First, the recoil frequency must be much smaller in comparison with the rate of spontaneous decay, and secondly, the momentum of a light field photon should be much smaller than the width of the momentum distribution of atoms. Later quantum methods were developed [3,4], for example, the secular approach which describes cooling and localization of atoms in the optical potential. In this approximation distance between the energy bands in the optical potential is greater than their broadening caused by optical pumping. At a fixed depth of the optical potential this approximation is valid in the limit of large detuning, and thus, for a given configuration is disrupted in a deep optical potential. Moreover, even when this condition, the secular approximation is valid only for the lower vibrational levels, and fails for the higher, where the distance between the levels becomes smaller due to the effects of anharmonicity. The more secular approximation is not applicable to atoms undergo above-barrier motion.

We have developed the new quantum method [5] to obtaining the stationary distribution of two-level atoms in a standing wave of arbitrary intensity, allowing us to take into full account the recoil effect. The method used is to decompose the density matrix elements in the Fourier series for the spatial harmonics, which is possible due to periodicity of the light field. Thus we obtain a system recursively coupled equations, where each harmonic is expressed through the previous one, and starting from free selected one (in our calculations, usually twenty or more) all the harmonics are equal to zero.

Using the developed method kinetics of atoms in light fields of varying intensity was investigated. The new and most important result was mode which we called the anomalous localization (Fig. 1). Usually at a low recoil and weak field stationary momentum distribution has a typical Gaussian profile and atoms are located in the region of minimum optical potential (at the antinodes of the standing wave in the red detuning). This result is well known and has been studied previously (see monograph [2,6] and references) However, in strong standing wave (Rabi frequency greater than the constant spontaneous relaxation) was detected a anomalous behavior of atoms, namely, the concentration at the peaks of the optical potential.

The research results have shown that such localization is always accompanied by a significant double-humped distribution of atoms in the momentum space (Fig. 1b). Also appearance of effect is required optical potential, we proposed following mechanism of anomalous localization: If in the case two-humped distribution the most probable kinetic energy of the atoms is greater than potential depth, atoms are concentrated in the peaks of the optical potential, but if the energy is less than depth of potential, localization will occur in the classical turning points. A bit later it has been successfully validated.

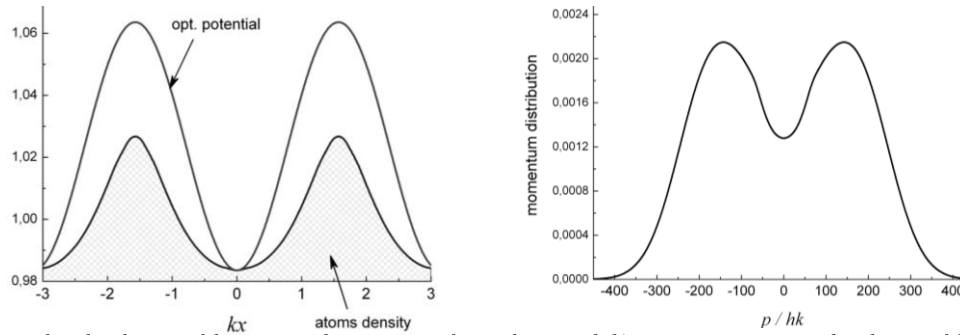


Fig.1. a) Anomalous localization of the atoms at the maximum of optical potential; b) stationary momentum distribution of the atoms in a strong field.

The next step in study of atomic kinetic was to examine the stationary distribution destruction with decreasing detuning. For small detunings of the momentum distribution (Fig. 2a) loses its Gaussian shape, wing area is increased, and, finally, at the approach to the turn of  $\delta = -1/200$  appear the non-physical narrow unstable structure (small peak around zero). Total exact quantum calculation confirmed statements quasiclassics and responded about how far you can reduce the detuning.

Further, it was decided to carry out a detailed comparison of the results of our method with the results of other authors [7,8], then should be noted that momentum distributions were compared because methods used by the authors do not allow us to study the spatial distribution of the atoms. In general, was obtained qualitative agreement forms, including narrow structures of order of  $\hbar k$ , for an example (Fig. 2b) the momentum distribution in a weak field ( $\delta = -0.5, \Omega = 0.1$ ) and for different parameters of recoil. In three cases, there was disagreement related to unphysical solutions obtained (negative probability, infinite space distribution) but to give a definitive answer to the question of whether stationary solution don't have there is still impossible. It is hoped to believe that in this case increasing points density will give an answer to this question. In fact, the main problem we face is the limited processing capacity of used computers but not fundamental limitations of the method.

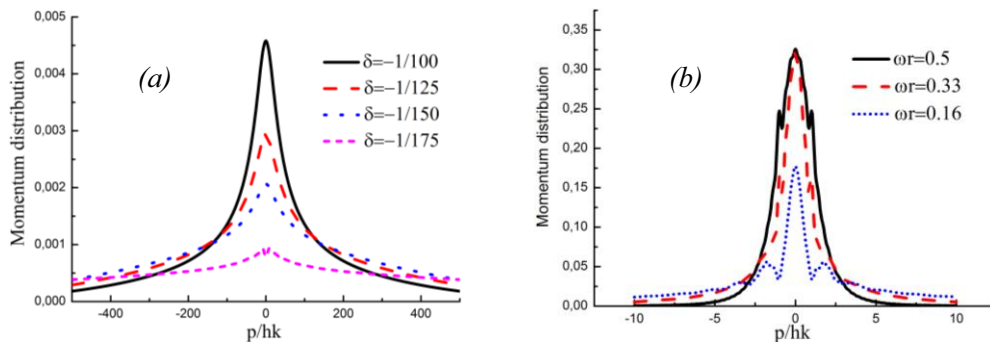


Fig.2. a) Momentum distribution of the atoms at low recoil; b) Quantum regime. Narrow structures of order of single photon recoil

The work is supported by the Ministry of Education and Science of the Russian Federation in the frame of the Program "Scientific and scientific-pedagogical personnel of innovative Russia" (the Contract no. 16.740.11.0466 and the Agreement no. 8387), by RFBR (grants nos. 12-02-00454, 12-02-00403, 11-02-00775, 11-02-01240), by the Russian Academy of Sciences, Presidium of Siberian Branch of Russian Academy of Sciences and the Russian Quantum Center. The young scientists D.V. Brazhnikov and R.Ya. Ilenkov are also supported by the Presidential Grant MK-3372.2912.2 and the RFBR Grant 12-02-31208-"mol\_a".

1. C. Cohen-Tannoudji, «Manipulating atoms with photons», Nobel Lecture, December 8, 1997.
2. A. P. Kazantsev, G. I. Surdutovich, and V. P. Yakovlev, «Mechanical Action of Light on Atoms», *World Sci., Singapore* (1990).
3. A. Aspect, E. Arimondo, R. Kaiser, N. Vansteenkiste, and C. Cohen-Tannoudji, *Phys. Rev. Lett.* **61**, 826 (1988).
4. S. M. Yoo and J. Javanainen, *J. Opt. Soc. Amer. B* **8**, 1341 (1991).
5. O. N. Prudnikov, R. Ya. Il'enkov, A. V. Taichenachev, A. M. Tumaikin, V. I. Yudin «Steady state of a low-density ensemble of atoms in a monochromatic field taking into account recoil effects», *Journal of Experimental and Theoretical Physics* June 2011, Volume 112, Issue 6, pp 939-945.
6. V.G. Minogin, V.S. Letochov, «Laser light pressure on atoms». New York u.a.: Gordon and Breach (1987).
7. Sung Mi Yoo and Juha Javanainen, Wigner-function approach to laser cooling in the recoil limit *JOSA B*, Vol. 8, Issue 6, pp. 1341-1347 (1991)
8. Doery M.R, Vredendregt E.J, Bergeman T. Quantum dynamics and cooling of atoms in one-dimensional standing-wave laser fields: Anomalous effects in Doppler cooling. *Phys Rev A*. 1995 Jun; 51(6):4881-4899.

# Elimination of Nonlinear Effects on Clock Frequency in a Lattice with a Blue Magic Wavelength

V. D. Ovsianikov<sup>1</sup>, V. G. Pal'chikov<sup>2</sup>, A. V. Taichenachev<sup>3</sup> and V. I. Yudin<sup>3</sup>

<sup>1</sup>*Physics Department, Voronezh State University, Voronezh 394006, Russia*

<sup>2</sup>*Institute of Metrology for Time and Space at National Research Institute for Physical-Technical and Radiotechnical Measurements, Mendeleevo, Moscow Region 141579, Russia*

<sup>3</sup>*Institute of Laser Physics SB RAS and Novosibirsk State University, Novosibirsk 630090, Russia  
e-mail:ovd@phys.vsu.ru*

**Abstract:** Nonlinear shift of clock levels disappears in a repulsive lattice. Uncertainties caused by multipole and hyperpolarizability contributions into linear shift of clock frequency are determined numerically for Sr lattice with a blue magic wavelength  $\lambda_{mag} = 389.889$  nm.

Spatial distributions of electric dipole  $\hat{V}_{E1} = E_0(\mathbf{r} \cdot \mathbf{e})$ , magnetic dipole  $\hat{V}_{M1} = E_0/(2c) ([\mathbf{n} \times \mathbf{e}] \cdot (\mathbf{L} + 2\mathbf{S}))$  and electric quadrupole  $\hat{V}_{E2} = E_0\omega/(\sqrt{6}c)r^2 (\{\mathbf{n} \otimes \mathbf{e}\}_2 \cdot \mathbf{C}_2(\theta, \phi))$  interactions between atom and lattice field  $\mathbf{E}(\mathbf{R}, t) = 2E_0\mathbf{e}\cos(\mathbf{k} \cdot \mathbf{R})\cos(\omega t)$ , produced by a laser wave of the amplitude  $E_0$ , polarization vector  $\mathbf{e}$  and the wave vector  $\mathbf{k} = \mathbf{n}\omega/c$  (the valence-electron position vector and its spherical coordinates  $\mathbf{r} = \{r, \theta, \phi\}$  originate in the atomic nucleus), may be presented as follows

$$\hat{V}(X, t) = \hat{V}_{E1} \sin(kX) \cos(\omega t) + (\hat{V}_{M1} + \hat{V}_{E2}) \cos(kX) \sin(\omega t), \quad (1)$$

where  $X$  is the coordinate of the position vector  $\mathbf{R}$  of atomic nucleus along the lattice axis with respect to the standing-wave node,  $k = 2\pi/\lambda_L$  is the wavenumber of the lattice radiation with the wavelength  $\lambda_L$ . The corresponding spatial distribution of ac shifts of clock levels in the lattice, up to the terms quadratic in the laser intensity may be written as [1, 2]

$$U_{g(e)}^L(X, I_L) = - \left[ \alpha_{g(e)}^{E1} \sin^2(kX) + \alpha_{g(e)}^{qm} \cos^2(kX) \right] I_L - \beta_{g(e)} I_L^2 \sin^4(kX), \quad (2)$$

where  $\alpha_{g(e)}^{E1}$  and  $\beta_{g(e)}$  are the electric dipole dynamic polarizability and hyperpolarizability of the ground-state (excited) atom at the lattice-wave frequency,  $\alpha_{g(e)}^{qm} = \alpha_{g(e)}^{E2} + \alpha_{g(e)}^{M1}$  is the sum of electric quadrupole (E2) and magnetic dipole (M1) dynamic polarizabilities, the absolute values of which are usually smaller than  $|\alpha_{g(e)}^{E1}|$  by nearly 7 orders of magnitude [2].

In contrast with the red-detuned attractive lattice with a positive dipole polarizability, the dipole terms (both polarizability  $\alpha_{g(e)}^{E1}$  and hyperpolarizability  $\beta_{g(e)}$ ) of the blue-detuned lattice potential (2) with a negative polarizability  $\alpha_{g(e)}^{E1} < 0$  disappear in its minimum, where the trapped atom mostly locates. Resolving the sine and cosine functions in power series of argument and confining ourselves to the lowest-order anharmonic terms ( $\propto X^4$ ), we get the Stark potential for an atom in a lattice with a blue-shifted wavelength in the form

$$U_{g(e)}^L(X, I_L) = -\alpha_{g(e)}^{qm} I_L - \alpha_{g(e)}^{dqm} I_L (kX)^2 + \left[ \frac{1}{3} \alpha_{g(e)}^{dqm} I_L - \beta_{g(e)} I_L^2 \right] (kX)^4. \quad (3)$$

This equation brings to evidence that the quadratic in  $I_L$  term with hyperpolarizability does not affect neither position-independent term, nor the harmonic term of the lattice potential (3) and appears first in the anharmonic part, the magnitude of which for sufficiently deep potential well is significantly suppressed in comparison with the harmonic part in the region where trapped atom locates. Therefore, the eigenfrequency of atomic vibrational motion  $\Omega_{g(e)} = \Omega_{g(e)}^{(0)} \sqrt{I_L}$  in the potential well (3) depends on only the difference between the dipole and multipole polarizabilities  $\alpha_{g(e)}^{dqm} = \alpha_{g(e)}^{E1} - \alpha_{g(e)}^{qm}$ , without any contribution from nonlinear hyperpolarizability-dependent effects:  $\Omega_{g(e)}^{(0)} = \sqrt{-2\alpha_{g(e)}^{dqm} k^2 / \mathcal{M}}$ , where  $\mathcal{M}$  is the mass of trapped atom.

Thus, the lattice-induced clock-frequency shift is caused by the difference between vibration-state energies of excited and ground-state atom, which may be presented as a mean value  $\mathcal{E}_{g(e)} = \langle n_{g(e)} | \hat{H}_{g(e)} | n_{g(e)} \rangle$

(or an eigenvalue) of the Hamiltonian  $\hat{H}_{g(e)} = \hat{P}^2/(2\mathcal{M}) + U_{g(e)}^L(X, I_L)$ , for an atom with momentum  $\hat{P}$ , oscillating in the potential well (3) in its eigenstate with a fixed quantum number  $|n_{g(e)}\rangle$ . So, the lattice-induced shift of the clock frequency  $\Delta\nu_{cl}(I_L, n) = \nu_{cl}(I_L, n) - \nu_{cl}^{(0)}$  may be resolved in powers of the laser beam intensity, as follows

$$\Delta\nu_{cl}(I_L, n) = \mathcal{E}_e - \mathcal{E}_g = b_{1/2}(n)I_L^{1/2} + b_1(n)I_L, \quad (4)$$

where  $\nu_{cl}^{(0)} = E_e - E_g$  is the standard clock frequency, defined as a difference between energies of excited and ground states in a free atom at rest. The square root of intensity comes from the  $I_L$ -dependence of the oscillator eigenfrequencies. The  $n$ -dependence of the coefficient  $b_{1/2}$  comes from the harmonic parts and that of  $b_1$  appears from anharmonic parts of the potentials (3). It is also noticeable that the dipole polarizability  $\alpha_{g(e)}^{E1}$  appears here in the difference  $\alpha_{g(e)}^{dqm}$  of the under-root expression for  $\Omega_{g(e)}^{(0)}$  and does not contribute to the linear in  $I_L$  term. Therefore, the square-root term in the shift (4) dominates, and the magic-wavelength condition for an atom in the blue-detuned lattice should be based on elimination of the square-root dependence of the clock-frequency shift on the laser intensity. Nevertheless, the definitions of the magic wavelength based on elimination of the linear dependence of the clock-frequency shift in the field of a travelling wave [3] is also valid since the difference between the values of the magic wavelengths determined in the two methods is on the order of the ratio  $[|\alpha_g^{qm}| + |\alpha_e^{qm}|] / |\alpha_{g(e)}^{E1}| \approx 10^{-7}$ .

An important feature of the mean value of the anharmonic potential consists in its inverse proportionality to the intensity. Therefore, the quadratic in  $I_L$  anharmonic term turns after averaging into linear one and the linear in  $I_L$  term turns into a constant value, independent of the laser intensity  $I_L$  and the clock-level polarizabilities. In the Lamb-Dicke regime for vibrational motion in a magic-wavelength potential, the oscillator quantum numbers for excited and ground-state atom coincide,  $n_e = n_g \equiv n$ . So, the  $I_L$ -independent term in the difference of energies (4) cancels out, whereas the hyperpolarizability appears in the coefficient  $b_1$ :

$$b_{1/2}(n) = [\Omega_e^{(0)} - \Omega_g^{(0)}] \left( n + \frac{1}{2} \right); \quad b_1(n) = -[\alpha_e^{qm} - \alpha_g^{qm}] + \frac{3k^2}{4\mathcal{M}} \left[ \frac{\beta_e}{\alpha_e^{dqm}} - \frac{\beta_g}{\alpha_g^{dqm}} \right] \left( n^2 + n + \frac{1}{2} \right). \quad (5)$$

Tuning the lattice laser to the magic wavelength so as to eliminate the square root term in the shift (4) means holding the condition  $\alpha_g^{dqm} = \alpha_e^{dqm}$ . It differs by only subtraction of  $2\alpha_g^{qm}$  from the left-hand side and  $2\alpha_e^{qm}$  from the right-hand side of the condition  $\alpha_g^\Sigma = \alpha_e^\Sigma \equiv \alpha_{mag}$ , which holds in definition of the magic wavelength in a travelling wave [3] ( $\alpha_{g(e)}^\Sigma = \alpha_{g(e)}^{E1} + \alpha_{g(e)}^{qm}$ ). In this case, however, the difference between eigenfrequencies in  $b_{1/2}$  amounts to only a small part of  $\Omega_{mag}^{(0)} = \sqrt{-2\alpha_{mag}k^2/\mathcal{M}}$ :

$$\Omega_e^{(0)} - \Omega_g^{(0)} = -\Omega_{mag}^{(0)} \frac{\alpha_e^{qm} - \alpha_g^{qm}}{\alpha_{mag}}. \quad (6)$$

Numerical calculations for Sr blue-detuned magic wavelength  $\lambda_{mag} = 389.889$  nm give

$$\alpha_{mag} = -92.68 \text{ kHz}/(\text{kW}/\text{cm}^2), \quad \alpha_e^{qm} - \alpha_g^{qm} = -13.62 \text{ mHz}/(\text{kW}/\text{cm}^2), \\ \Omega_{mag}^{(0)} = 74.36 \text{ kHz}/\sqrt{\text{kW}/\text{cm}^2}, \quad \beta_e - \beta_g = 1.147 / (\text{mHz}/(\text{kW}/\text{cm}^2)^2).$$

This data demonstrates, that for the laser intensity  $I_L = 10 \text{ kW}/\text{cm}^2$ , the Sr atoms cooled to  $1 \mu\text{K}$  energy may be trapped into the lowest,  $n = 0$ , vibrational states inside the wells of the magic-wavelength lattice. The uncompensated multipole and hyperpolarizability effects induce the sum of square-root and linear in  $I_L$  clock-frequency shifts (4) of about 100 mHz. The control of uncertainties for these shifts at the level of 0.5% ensures corresponding control of the fractional uncertainties of the clock frequency at the level of  $10^{-18}$ .

- [1] A.V. Taichenachev et al, "Frequency Shifts in an Optical Lattice Clock Due to Magnetic-Dipole and Electric-Quadrupole Transitions" Phys. Rev. Lett. **101**, 193601 (2008).
- [2] H. Katori et al, "Magic Wavelength to Make Optical Lattice Clocks Insensitive to Atomic Motion", Phys. Rev. Lett. **103**, 153004 (2009).
- [3] M. Takamoto et al, "Prospects for optical clocks with a blue-detuned lattice", Phys. Rev. Lett. **102**, 063002 (2009).

# Static Polarizability Measurements of the 5D Level in Rubidium-87

**A.A. Golovizin, S.A. Snigirev, A.V. Akimov, N.N. Kolachevsky, V. N. Sorokin**

*P.N. Lebedev Physical Institute of the Russian Academy of Sciences, Leninsky prosp. 53, 119991 Moscow, Russia  
Moscow Institute of Physics and Technology, Dolgoprudny, 141700, Russia  
Russian Quantum Center, SKOLKOVO, Moscow region, 143025, Russia  
e-mail: [artem.golovizin@gmail.com](mailto:artem.golovizin@gmail.com)*

**Abstract:** We performed a sensitive measurements of static polarizability of the  $5D_{5/2}$  and  $5D_{3/2}$  fine structure levels in laser-cooled Rb-87 atoms placed in static electric field of a few kV/cm. 5D level was excited either by cascade excitation from the ground state or by Stimulated Raman Adiabatic Passage. Preliminary results are discussed.

Accurate theoretical prediction of scalar polarizabilities of atomic levels is of vital importance in the field of ultra-stable atomic clocks, where the Stark shift (static and dynamic, including blackbody radiation) is one of the strong limiting factors. There are numerous accurate measurements of the ground state polarizability in Cs, Rb, Sr, etc., which allow for accurate tests of theoretical models. Theory for highly excited states (Rydberg states) is also well elaborated. Still there are certain theoretical difficulties in calculating of scalar and tensor polarizabilities of intermediate excited states in alkali atoms. Different theoretical approaches give predictions which significantly deviate from each other. For example, theoretical predictions for the 5D state polarizability in Rb differ up to 20% [1-3]. An accurate measurement of the static Stark effect of 5D level in Rb will give an important input allowing to validate the accuracy of theoretical approximations. To our knowledge, such measurements have not been performed up to date.

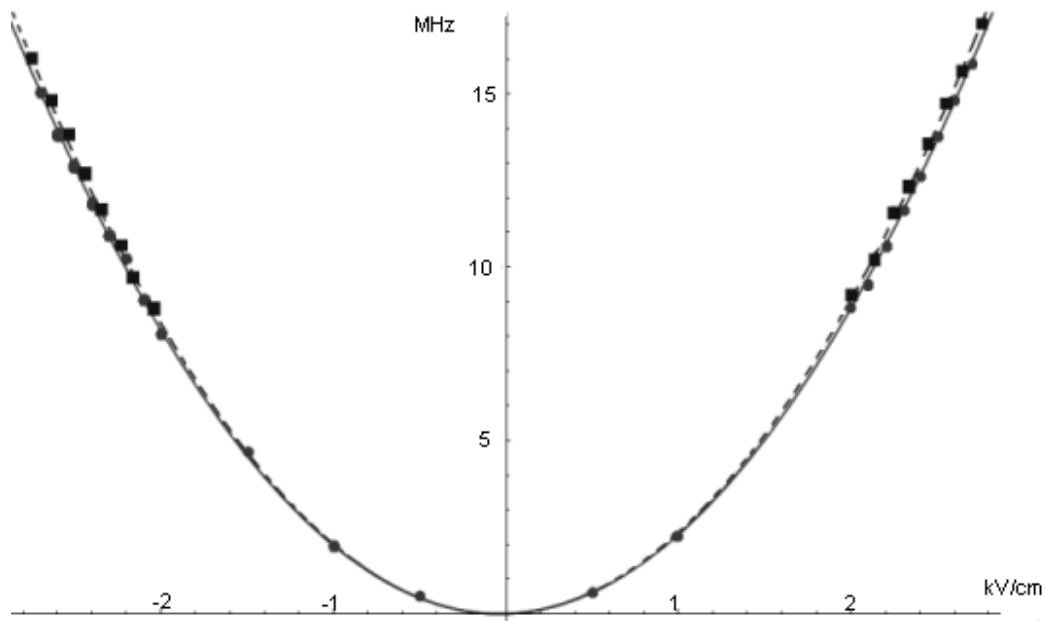


Figure 1. Experimental data (dots) and its parabola fits (curves) for line shift vs. applied electric field for light polarizations along (solid) and orthogonal (dashed) in respect to the field axis.

In our spectroscopic experiment the polarizability of  $5D_{5/2}$  and  $5D_{3/2}$  sublevels is determined from the frequency shift of corresponding  $5P_{3/2} \rightarrow 5D$  transition in Rb atoms placed in homogenous electric field. We address 5D level by two methods (i) the cascade excitation  $5S \rightarrow 5P$  at 780 nm and then  $5P \rightarrow 5D$  at 776 nm [4] and (ii) Stimulated Raman Adiabatic Passage with the reverse pulse sequence [5]. Experiments are performed on the laser cooled atomic cloud containing up to  $10^6$  atoms at the temperature of  $\sim 100$   $\mu$ K. Atoms are trapped in the magneto-optical trap (MOT) placed between two parallel highly-transparent metal meshes which form a plane capacitor. Stark shift measurement is performed in the pulsed regime with MOT beams switched off to prevent shifts from strong cooling beams. The population of the 5D level is detected by a photomultiplier tube counting 420 nm photons resulting from 5D level decay. Lines recorded at different electric field strengths are fitted by the same fit model.

The dependency of the line shift vs. applied electrical field is shown in Fig.1. Typical statistical measurement uncertainty of the 5D level scalar polarizability is at sub-percent level which should be enough to distinguish between different theoretical models. Varying polarization of the  $5P \rightarrow 5D$  excitation light in respect to the field axis we can address different magnetic sublevels and thus observe the influence of tensor polarizability (Fig.1). Different dependencies on laser polarization were also observed for  $5D_{5/2}$  and  $5D_{3/2}$  levels. At a moment we are studying contribution of systematic effects: magnetic field, line shape, field homogeneity, etc.

## References

- [1] M. S. Safronova, C. J. Williams, and C. W. Clark, *Phys. Rev. A* **69**, 022509 (2004).
- [2] A. A. Kamenski and V. D. Ovsianikov, *J. Phys. B: At. Mol. Opt. Phys.* **39**, 2247 (2006).
- [3] D.A. Kondrat'ev, I.L. Beigman, L.A. Vainshtein, *J. of Russian Las. Res.* **31**, 294 (2010).
- [4] A.V. Akimov et al., *Quant. Electron.* **40**, 139 (2010).
- [5] S A Snigirev et al., *Quant. Electron.* **42**, 714 (2012).

# Atomic Ratchet Driven by the Weak Perturbation with Broadband Spectrum

Makarov D.V., Kon'kov L.E.  
V.I.Ilichev Pacific Oceanological Institute  
43, Baltiyskaya Str., Vladivostok, 690041, Russia

**Abstract:** We present a scheme of atomic ratchet in a deep optical lattice perturbed by two additional low-amplitude lattices whose amplitudes are subjected to almost-periodic modulation with impact of randomness. This scheme provides activation of the net current even if the initial atomic ensemble is localized near the minima of the optical potential.

## 1. Introduction

Ratchet effect with cold atoms in optical lattices has recently attracted considerable attention. It can be regarded, for example, as a way for producing atomic chips which can be used in quantum computers. In the simplest setup for the atomic ratchet, one uses far-detuned deep optical lattice. This case provides the better localization of initial atomic cloud and can be fairly described in the framework of the semiclassical approximation. Activation of net current requires escaping of atoms from the potential wells, therefore, the experiments were usually conducted with relatively strong perturbation of the optical potential. Another promising approach is the usage of high-frequency driving leading to the lowering of the effective optical potential. In the present paper we propose a simple scheme which provides generation directed atomic transport using small-amplitude perturbation, even if atoms are predominantly localized near the minima of the potential. Usage of a small-amplitude perturbation allows one to avoid excessive heating of atoms. Our approach is based on the usage of two additional optical lattices. Amplitude of each lattice is subjected to almost-periodic modulation, that is, the respective modulating signal has finite spectral width. As a model of such signal, we use the two-dimensional Ornstein-Uhlenbeck process, or the so-called harmonic noise [1]. Presence of noisy component leads to efficient destruction of classical phase space barriers impeding the atom escaping from the potential wells.

## 2. Model

We consider ensemble of non-interacting atoms loaded into an optical lattice with tight confinement in the transversal direction, that is, atom dynamics can be fairly described by one-dimensional Schrödinger equation. In dimensionless units, it reads

$$i\hbar \frac{\partial \Psi(x,t)}{\partial t} = -\frac{\hbar^2}{2} \frac{\partial^2 \Psi(x,t)}{\partial x^2} + U(x,t) \Psi(x,t). \quad (1)$$

We consider the case of a deep lattice  $\hbar \ll 1$  and propose the following configuration of the optical potential:

$$U(x,t) = -\cos(x) + y(t) \sin x - \beta y(t+\Delta) \cos x, \quad (2)$$

where  $y$  is the harmonic noise. Note that there are two identical harmonic noises in (2), differing only by the time shift  $\Delta$ . Harmonic noise obeys the coupled stochastic differential equations

$$\dot{y} = s, \quad \dot{s} = -\Gamma s - \Omega^2 y + \varepsilon \sqrt{2\Gamma} \eta(t), \quad (3)$$

where  $\eta(t)$  is Gaussian white noise with

$$\langle \eta(t) \rangle = 0, \quad \langle \eta(t) \eta(t') \rangle = \delta(t-t'). \quad (4)$$

The power spectrum of harmonic noise  $y(t)$  is given by

$$S(\omega) = \frac{\varepsilon^2 \Gamma}{\omega^2 \Gamma^2 + (\omega^2 - \Omega^2)^2} \quad (5)$$

In the case of low values of  $\Gamma$ , the power spectrum (5) has the peak at the frequency

$$\omega_p = \sqrt{\Omega^2 - \Gamma^2/2}. \quad (6)$$

We take  $\Delta = \pi/(2\Omega)$ . Then, in the limit  $\Gamma \rightarrow 0$  the optical potential  $U(x,t)$  tends to the superposition of the standing and running waves

$$U = -\cos x + \varepsilon \sin(x - \beta\Omega t). \quad (7)$$

The Hamiltonian corresponding to this potential is not symmetric in the momentum space that results in the asymmetry of the ballistic atomic current [2]. However, if atoms are initially localized near the potential minima, the ballistic current is suppressed by classical invariant tori which act as dynamical barriers for transition into the ballistic states. In this sense, adding some amount of noise plays the constructive role, resulting in crossing the barriers due to noise-induced diffusion in the energy space. As long as noise doesn't alter asymmetry of the Hamiltonian in the momentum space, there occurs directed atomic transport. It is confirmed by results of numerical simulation of quantum atom dynamics (see Fig. 1).

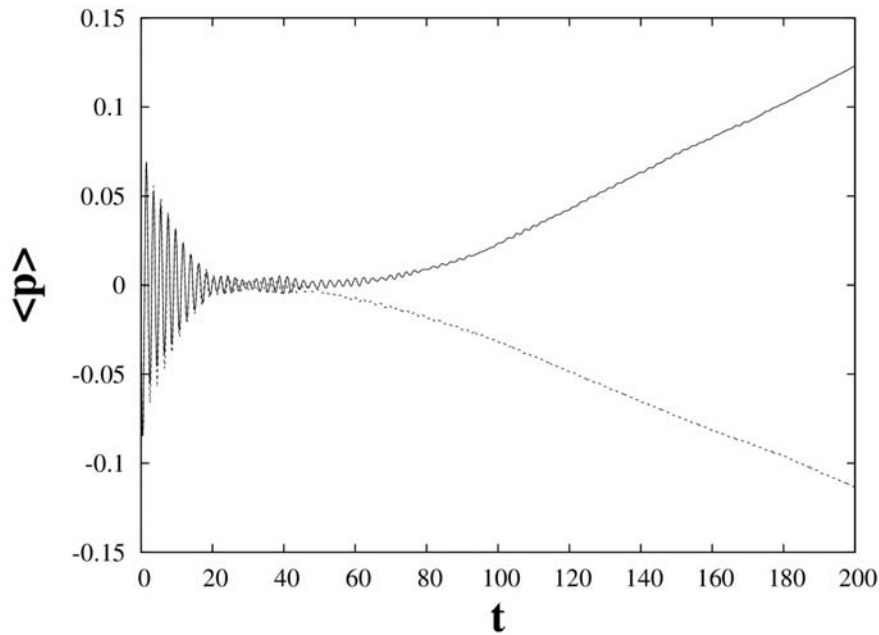


Fig. 1 Mean momentum as function of time for  $\hbar=0.1$ ,  $\varepsilon=0.05$ ,  $\Gamma=0.1$ ,  $\Omega=1.0$ ,  $\beta=1$  (solid) and -1 (dashed).

### 3. References

- [1] A. Neiman, L. Schimansky-Geier, "Stochastic resonance in bistable systems driven by harmonic noise", *Phys. Rev. Lett.* **72**, 2988-2991 (1994)
- [2] D. V. Makarov, M. Yu. Uleysky, "Generation of the ballistic particle transport in a periodic Hamiltonian system subjected to small time-dependent perturbation", *JETP Letters* **83**, 522-525 (2006).

# Bernstein's paradox in multiqubit states

A.V. Belinsky, A.S. Chirkin

Faculty of Physics and International Laser Center, M.V. Lomonosov Moscow State University, Leninskie Gory, Moscow  
119991, Russia;

FAX: +7 495/939-3113; email: [aschirkin@rambler.ru](mailto:aschirkin@rambler.ru) :

**Abstract:** An implementation of an analog of classical Bernstein's paradox on discrete quantum variables is discussed. In the case of three variables, this paradox consists in that the pair independence of events does not imply their mutual independence.

Entangled quantum states play an extremely important role in understanding quantum mechanics and in many applications: quantum information, quantum computations and quantum imaging. The clearest demonstration of the nonclassical character of correlations in entangled states is the violation of the relations of the classical model approach. These are the EPR paradox, Bell's inequality, the Greenberger–Horne–Zeilinger (GHZ) paradox, multiphoton interference, etc. [1- 4].

In this paper, we draw attention to the possibility of implementing in multiqubit states counterpart of the classic Bernstein's paradox from probability theory. In the case of three variables, for example,  $A, B, C$ , it consists in that the pair statistical independence of events ( $B$  doesn't depend on  $A$ ,  $C$  on  $B$  and  $A$  on  $C$ ) does not imply their statistical independence in aggregate that is  $ABC$  is statistically connected. We have examined GHZ and W states and Dicke and cluster ones too. It is established in [5] that quantum paradoxes are related to interference terms of the normally ordered characteristic function (NOCF) of Bose operators.

In order to observe the quantum Bernstein paradox the interference terms of the NOCF should transform into photon number correlation by means of polarization beam splitters (PBSs) on which orthogonally polarized photons come. After the PBSs, photons are detected by photon counters. In the case of four-qubit GHZ state after four PBSs the interference terms take the form  $\Gamma_{GHZ} = \langle \hat{N}_1 \hat{N}_2 \hat{N}_3 \hat{N}_4 \rangle = 1$  (index  $j$  denotes the number of channel). Value  $\Gamma_{GHZ} = 1$  corresponds to symmetric PBSs and to certain photon delays. Value  $+1$  or  $-1$  is shown to match the operator  $\hat{N}_j$  depending on that what counter registers a photon. Consequently, only eight of 16 possible outcomes are realized. The value “+1” and “-1” in each channel has probability  $1/2$ , while the pair of “+1” or “-1” in any two channels equals  $1/4$ . The probability of three simultaneous “+1” is  $1/8$ . However, the probabilities of four simultaneous “+1” is  $1/8$  too. Thus we have a paradoxical situation when the statistical independence in all possible triple correlations leads to the statistical dependence in fourth-order correlations.

## Reference

- [1] A. V. Belinsky and D. N. Klyshko, *Phys.—Usp.* **36** (8), 653 (1993).
- [2] A. V. Belinsky and D. N. Klyshko, *JETP* **75** (4), 606 (1994).
- [3] G. S. Greenstein and A. G. Zajonc, *The Quantum Challenge: Modern Research on the Foundations of Quantum Mechanics* (Jones and Bartlett, London, 2005; Intellect, Moscow, 2008).
- [4] J. W. Pan, Z. B. Chen, C. Y. Lu, H. Weifurter, A. Zeilinger, and M. Zukovski, *Rev. Mod. Phys.* **84**, 777 (2012).
- [5] A.S. Chirkin, I.V., O.V. Belyaeva, A.V. Belinsky *JETP* **116**, 39 (2013).

# Four-mode entangled quantum states in coupled intracavity optical parametric processes

M.S.Gevorgyan<sup>1</sup>, A.S. Chirkin<sup>2</sup>

<sup>1</sup> Faculty of General and Applied Physics, Moscow Institute of Physics and Technology, Moscow 141700, Russia;

email: [menua.gevorgyan@phystech.edu](mailto:menua.gevorgyan@phystech.edu)

<sup>2</sup> Faculty of Physics and International Laser Center, M.V. Lomonosov Moscow State University, Leninskie Gory, Moscow 119991, Russia;

FAX: +7 495/939-3113

**Abstract:** Quantum theory of laser generation, nondegenerate parametric down-conversion and up-conversion occurring simultaneously in active nonlinear crystals with aperiodic domain structure is presented. Entanglement of the quadrature Fourier components of generated frequencies is studied.

As is known, multi-mode entangled quantum states broaden the ability of using quantum light fields in quantum communication and quantum computing. In the paper we present the results of quantum theory of coupled five-frequency interactions in active aperiodic poled nonlinear crystals (AAPNCs). The interaction under study includes process of laser generation, nondegenerate parametric down-conversion followed by two up-conversions occurring simultaneously in a single AAPNC under quasiphase matching conditions. Describing the processes is based on the Heisenberg-Langevin equations. Steady state regime of generation is considered and the thresholds of laser generation and parametric down-conversion are determined. The spectral density of fluctuations of the quadrature components at frequencies both below and above the laser frequency, as well as their mutual spectral density is studied. The analysis in terms of the formation of EPR pairs (correlation of the Einstein-Podolsky-Rosen) between the Fourier components at different carrier frequencies is carried out too.

# Nonthreshold single-qubit laser

**T.B.Karlovich and S.Ya.Kilin**

*B. I. Stepanov Institute of Physics NASB, 220072, Minsk, Belarus*

*E-mail: [tbkar@mail.ru](mailto:tbkar@mail.ru)*

**Abstract:** Two definitions of microlaser threshold on the basis of P- and Q-distribution functions are presented. The conditions of nonthreshold generation of a one-qubit laser are obtained. The influence of the dephasing on P-distribution is considered.

## 1. Introduction

The definition of the threshold of a single-atom laser was the question of the great discussion during a long period of time. For the macroscopic laser the threshold is determined as the breakpoint in the dependency of mean photon number in the cavity or intensity of the intracavity field versus the intensity of the incoherent pump. So simple definition is absent in the microlaser case because in this situation the most of the spontaneous emission is realized into the single cavity field mode. With the suppression of the spontaneous emission into noncavity field modes threshold must be very low [1]. According to the rate laser equations for the ideal cavity QED laser the mean intracavity field number is linearly increased with the increasing of the intensity of the incoherent pump. In this case both the threshold and the breakpoint are disappeared in the dependency of the intracavity field intensity on the external field [2].

On the other hand in the work [3] authors confirm that any microlaser has the threshold, moreover this threshold can be achieved in the absence of the population inversion. Microlaser is described on the basis of the quantum Langevin equations for the semiconductor laser. The threshold is defined as the equality of the mean intracavity photon number to the unity. The existence of the threshold is based on the presence of the transition from the linear amplification regime to the nonlinear generation regime. In our previous work [4] we proposed to determine two thresholds for the one-atom laser on the basis of P-function quasiprobability and Q-distribution function (see Fig.1). The first one is connected with the generation of the light with nonzero amplitude and the second one is coincide with the previous definition  $\langle n \rangle = 1$ . Between the first and the second thresholds a single-atom laser can generate nonclassical light. Above the second threshold laser can generate radiation in the state close to the coherent state [5]. Also the lasing without threshold is investigated [4]. This type of lasing is considered in experimental work [6]. In this work we investigate the properties of radiation of single-qubit laser using the same definitions of the threshold as for single-atom laser.

## 2. Model of single-qubit laser

In this section we present the description of the single-qubit laser. It consists of a Josephson-junction charge qubit embedded in a superconducting resonator. A strong coupling between superconducting qubit (artificial atom) and electric resonator was implemented in the experiments [7,8]. Such system has a number of advantages over single-atom lasers and masers: artificial atom is fixed in the resonator and strongly and controllably coupling to the resonator modes due to the large dipole moment. Laser action of single-qubit laser is demonstrated in work [9]. In this work qubit is well described by two charge states  $|0\rangle$  and  $|2\rangle$  differing by one Cooper pair characterized by Josephson energy  $E_J$  and single-electron charging energy  $E_C$ . The mode of superconducting coplanar waveguide resonator is described by the harmonic oscillator with frequency  $\omega_R$ . The coupling between Cooper pair and harmonic oscillator is described by Jaynes-Cummings Hamiltonian:

$$H_{JC} = \frac{1}{2} \hbar \omega_Q \sigma_z + \hbar \omega_R a^\dagger a + \hbar g (\sigma_+ a + \sigma_- a^\dagger), \quad (1)$$

where qubit's level spacing is  $\hbar \omega_Q = \sqrt{E_C^2 + E_J^2}$ ,  $g$  is the qubit-resonator coupling strength.

The interaction with environment in single-qubit laser is accounted as a dissipation of the cavity and a dissipation of the qubit. The driving of the qubit is described by the incoherent pump. The reduced qubit-resonator density matrix  $\rho$  obeys the master equation in the Lindblad form:

$$\dot{\rho} = -\frac{i}{\hbar} [H_{JC}, \rho] + L_Q \rho + L_R \rho. \quad (2)$$

In Eq. (2) Liouvillian  $L_Q$  describes dephasing with rate  $\Gamma_\phi^*$ , relaxation of qubit with rate  $\Gamma_{21}$  and excitation of qubit with rate  $\Gamma_{12}$ :

$$L_Q \rho = \frac{\Gamma_\phi^*}{2} (\sigma_z \rho \sigma_z - \rho) + \frac{\Gamma_{21}}{2} ([\sigma_- \rho, \sigma_+] + [\sigma_-, \rho \sigma_+]) + \frac{\Gamma_{12}}{2} ([\sigma_+ \rho, \sigma_-] + [\sigma_+, \rho \sigma_-]). \quad (3)$$

Liouvillian  $L_R$  describes relaxation and excitation of resonator field mode with damping rate  $k$ :

$$L_R \rho = k(n_{th} + 1)([a \rho, a^+] + [a, \rho a^+]) + kn_{th}([a^+ \rho, a] + [a^+, \rho a]), \quad (4)$$

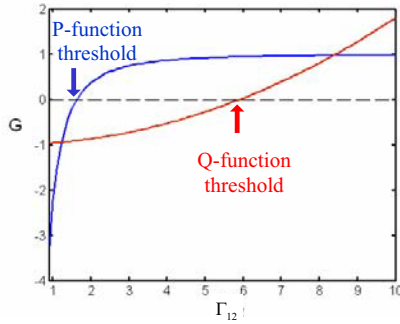
where  $n_{th}$  is the thermal photon number.

### 3. Results

On the basis of the analytical solution for the P-function of single-qubit laser in the strong coupling regime the condition for single-qubit laser generation is obtained:

$$G = \bar{a}^4 - \nu(\nu - 1) > 0, \quad (5)$$

where  $2\bar{a}^2 = \frac{\Gamma_{12}}{2k}$  is the normalized intensity of incoherent pump,  $\nu = \frac{\Gamma_{21}}{4k} - \frac{1}{2}$  is normalized decay rate of the excited state. When parameter  $\nu \in [0, 1]$  one-qubit laser can generate radiation at any excitation rate and consequently demonstrates the thresholdless behavior (see Fig.2).



Parameters:  $\Gamma_{12} = 4$ ,  $k = 0.5$ ,  $n_{th} = 0.1$   
Fig.1. Two thresholds of the microlaser

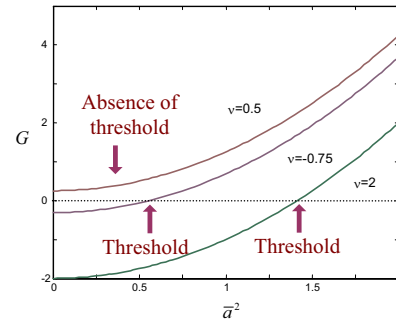


Fig.2. Thresholdless generation of single-qubit laser

### 4. Conclusions

It is found that one-qubit laser can generate radiation without threshold approximately under the same conditions as single-atom laser (5). In this case dephasing rate does not strongly influence on the shape of P-function and on the threshold conditions for single-qubit laser.

- [1] G. Björk and Y. Yamamoto "Analysis of semiconductor microcavity lasers using rate equations," IEEE J. Quantum Electron. **27**, 2386-2396 (1991).
- [2] P.R. Rice, H.J. Carmichael "Photon Statistics of a Cavity-QED Laser: A comment on the laser-phase-transition analogy," Phys.Rev. A **50**, 4318-4329 (1994).
- [3] G. Björk, A. Karlsson, and Y. Yamamoto "Definition of a laser threshold," Phys.Rev. A **50**, 1675-1680 (1994).
- [4] T.B. Karlovich, S.Ya. Kilin "Quantum statistical properties of a single-atom-laser," Opt. i Spectr. **91**, 375-383 (2001).
- [5] S.Ya. Kilin, T.B. Karlovich "Single-atom laser. Coherent and nonclassical effects in the regime of strong coupling," JETP **122**, 933-949 (2002).
- [6] J. McKeever, A. Boca, A.D. Boozer, J.R. Buck and H.J. Kimble "Experimental realization of a one-atom laser in the regime of strong coupling," Nature (London) **425**, 268-271 (2003).
- [7] A. Wallraff, D.I. Schuster, A. Blais, L. Frunzio, R.-S. Huang, J. Majer, S. Kumar, S.M. Girvin and R.J. Schoelkopf "Strong coupling of a single photon to a superconducting qubit using circuit quantum electrodynamics," Nature **431**, 162-167 (2004).
- [8] I. Chiorescu, P. Bertet, K. Semba, Y. Nakamura, C.J.P.M. Harmans and J.E. Mooij "Coherent dynamics of a flux qubit coupled to a harmonic oscillator," Nature **431**, 159-162 (2004).
- [9] O. Astafiev, K. Inomata, A.O. Niskanen, T. Yamamoto, Yu.A. Pashkin, Y. Nakamura and J.S. Tsai "Single artificial-atom lasing," Nature **449**, 588-590 (2007).